DE[redacted]ED

293

Copy
RM L57A31

NACA RM L57A31

[redacted]

NACA

RESEARCH MEMORANDUM

Declassified by authority of NASA
Classification Change Notices No. 413
Dated ** 12/29/65

WIND-TUNNEL INVESTIGATION AT HIGH SUBSONIC SPEEDS OF THE EFFECTS ON STATIC STABILITY CHARACTERISTICS OF VARIOUS MODIFICATIONS TO A SWEPT-WING FIGHTER-TYPE AIRPLANE MODEL

By Kenneth W. Goodson

Langley Aeronautical Laboratory
Langley Field, Va.

DECLASSIFIED:
ATS 480

AUTHORITY:
DROBKA TO LEBOW
MEMO DATED 12/13/65

[redacted]

[redacted]

NATIONAL ADVISORY COMMITTEE
FOR AERONAUTICS
WASHINGTON
April 30, 1957

[redacted]

 DECLASSIFIED CONFIDENTIAL

NATIONAL ADVISORY COMMITTEE FOR AERONAUTICS

RESEARCH MEMORANDUM

WIND-TUNNEL INVESTIGATION AT HIGH SUBSONIC SPEEDS OF THE EFFECTS ON STATIC STABILITY CHARACTERISTICS OF VARIOUS MODIFICATIONS TO A SWEPT-WING FIGHTER-TYPE AIRPLANE MODEL

By Kenneth W. Goodson

SUMMARY

An investigation was made at high subsonic speeds of a model of a twin-engine swept-wing fighter-type airplane. The model was tested with several different tail configurations and with several wing and engine inlet modifications. The investigation was concerned primarily with longitudinal stability at a stabilizer incidence of 0°; however, a few stabilizer and lateral-derivative tests also were made. The model was tested in the Langley high-speed 7- by 10-foot tunnel at Mach numbers from 0.60 to 0.92.

The results showed that a horizontal tail raised to the top of the vertical tail and moved forward from the original position gave substantial improvements in stability and delayed the angle of attack and lift coefficient at which pitch-up instability occurred. Use of a fixed horizontal surface, attached below the engine tail pipes, in combination with either the original or new horizontal tail (biplane arrangement) also provided substantial improvements in stability; however, the combination that included the new horizontal tail had better characteristics. Some additional but smaller improvements were obtained when wing leading-edge chord-extensions, modified wing trailing-edge fillets, and modified engine inlets were used.

INTRODUCTION

Many swept-wing high-speed airplanes experience abrupt changes in longitudinal stability (pitch-up) at moderate and high lift coefficients. The present investigation was undertaken to investigate various possibilities of alleviating or possibly eliminating the pitch-up problem on

[redacted]

a twin-engine swept-wing fighter-type configuration. Results of rocket-model investigations of this configuration are published in reference 1.

The present model was tested in the Langley high-speed 7- by 10-foot tunnel through a Mach number range from 0.60 to 0.92 over an angle-of-attack range of 0° to 27° (for the lower Mach numbers.) Several lateral derivative tests were made through the angle-of-attack range at sideslip angles of $\pm 4^{\circ}$. Analysis of these data has been limited in order to expedite publication.

SYMBOLS

The data are presented about the system of axes shown in figure 1. The pitching-moment coefficients are referred to a center of gravity at the 28.57-percent mean aerodynamic chord of the theoretical wing.

C_L lift coefficient, $\frac{\text{Lift}}{qS}$

C_D drag coefficient, $\frac{\text{Drag}}{qS}$

C_m pitching-moment coefficient, $\frac{\text{Pitching moment}}{qS\bar{c}}$

C_l rolling-moment coefficient, $\frac{\text{Rolling moment}}{qSb}$

C_n yawing-moment coefficient, $\frac{\text{Yawing moment}}{qSb}$

C_Y side-force coefficient, $\frac{\text{Side force}}{qS}$

q dynamic pressure, $\frac{\rho V^2}{2}$, lb/sq ft

ρ mass density of air, slugs/cu ft

V free-stream velocity, ft/sec

M Mach number

S wing area (theoretical area, neglects inboard wing fillets, see fig. 2), sq ft

[redacted]

c	local chord parallel to plane of symmetry, ft
$\bar{c}$	wing mean aerodynamic chord, $\frac{2}{S}\int_0^{b/2} c^2 dy$, ft
$\bar{c}_h$	horizontal-tail mean aerodynamic chord, ft
$\bar{c}_v$	vertical-tail mean aerodynamic chord, ft
b	wing span, ft
y	spanwise distance from plane of symmetry, ft
α	angle of attack of wing, deg
β	angle of sideslip, deg
i_t	stabilizer incidence, positive with trailing edge down, deg
Γ	dihedral angle, positive with tips up, deg
Λ_{le}	surface leading-edge sweep, deg

Subscripts:

β	denotes partial derivative of coefficient with respect to sideslip angle; for example $C_{l_\beta} = \frac{\partial C_l}{\partial \beta}$

The various components of the configurations presented herein are designated as follows:

W	wing
F	fuselage
V_o	original vertical tail
V_1	new vertical tail
H_o	original horizontal tail
H_1	new horizontal tail

[redacted]

H_2 fixed horizontal surface attached below engine tail pipes

H_3 original horizontal-tail plan form in low position

H_4 low-aspect-ratio highly swept horizontal surface

MODEL AND APPARATUS

A two-view drawing of the basic complete model (WFV_oH_o) is shown in figure 2. The model wing had an aspect ratio (neglecting fillets) of 4.270, taper ratio of 0.284, 1.67-percent positive leading-edge camber, and 41.1° leading-edge sweep. This nominal plan form had been modified to accommodate the engines by extending the inboard portion of the trailing edge. The original (basic) vertical- and horizontal-tail configuration also is shown in figure 2. The indicated difference between model and airplane (fig. 2) is a result of the model being adapted to the sting support.

A new vertical- and horizontal-tail combination (V_1H_1) was designed (fig. 3) so that the mean aerodynamic chord of the horizontal tail was moved forward to a higher position. In order to accomplish this, the leading-edge sweep of the vertical tail was reduced from 52.0° to 35.0° by shearing the original surface about the root chord. Also, the horizontal tail was redesigned to move its mean aerodynamic chord forward and upward by changing the plan form and incorporating 20° of positive dihedral. This horizontal tail was mounted on the reduced-sweep vertical tail in a T-tail arrangement with the apex of the horizontal tail coincident with the leading edge of the tip chord of the vertical tail. These modifications reduced the horizontal-tail length from $2.85\bar{c}$ to $2.47\bar{c}$ and increased the horizontal-tail height from $0.97\bar{c}$ to $1.22\bar{c}$ when referenced to the assumed center of gravity.

Drawings of several additional horizontal surfaces that were investigated are shown in figure 4. Horizontal tail H_2 was located below the jet-exit ducts to give a tail position below the wing-chord plane. A horizontal tail H_3 having the same plan form as the original horizontal tail H_o was mounted in a position directly beneath the original horizontal tail and above the wing-chord plane. This tail was given -15.0° dihedral in order to lower the surface further. A low-aspect-ratio, highly swept, fixed horizontal surface or strake H_4 was also tested in combination with the new T-tail arrangement. This tail also had -15° dihedral.

[redacted]

Two-engine inlet modifications are shown in comparison with the original inlet in figure 5. The modified inlet areas were made equal to that of the basic inlet and the ducts were kept open for all the present tests. When the inlet was first modified (modified inlet 1), the accessory housing bodies located inside the ducts were removed to facilitate model changes in the inlet region. These bodies were left out of the model for the remaining tests, inasmuch as their effect was believed to be negligible for the present investigation. The small differences in configurations (accessory bodies in or out or the inlet modification used) are indicated in table I.

Various modifications to the wing are shown in figure 6. These modifications include leading-edge chord-extensions, wing trailing-edge fillets or extensions, inboard-upper-surface spoilers, and fences located on the lower surface of the inlets. The $0.35\frac{b}{2}$ chord-extension was extended in the wing-chord plane, whereas the $0.65\frac{b}{2}$ chord-extension (previously tested at CWT) was extended along the leading-edge camber line. The 1/2-inch-lower surface inlet fences were constructed of 1/32-inch-thick material. For one test a 1/8-inch-wide transition strip (made with number 60 carborundum) was located at the 10-percent-chord line of the wing upper and lower surface and a 1/8-inch band was located on the fuselage 1 inch behind the nose.

Additional information concerning the model and the various tails is presented in table II. Photographs of the model with the new vertical- and horizontal-tail combination (WFV_1H_1) are presented in figures 7 and 8. The inlet modifications are also shown in these photographs.

TESTS

The sting-supported model was tested in the Langley high-speed 7- by 10-foot tunnel through a Mach number range of 0.60 to 0.92 and through an angle-of-attack range that varied with Mach number because of load limits of the balance (the maximum range being about 0° to 27°). The Reynolds number (based on the mean aerodynamic chord) varied with Mach number from about 1.50×10^6 to 2.0×10^6. The Mach range was limited in some cases by temperature and tunnel power.

Longitudinal stability tests were made for the complete model with the various tail, wing, and inlet modifications. Stabilizer effectiveness tests and lateral derivative tests ($\beta = \pm 4^{\circ}$) were made for the complete model with the new vertical and horizontal tails (WFV_1H_1).

CORRECTIONS

Blockage corrections were applied to the results by the method of reference 2. Jet-boundary corrections to the angle of attack and drag were applied in accordance with reference 3. Corrections for effects of the longitudinal pressure gradient in the wind-tunnel test section have been applied to the data.

Model support tares have not been applied except for a fuselage base-pressure correction to reduce the drag to a condition of free-stream static pressure at the fuselage base. No corrections have been applied for the internal drag of the duct. From past experience, it is expected that the influence of the sting support on the model characteristics with tails H_0, H_1, and H_2 is small with regard to the lift and pitching moment; however, for configurations with tails H_3 and H_4 the sting effects could be quite large.

The angle of attack has been corrected for deflection of the balance and sting support. No attempt has been made to correct the data for aeroelastic distortion of the steel model.

PRESENTATION OF RESULTS

The results are presented in figures 9 to 17 as follows:

	Figure
Effect of several tail modifications on the longitudinal aerodynamic characteristics of the model	9 to 11
Effect of duct-inlet modifications on the longitudinal aerodynamic characteristics of the model	12
Effect of wing modifications and fixes on the longitudinal aerodynamic characteristics of the model	13 to 15
Effect of stabilizer deflection on the longitudinal aerodynamic characteristics of the model with the new vertical and horizontal tails (WFV_1H_1)	16
Lateral stability derivatives of the model with the new vertical and horizontal tails (WFV_1H_1)	17

[redacted]

The results are presented about a center of gravity at the 28.57-percent mean aerodynamic chord of the nominal wing (without fillets). Small variations in model configurations (accessory bodies in or out and duct-inlet configuration) are shown in the tabulation of the detailed test program given in table I.

DISCUSSION

Pitching-Moment Characteristics

Presented in figure 9 are data showing the effect of several tail configurations on the longitudinal characteristics of the model over the angle-of-attack and Mach number range tested. For the complete model with the original vertical and horizontal tail (WFV_oH_o), there is a reduction in stability at $\alpha = 5^o$ to 7° and an instability at about $\alpha = 15^o$ for Mach numbers of 0.60 to 0.85. Comparison of the tail-on and tail-off configurations shows that the initial reduction in stability is caused by the wing-fuselage configuration and that the abrupt instability near the stall results primarily from the downwash at the tail. Experience has shown this tail-on instability to be peculiar to configurations having the tail located above the wing-chord plane in such a way that the tail traverses the wing wake and region of maximum downwash at high angles of attack. Tuft probe studies (at very low speed) in the vicinity of the model showed that the initial reduction in stability may have been influenced by the lifting properties of the engine inlets and that the instability at the higher lift was associated with the tail entering the high downwash region. The tuft survey showed that at high angles of attack the downwash angle at the tail approached and possibly exceeded the angle of attack, a condition which would make the tail ineffective in adding to the stability of the wing-body combination.

The new vertical- and horizontal-tail configuration (WFV_1H_1) was designed to move the horizontal tail above the wing wake by reducing the sweep of the vertical tail and mounting a modified horizontal tail (with reduced sweep and increased dihedral) on the vertical-tail tip chord in a T-tail arrangement. This combination raised the mean aerodynamic chord of the horizontal tail about $0.25\bar{c}$ and moved it forward about $0.38\bar{c}$. This configuration improved the stability at low angles of attack ($\alpha = 5^o$ to 7°) and delayed the occurrence of instability by an increment of about 8° in angle of attack or 0.15 in lift coefficient at $M = 0.60$. The improvement in lift or angle-of-attack range became progressively smaller as the Mach number increased. Perhaps a more realistic reference for comparison of improvements in lift or angle-of-attack range would be the point where the reduction in stability is first observed (for example, see fig. 9(a), $M = 0.80$), since in some type of

maneuvers a sudden reduction in stability at moderate angles of attack might be felt as pitch-up. From this point of view the improvement in lift or angle-of-attack range would be larger than that previously indicated.

Another, but perhaps less practical, modification was the addition of a fixed horizontal surface to the lower surface of the engine-tail pipes to provide a horizontal stabilizing surface below the wing wake. This surface was tested in combination with the T-tail configuration in a biplane tail arrangement ($WFV_1H_1 + H_2$ + modified inlet 1). It will be shown later that the change in inlet modification for this configuration had only a small effect on the results.

The biplane tail gave the best overall stability characteristics of any of the configurations tested. Note, however, that the pitch-up at high angles of attack still exists but is delayed to a higher angle of attack and lift coefficient. When H_2 was tested in combination with the original horizontal tail (configuration $WFV_oH_o + H_2$ of fig. 10), a very substantial improvement over the original configuration was obtained, although the results were somewhat inferior to those obtained with the biplane tail configuration having the higher horizontal tail (configuration $WFV_1H_1 + H_2$ of fig. 9). This condition probably exists because the original horizontal tail encounters the region of maximum downwash at a much lower angle of attack in such a way that the tail nonlinearities do not cancel the wing nonlinearities. The result of lowering the original horizontal-tail plan form to a position just above the wing-chord plane was detrimental. (See configuration $WFV_oH_3 + H_2$ in fig. 10.) The configuration with only the horizontal tail H_2 experiences rather large losses in stability at moderate angles of attack (figs. 10(a) and 10(b)). At the higher angles of attack, however, the stability increases as the tail (H_2) emerges from the wing wake. The addition of transition to the leading edge of the wing did not appreciably affect the pitching-moment characteristics (fig. 10). The effects on stability of the highly swept horizontal tail or strake H_4 (fig. 11) were small.

The configuration with the new tail assembly (WFV_1H_1) was tested with various wing and inlet modifications. The effects of lower-surface inlet fences were negligible (fig. 11). The inlet modifications of figure 5 were made in an effort to reduce the lifting efficiency of the inlets in the hope of improving the tail-off characteristics as well as the downwash at the tail. Some stability improvements resulted from the modified inlets, although they were rather small. (See fig. 12.) Some improvement in the pitching-moment-curve linearity was obtained, however, with the wing trailing-edge fillets. (See fig. 13.) No improvement was obtained with the wing trailing-edge spoiler or with

[redacted]

the tail assembly moved forward (fig. 14). A somewhat larger gain in pitching-moment-curve linearity was obtained with chord-extensions running from $0.65\frac{b}{2}$ to the wing tip (fig. 15); however, they provided little change in the angle of attack at which instability occurs.

Since the new vertical- and horizontal-tail configuration (WFV_1H_1) showed considerable improvement in longitudinal stability characteristics, it was thought to be desirable to determine the effect of stabilizer deflection on the aerodynamic characteristics. These results are shown in figure 16. The small nonlinearity at $M = 0.80$ and $M = 0.85$ is magnified somewhat by the -6° stabilizer deflection; otherwise, the results are typical of the usual stabilizer effects.

Lift and Drag Characteristics

Use of the new tail assembly V_1H_1 did not appreciably affect the lift characteristics; however, addition of the horizontal surface H_2 below the tail pipe (figs. 9 and 10) extended the lift coefficients to higher values at subcritical Mach numbers. Addition of wing trailing-edge fillets or leading-edge chord-extensions gave small increases in lift-coefficient range (figs. 11(c), 13(c), and 15(c)) at some Mach numbers.

The configuration with the new tail assembly WFV_1H_1 had a minimum drag approximately equal to that of the basic configuration WFV_oH_o. Drag values obtained for configurations having H_2 below the tail pipes are regarded as unrealistic since no attempt was made to obtain a clean installation of this tail on the model. Small changes in drag were obtained when trailing-edge fillets and leading-edge chord-extensions were used.

Lateral Derivatives

Lateral stability derivatives (from tests at $\beta = \pm 4^{\circ}$) were obtained with the new tail assembly WFV_1H_1 as shown in figure 17. These results show that the model is directionally stable through the angle-of-attack range tested, although there is considerable reduction in stability at the higher angles of attack. The effective dihedral increases with angle of attack.

[redacted]

SUMMARY OF RESULTS

An investigation of the stability characteristics at high subsonic speeds (Mach numbers of 0.6 to 0.92) of a model of a twin-engine fighter-type airplane indicate the following results:

The results showed that a new horizontal tail raised to the top of the vertical tail and moved forward from the original position gave substantial improvements in stability and delayed the angle of attack and lift coefficient at which pitch-up instability occurred. Use of a fixed horizontal surface, attached below the engine tail pipes, in combination with either the original or new horizontal tail (biplane arrangement) also provided substantial improvements in stability; however, the combination that included the new horizontal tail had better characteristics. Some improvement was obtained when wing leading-edge chord-extensions, modified wing trailing-edge fillets, and modified engine inlets were used.

Langley Aeronautical Laboratory,
National Advisory Committee for Aeronautics,
Langley Field, Va., January 7, 1957.

REFERENCES

1. Mitcham, Grady L.: A Summary of the Longitudinal and Lateral Stability and Control Characteristics Obtained From Rocket-Model Tests of a Swept-Wing Fighter-Type Airplane at Mach Numbers From 0.5 to 1.9. NACA RM L56K19, 1957.

2. Herriot, John G.: Blockage Corrections for Three-Dimensional-Flow Closed-Throat Wind Tunnels, With Consideration of the Effect of Compressibility. NACA Rep. 995, 1950. (Supersedes NACA RM A7B28.)

3. Gillis, Clarence L., Polhamus, Edward C., and Gray, Joseph L., Jr.: Charts for Determining Jet-Boundary Corrections for Complete Models in 7- by 10-Foot Closed Rectangular Wind Tunnels. NACA WR L-123, 1945. (Formerly NACA ARR L5G31.)

[redacted]

TABLE I.- MODEL CONFIGURATIONS TESTED

Figure	Configuration	Duct inlet	Accessory housing bodies
9	WFV_oH_o	Original	Out
	WFV_1H_1	Original	Out
	$WFV_1H_1 + H_2$	Modification 1	Out
	WF	Original	In
10	WFV_oH_o	Original	Out
	WFV_oH_2	Original	Out
	$WFV_oH_o + H_2$	Original	Out
	$WFV_oH_3 + H_2$	Original	Out
	WFV_oH_o + 0.10c transition	Original	Out
11	WFV_1H_1	Original	Out
	$WFV_1H_1 + H_4$	Original	In
	$WFV_1H_1 + H_4$ + Lower surface inlet fences	Original	In
	$WFV_1H_1 + H_4$ + Wing fillet 2	Original	In
12	WFV_1H_1	Original	Out
	WFV_1H_1	Modification 1	Out
	WFV_1H_1	Modification 2	Out
13	WF	Original	In
	WF + Wing fillet 2	Original	In
	WFV_1H_1	Original	Out
	WFV_1H_1 + Wing fillet 2	Original	In
	WFV_1H_1 + Wing fillet 3	Modification 1	Out
14	WFV_1H_1	Modification 1	Out
	WFV_1H_1 (Tail moved forward 2 inches)	Original	Out
	WFV_1H_1 + Trailing-edge spoiler	Modification 1	Out
15	WFV_1H_1	Original	Out
	$WFV_1H_1 + 0.65\frac{b}{2}$ chord-extension (CWT)	Original	Out
	$WFV_1H_1 + 0.35\frac{b}{2}$ chord-extension	Original	In
16	WFV_1H_1; $i_t = 0^\circ$	Original	Out
	WFV_1H_1; $i_t = -6^\circ$	Original	Out
17	WFV_1H_1; $i_t = -6$; Lateral derivatives	Original	Out

CONFIDENTIAL

TABLE II.- MODEL GEOMETRIC CHARACTERISTICS

Characteristic	Wing	Vertical tail		Horizontal tail				
		V_o	V_1	H_o	H_1	H_2 (*)	H_3	H_4 (*)
Area, sq ft	0.922 Theoretical**	0.212	0.212	0.189	0.189	0.113	0.189	0.095
Aspect ratio	4.272 Theoretical**	.662	.662	3.301	3.32	2.22	3.301	.557
Taper ratio	0.284 Theoretical**	.509	.509	.460	.25	.50	.460	.100
Λ_{le}, deg	41.1	52.0	35.0	39.8	35.9	45.0	39.8	
Dihedral, deg	0	0	0	10	20	0	-15	-15
Incidence, deg	1.0	0	0	0	0	0	0	0
Airfoil-section root tip	NACA 65A007 modified***	NACA 65A007	NACA 65A006	NACA 65A007	NACA 65A006	1/16-inch flat plate	1/16-inch flat plate	1/16-inch flat plate
	NACA 65A006 modified***	NACA 65A007	NACA 65A006	NACA 65A006	NACA 65A006			
Mean aerodynamic chord, in.	6.146	7.03	7.03	2.988	3.207		2.988	
Root chord, c_r, in.	8.663	9.000	9.000	3.925	4.582	3.60	3.925	9.00
Tip chord, c_t, in.	2.464	4.582	4.582	1.795	1.146	1.80	1.795	.90
Span, in.	23.812	4.500	4.500	9.450	9.450	6.00	9.450	2.75

*Based on theoretical exposed area.

**Neglects wing fillet area.

***The wing basic airfoil section was modified by extending the portion forward of the 0.16c line by 5 percent and adding 1.67-percent positive camber.

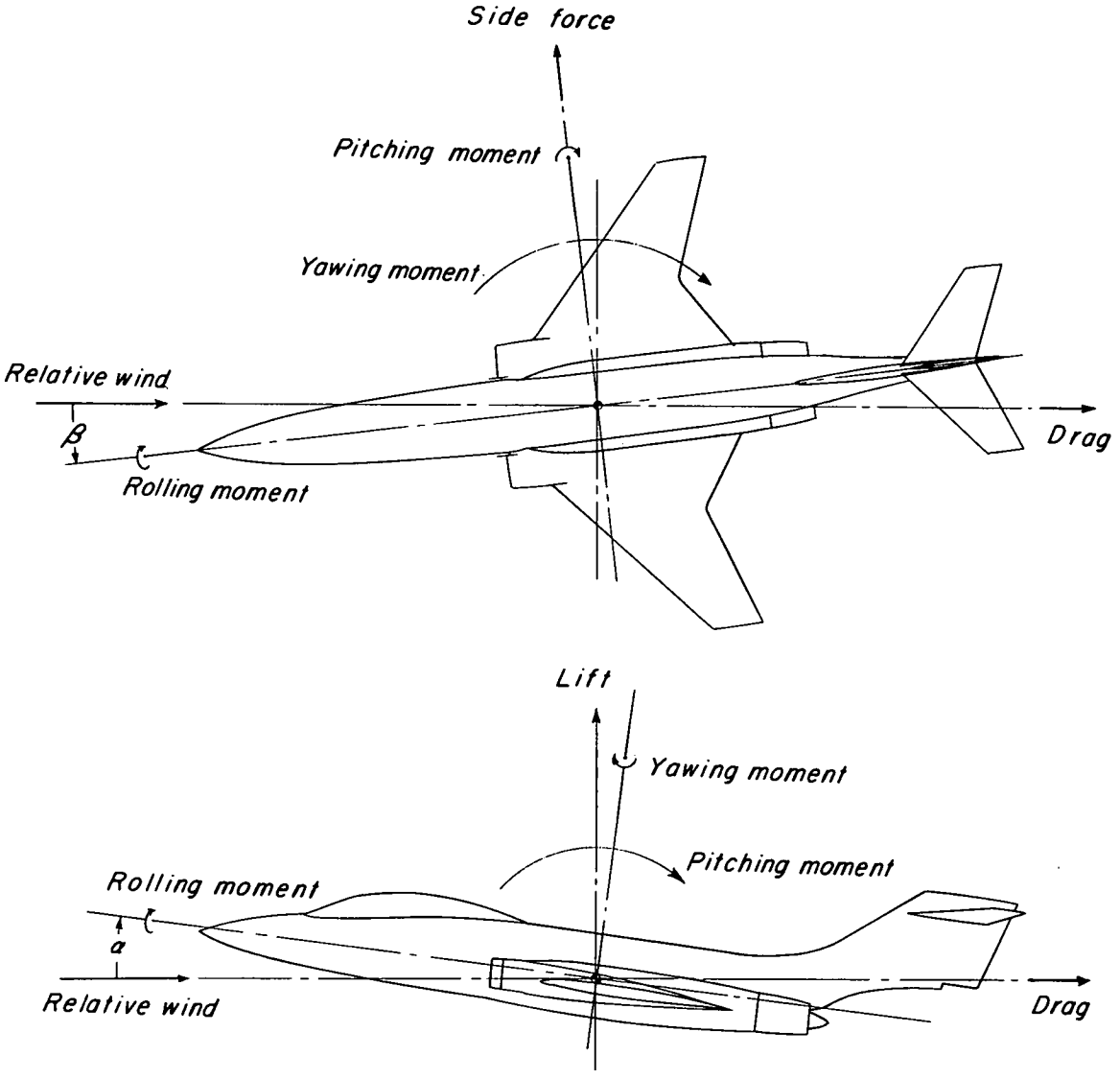

Figure 1.- System of axes. (Positive values of forces, moments, and angles are indicated by arrows.)

[redacted]

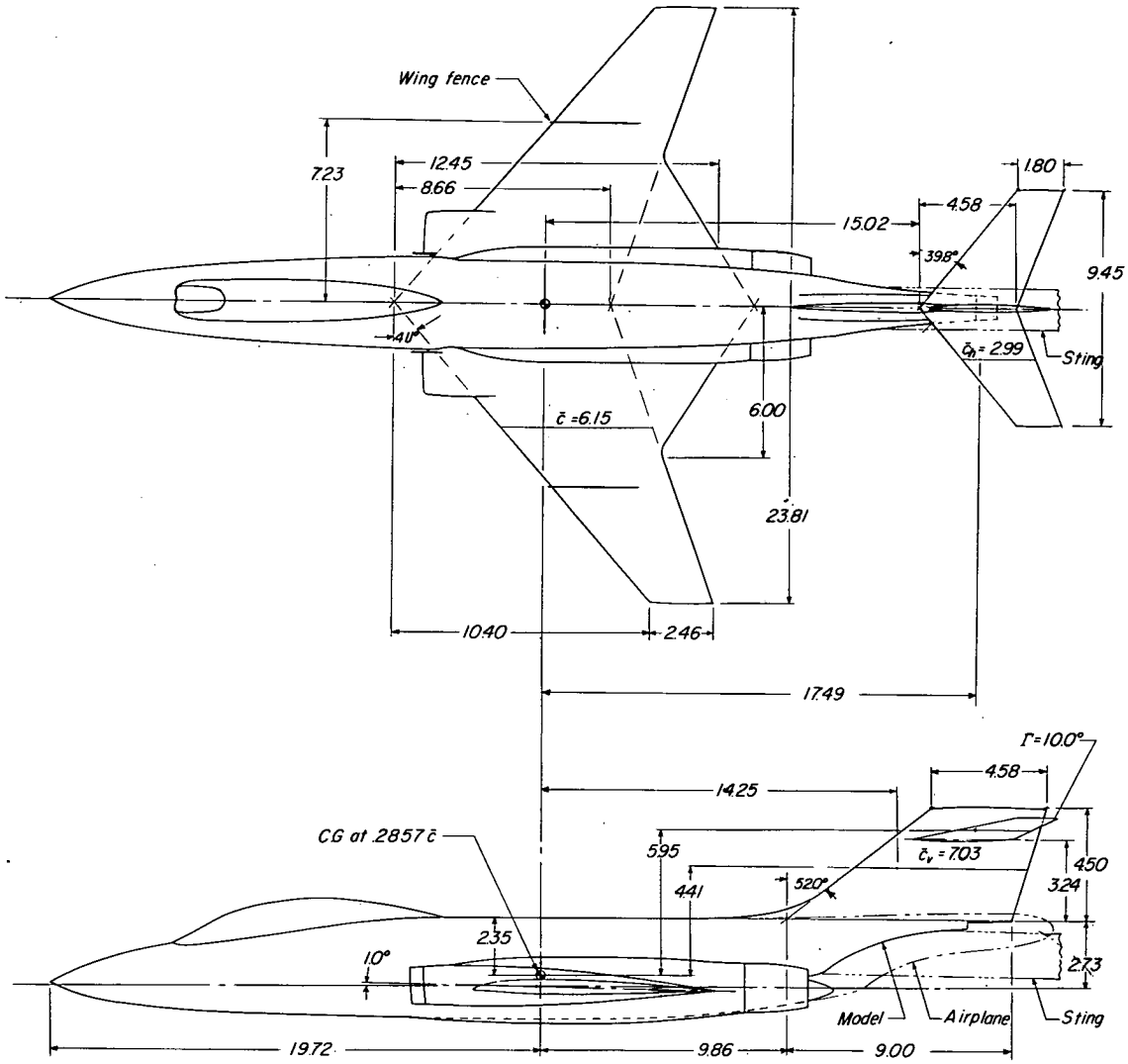

Figure 2.- Two-view drawing of basic model (WFV_oH_o). All dimensions are in inches.

[redacted]

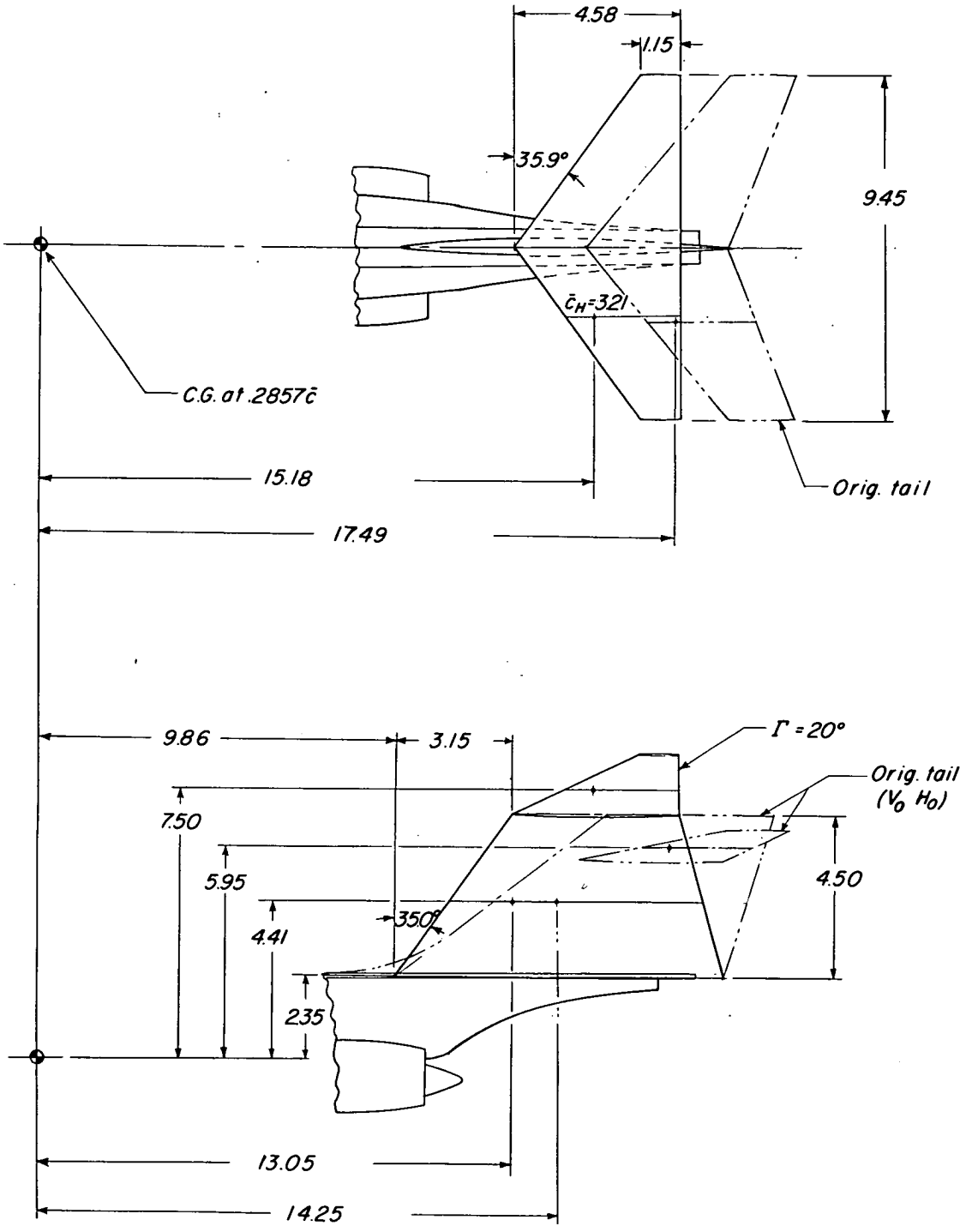

Figure 3.- Two-view drawing of a new vertical and horizontal T-tail arrangement (WFV_1H_1). All dimensions are in inches.

[redacted]

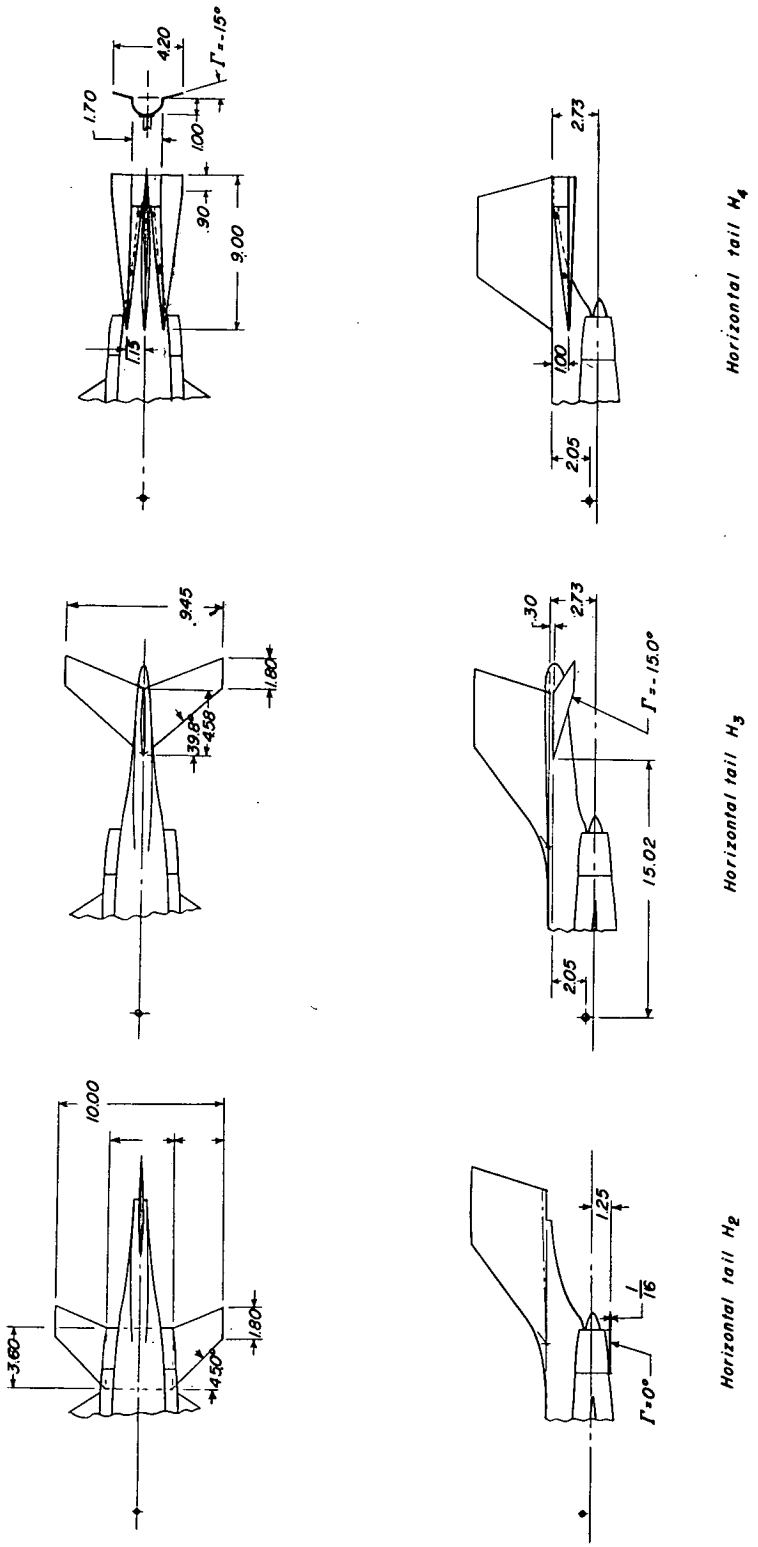

Figure 4.- Drawings of several additional horizontal-tail configurations (H_2, H_3, H_4). All dimensions are in inches.

[redacted]

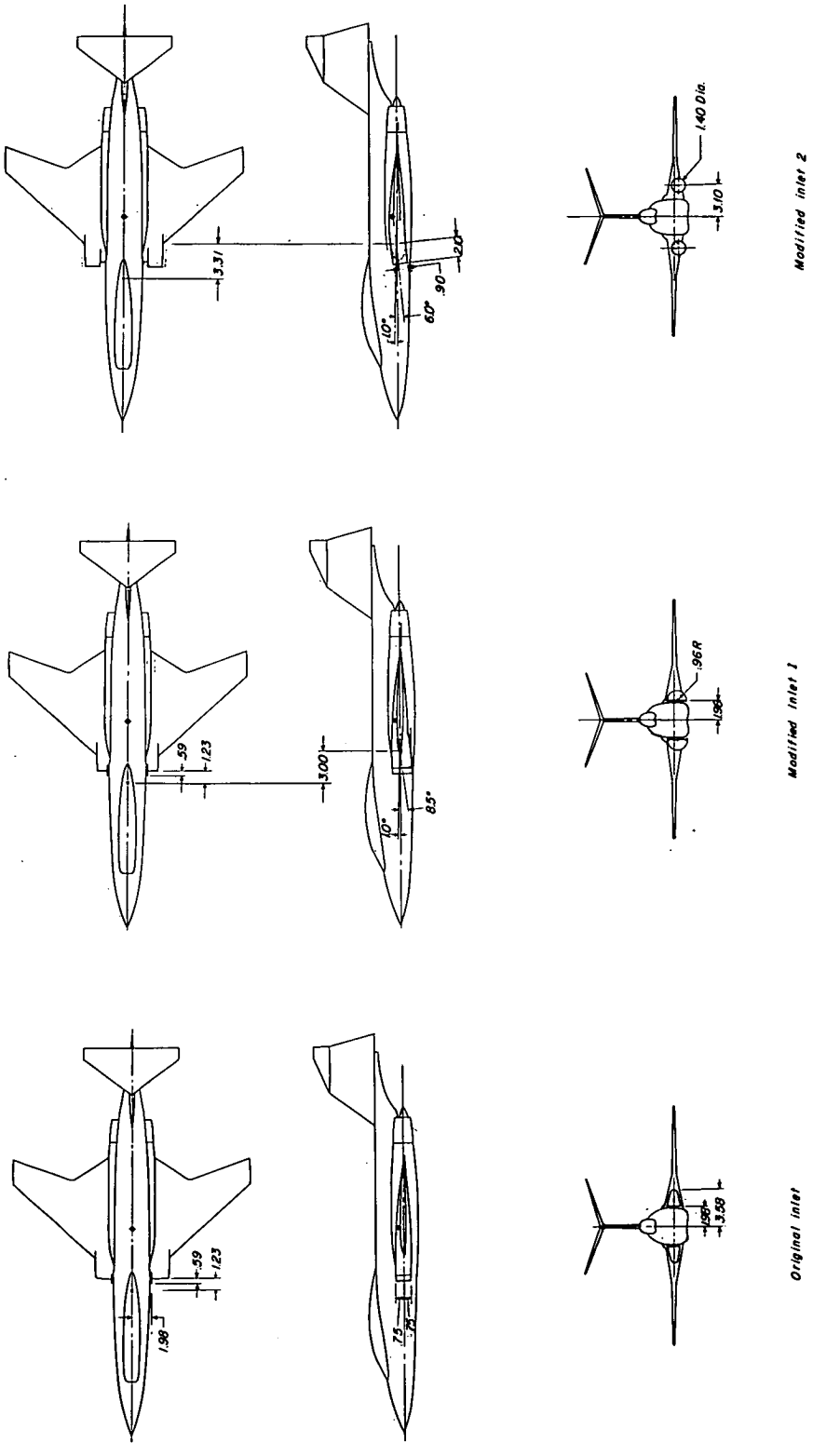

Figure 5.- Three-view drawings of several duct inlet configurations. All dimensions are in inches.

[redacted]

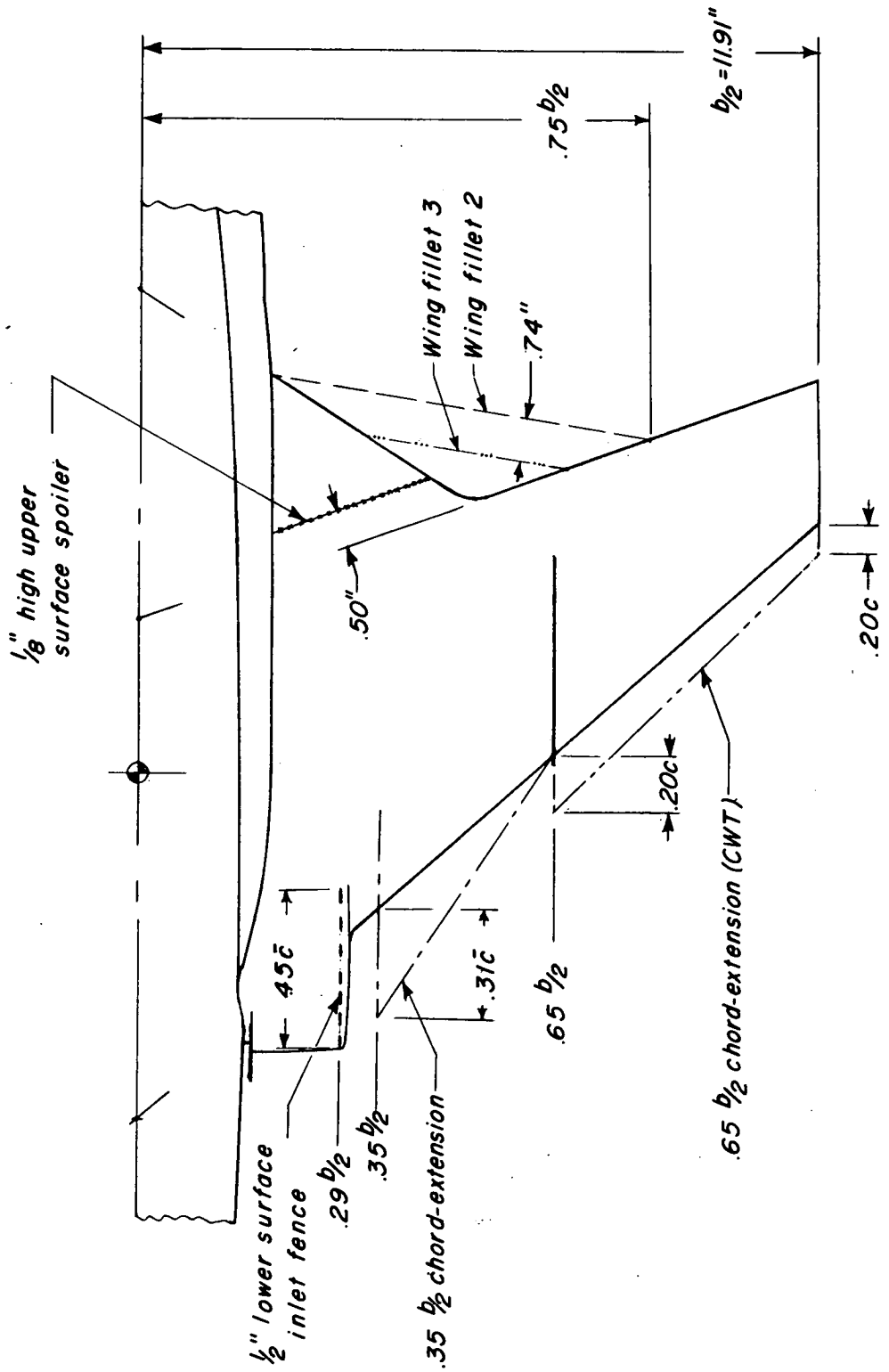

Figure 6.- Sketches of several wing modifications.

[redacted]

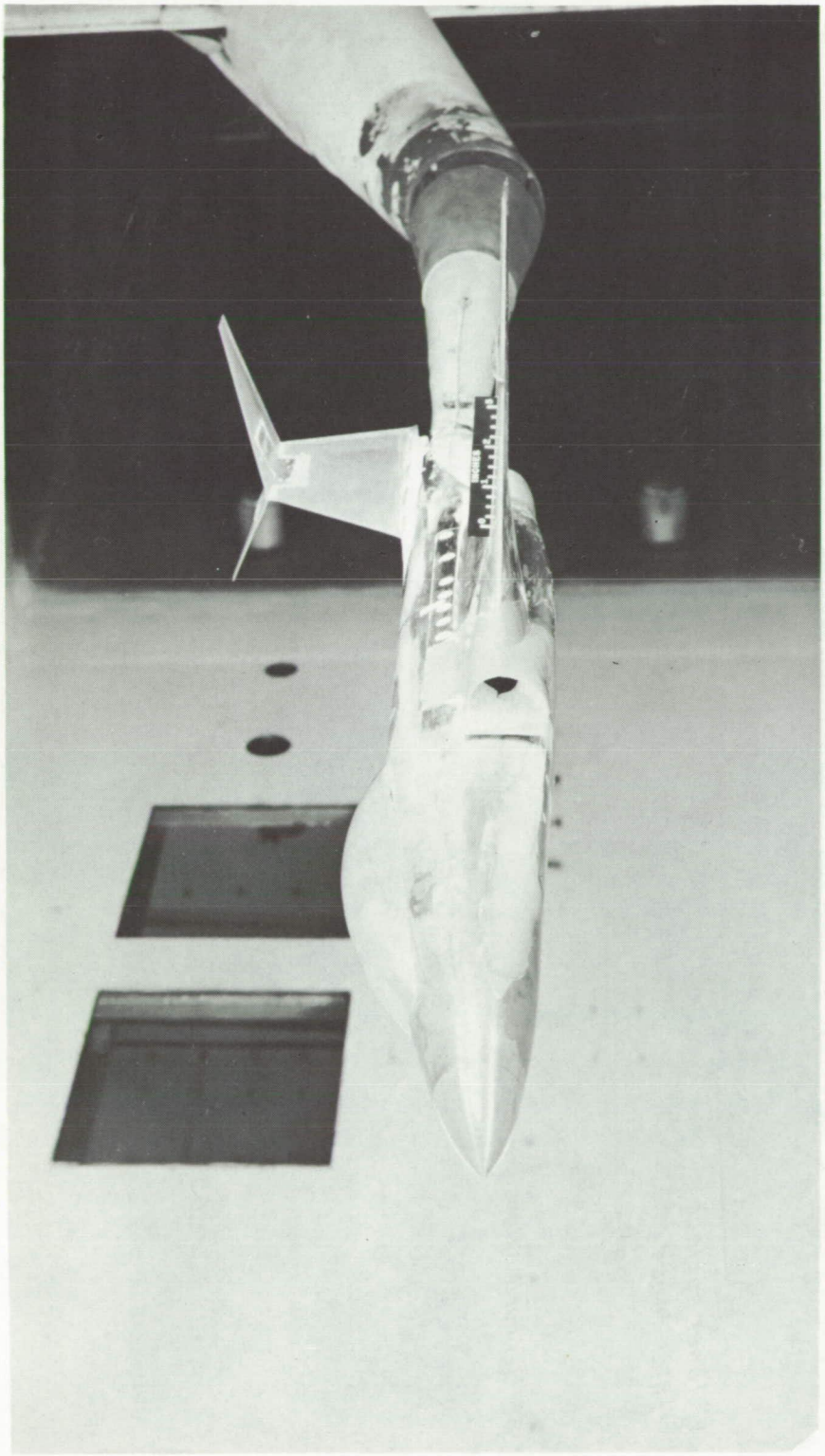

(a) Three-quarter front view. L-94994

Figure 7.- Photographs of the model with the new vertical- and horizontal-tail assembly. WFV_1H_1. Duct inlet 1.

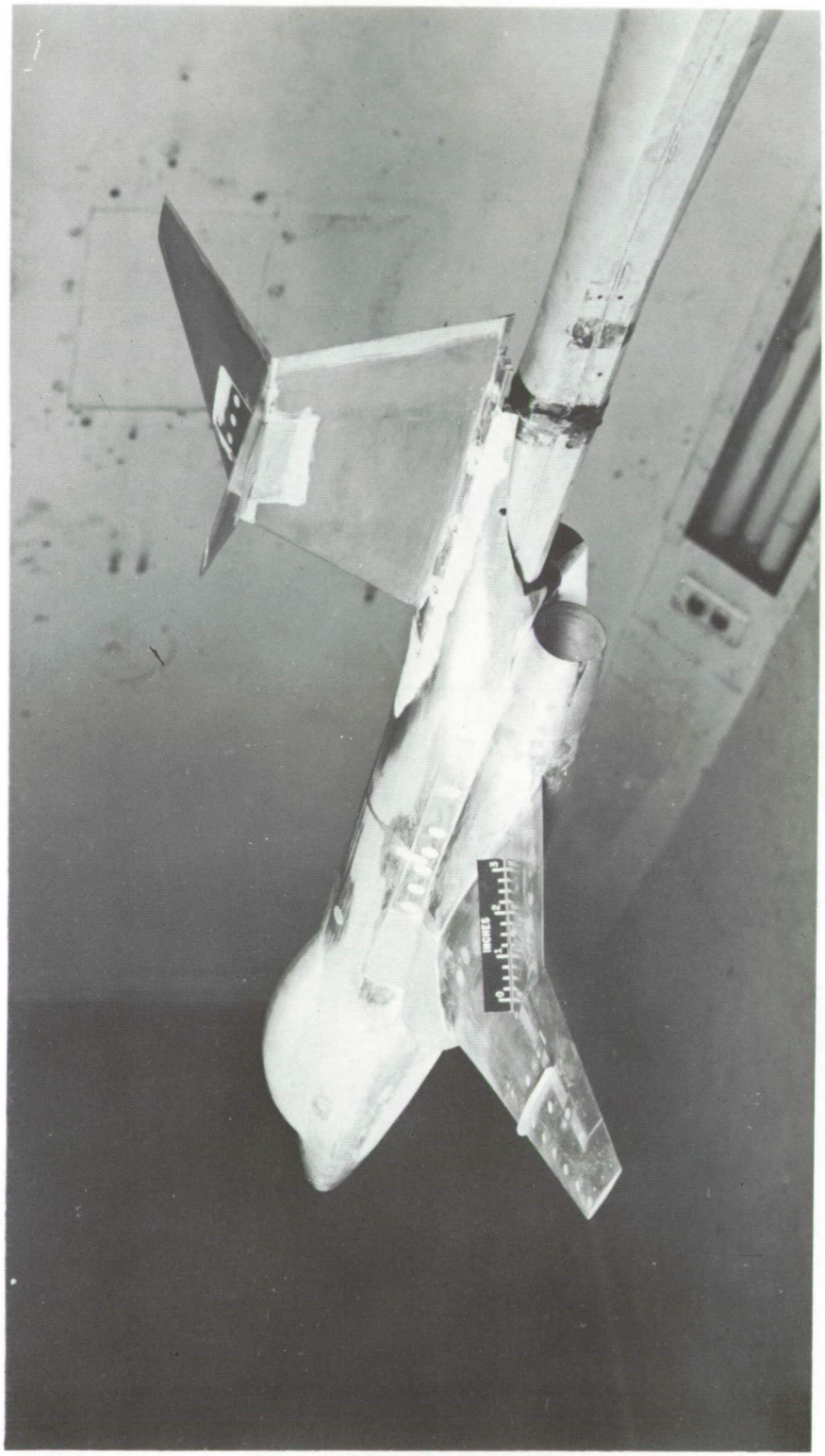

L-94995

(b) Three-quarter rear view.

Figure 7.- Concluded.

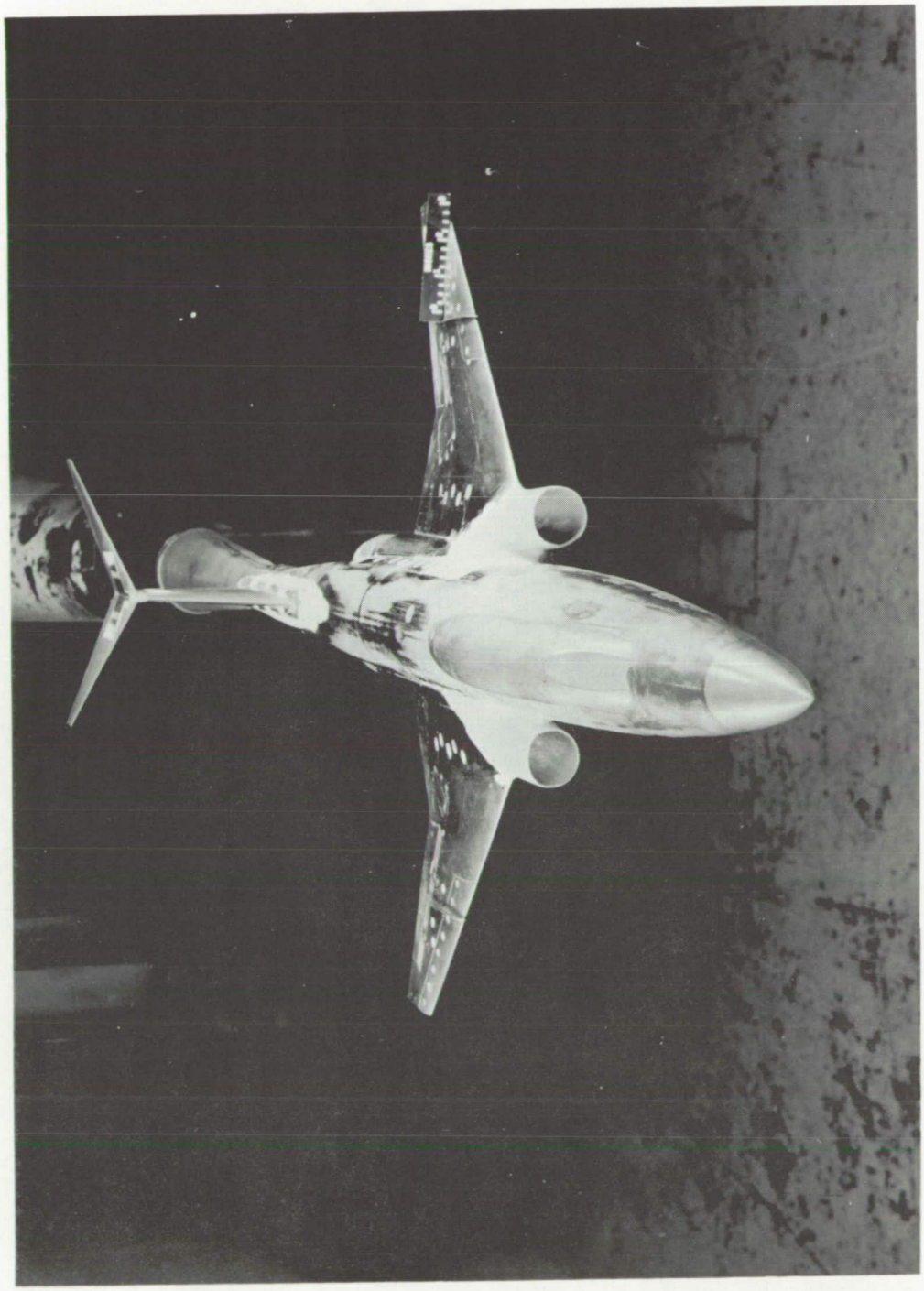

L-95012

Figure 8.- Photograph showing three-quarter view of the model with the new vertical-horizontal tail assembly. WFV_1H_1. Duct inlet 2.

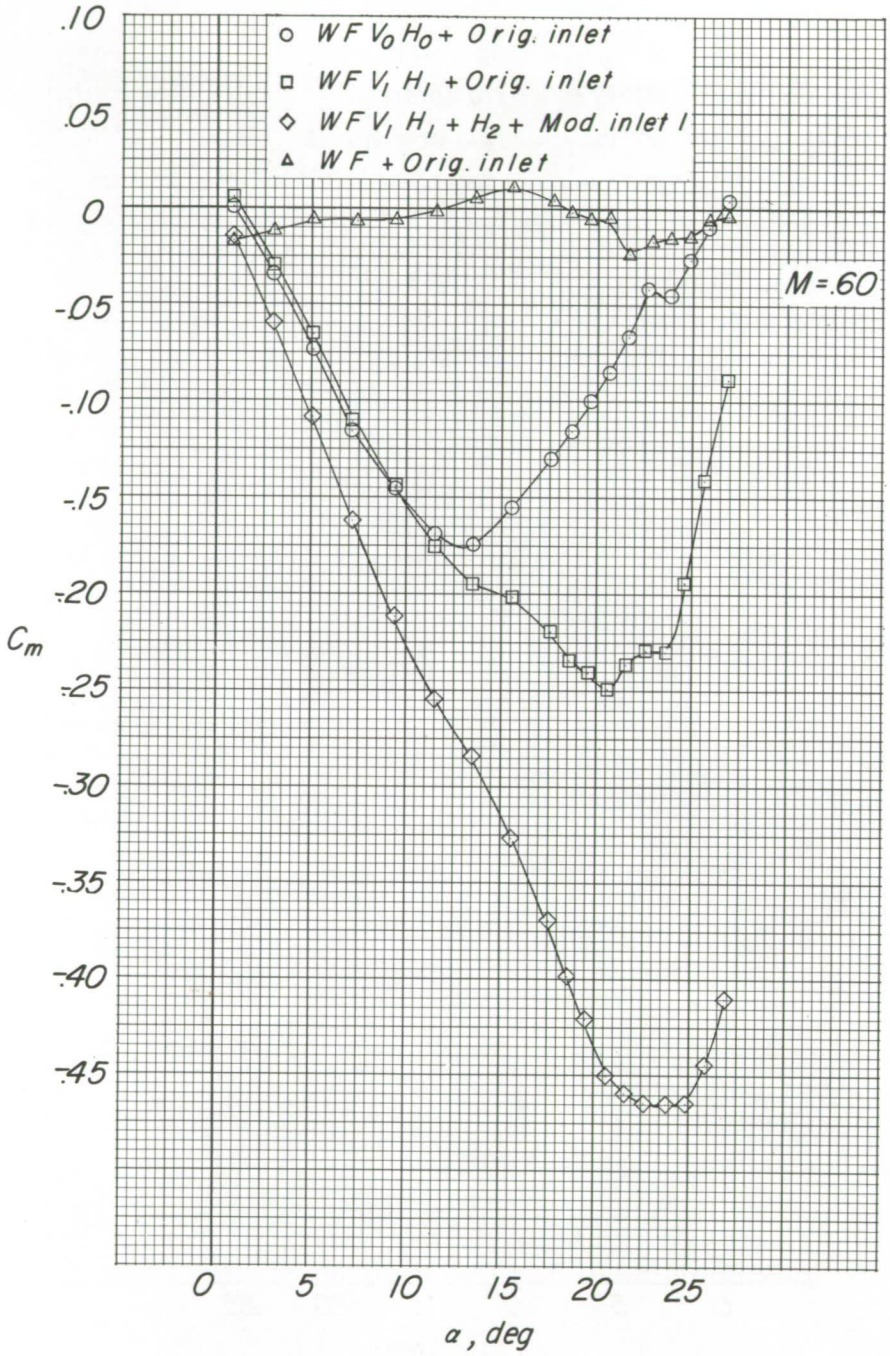

(a) C_m against α.

Figure 9.- Effect of several tail configurations on the longitudinal aerodynamic characteristics of the model. $i_t = 0^o$.

(a) Continued.

Figure 9.- Continued.

(a) Continued.

Figure 9.- Continued.

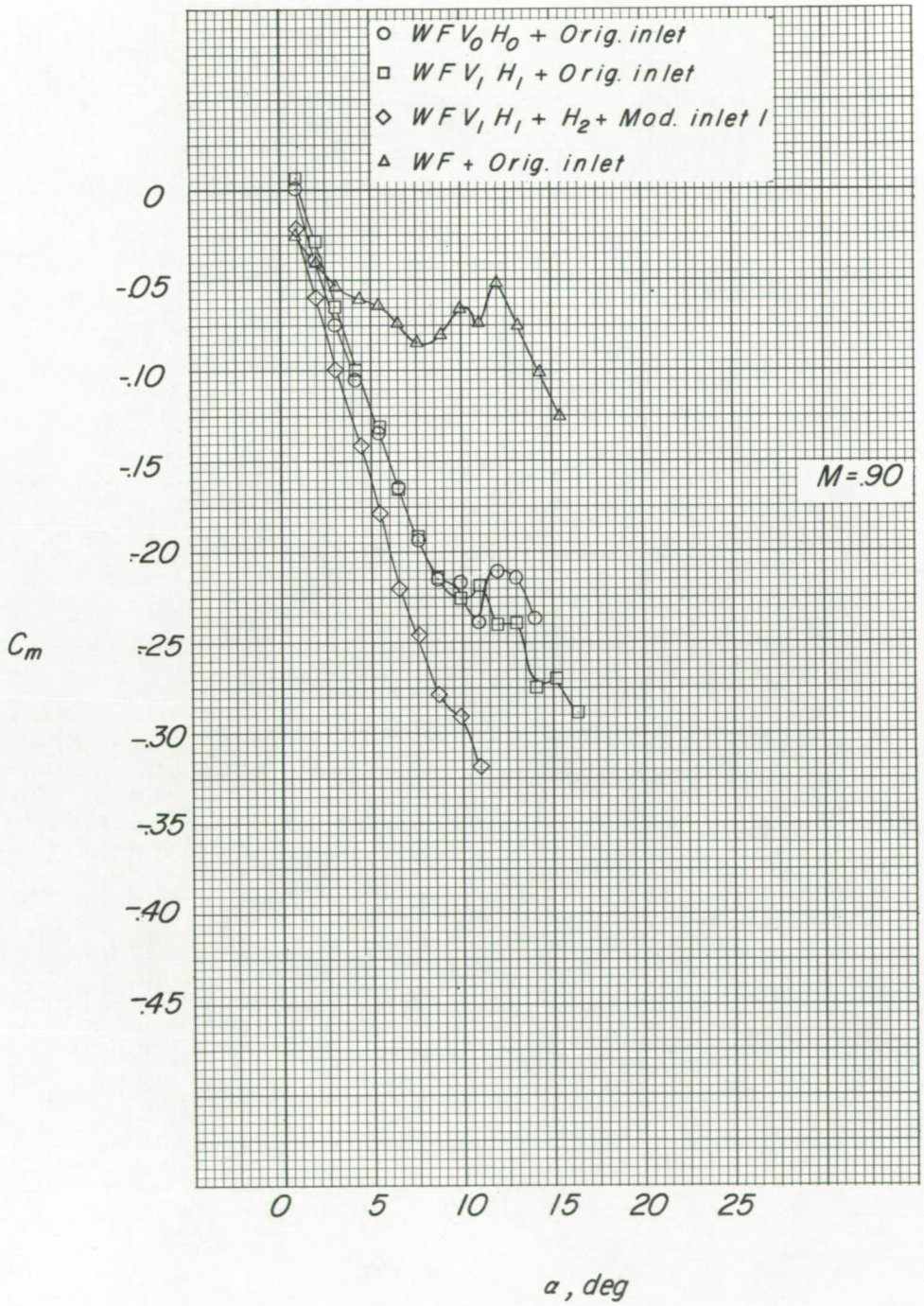

(a) Continued.

Figure 9.- Continued.

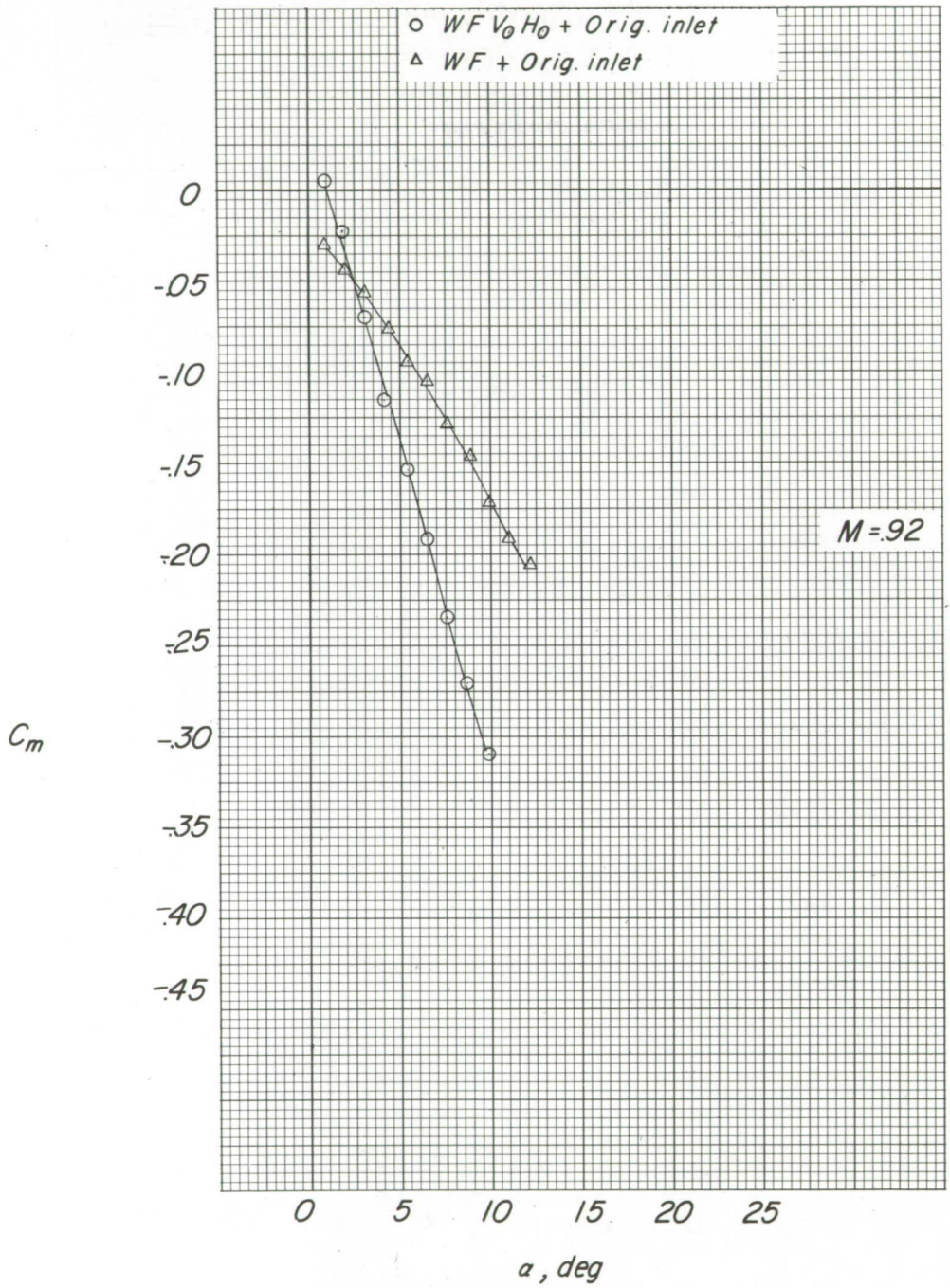

(a) Concluded.

Figure 9.- Continued.

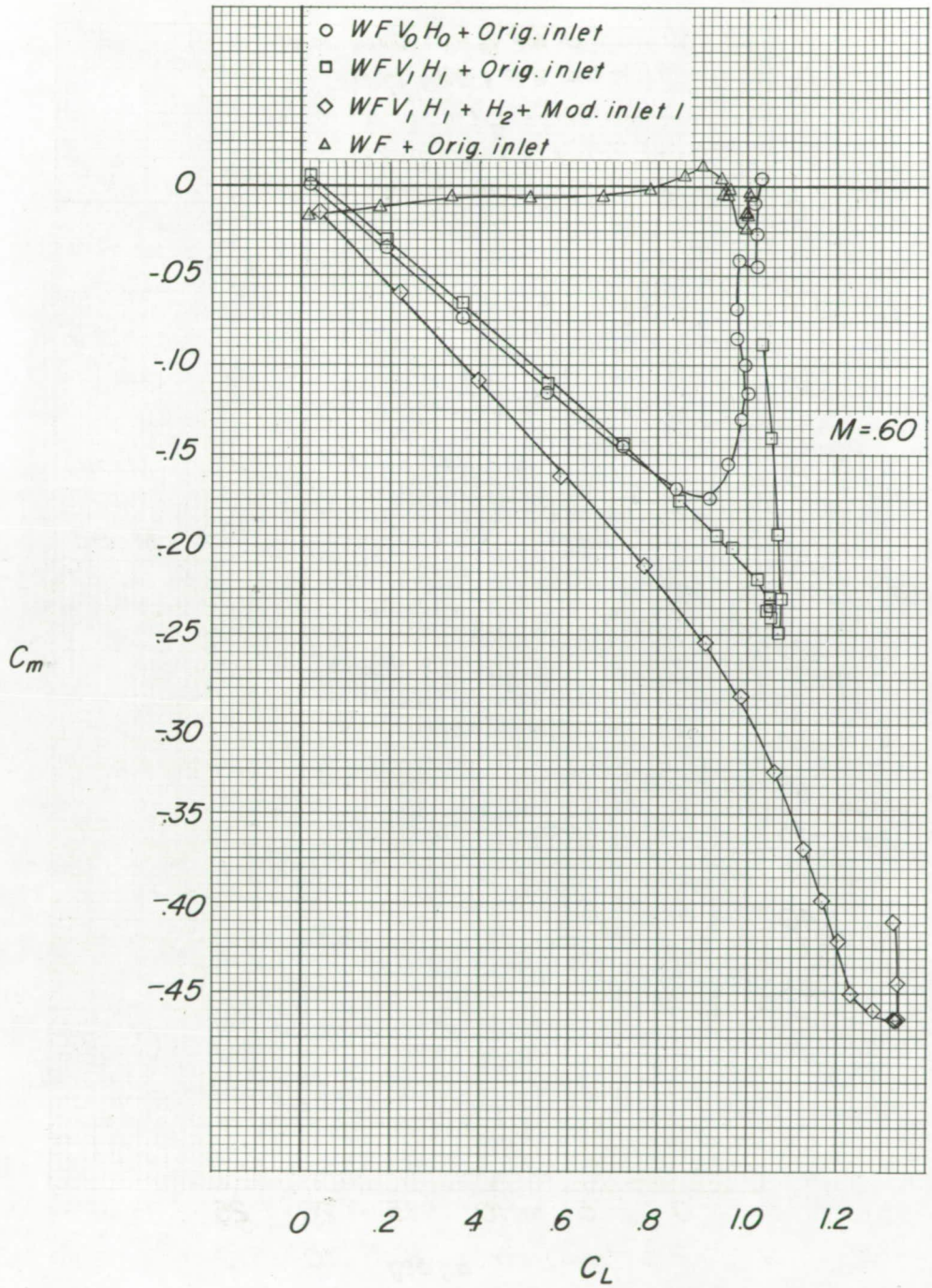

(b) C_m against C_L.

Figure 9.- Continued.

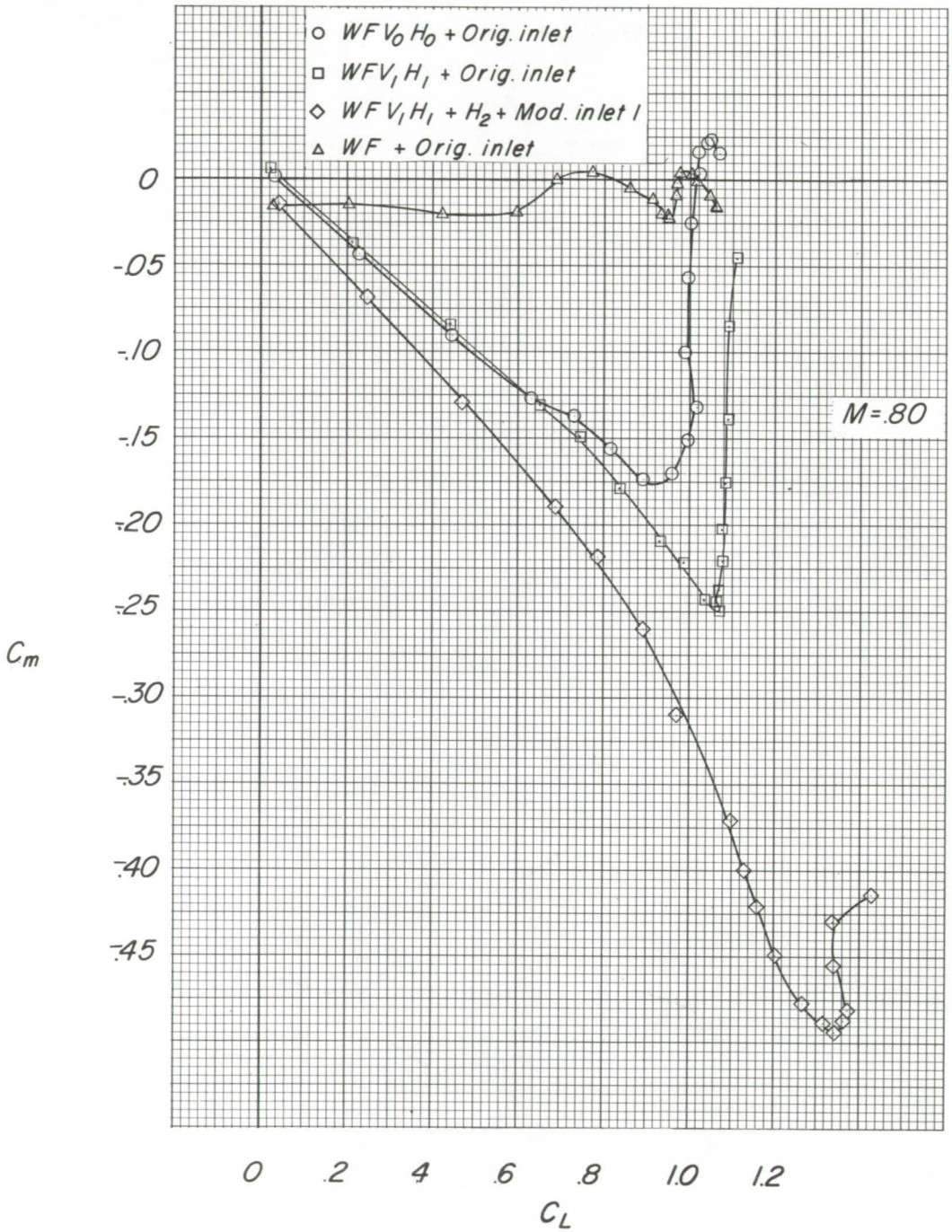

(b) Continued.

Figure 9.- Continued.

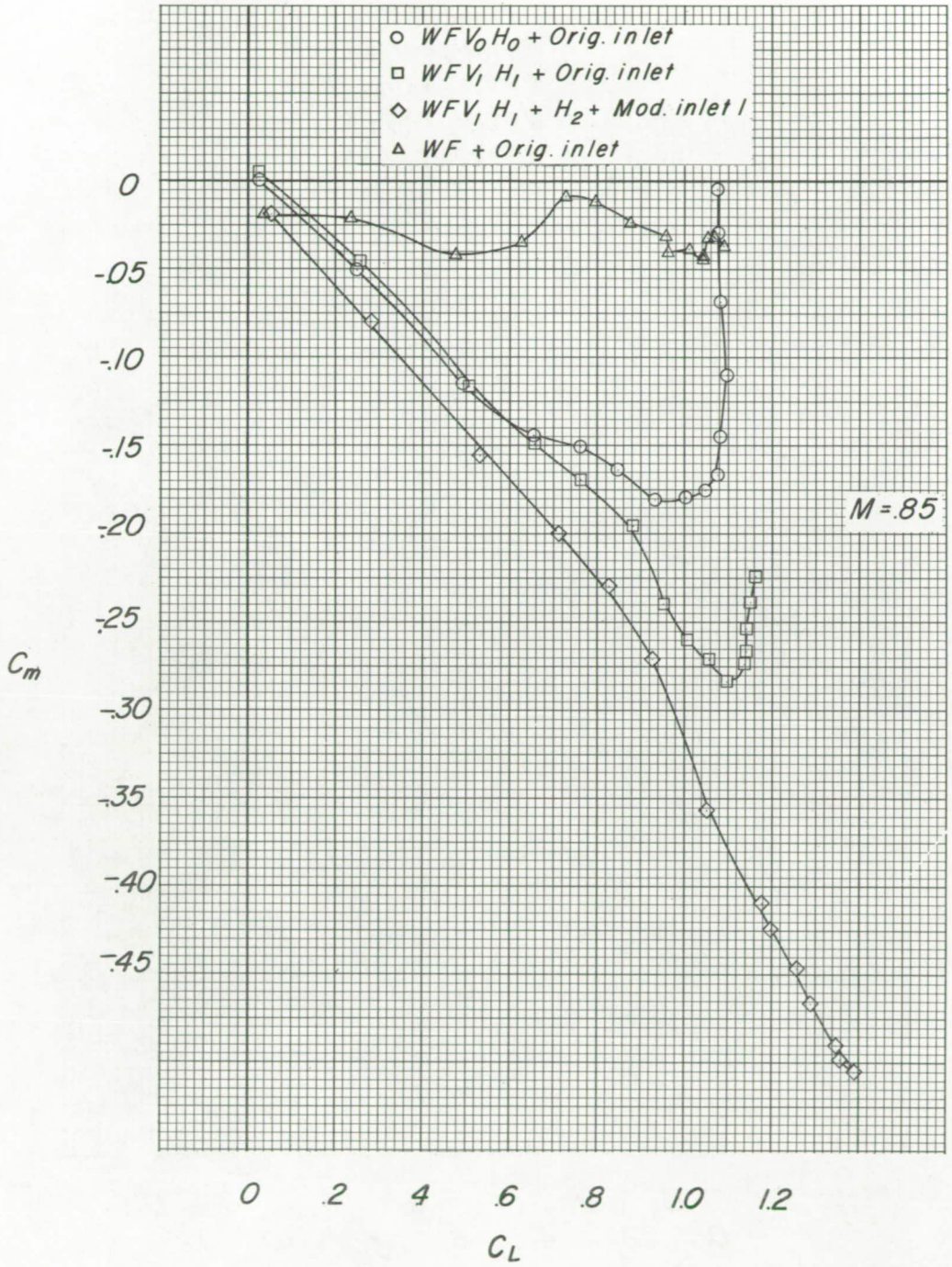

(b) Continued.

Figure 9.- Continued.

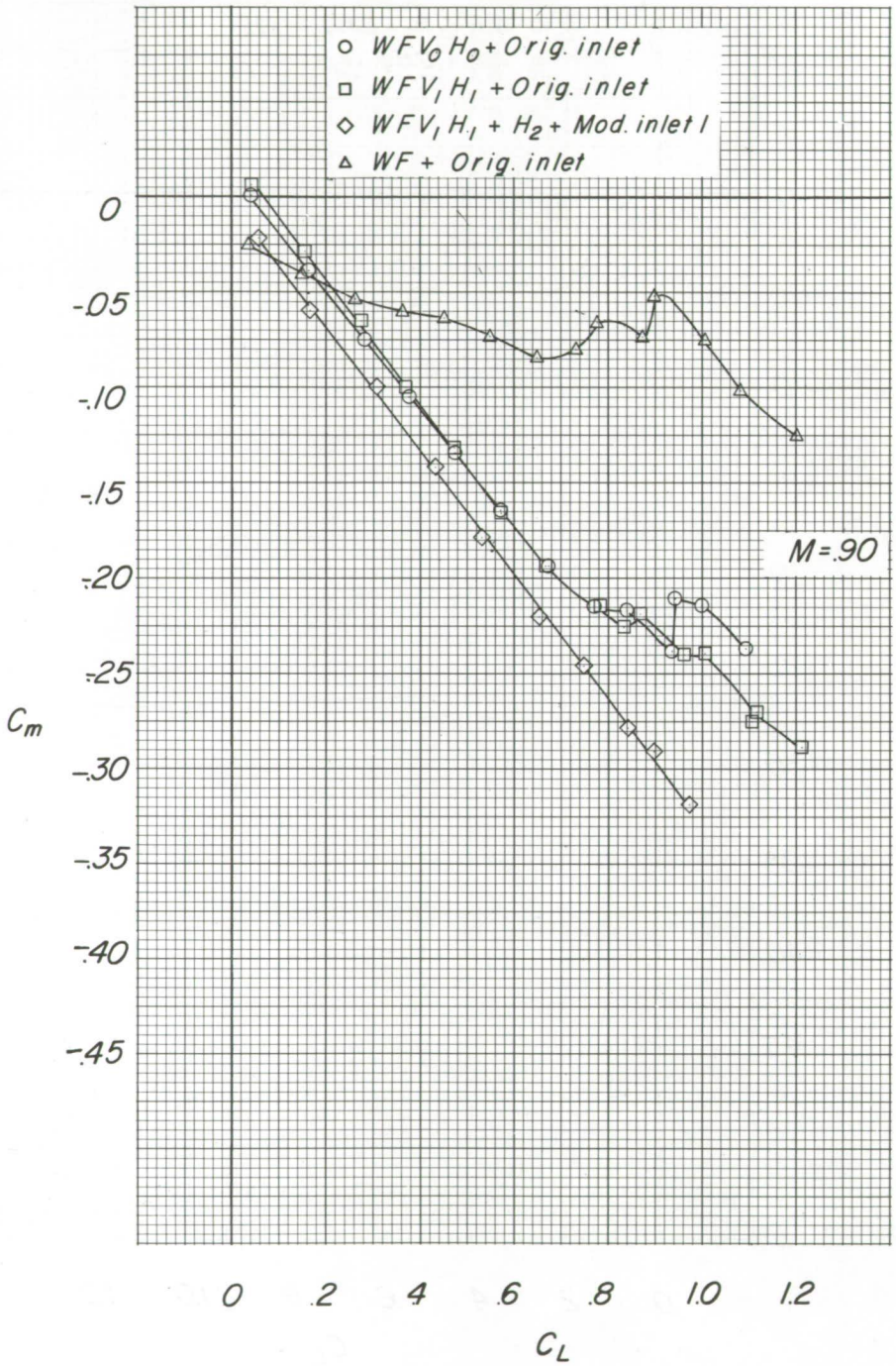

(b) Continued.

Figure 9.- Continued.

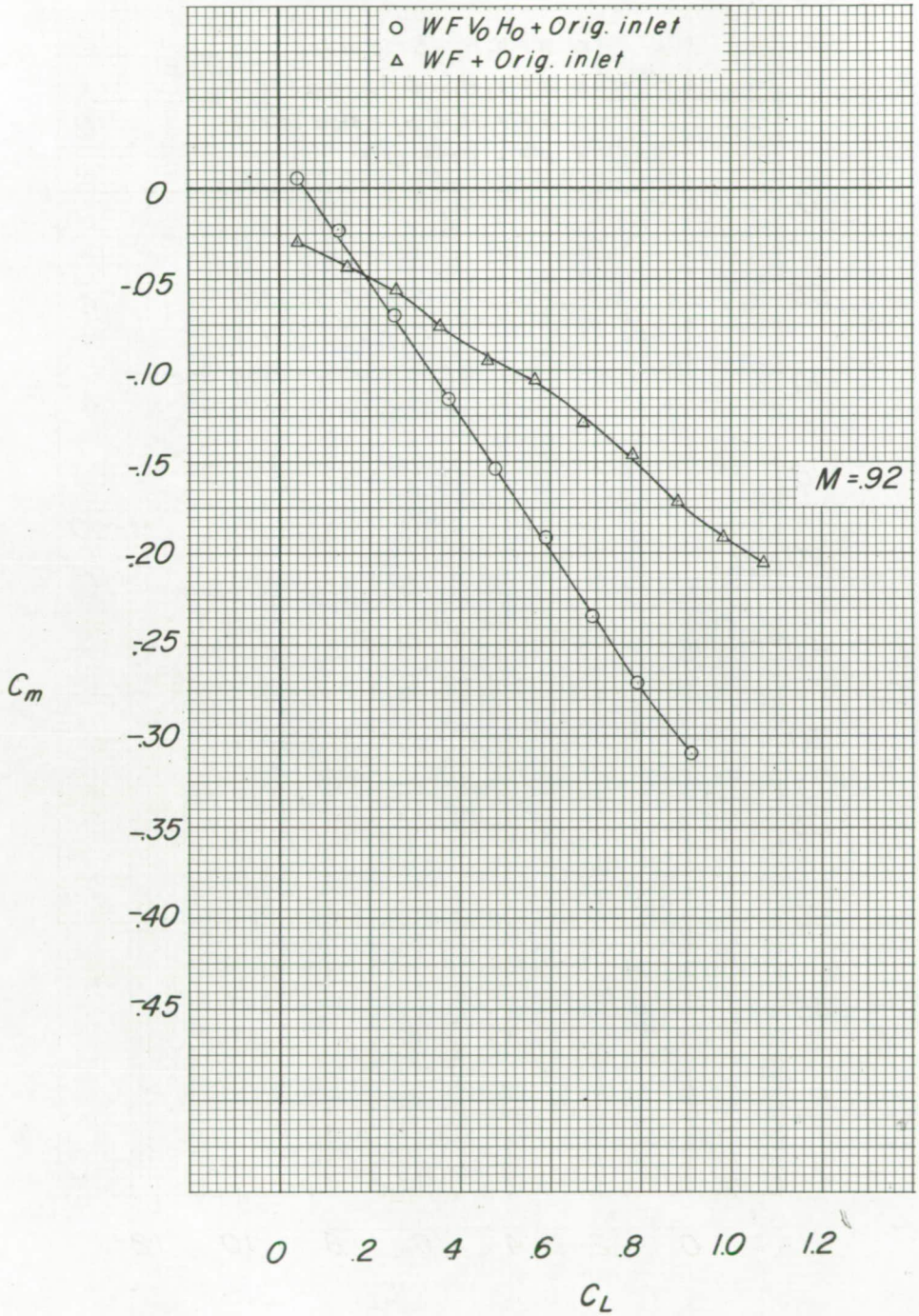

(b) Concluded.

Figure 9.- Continued.

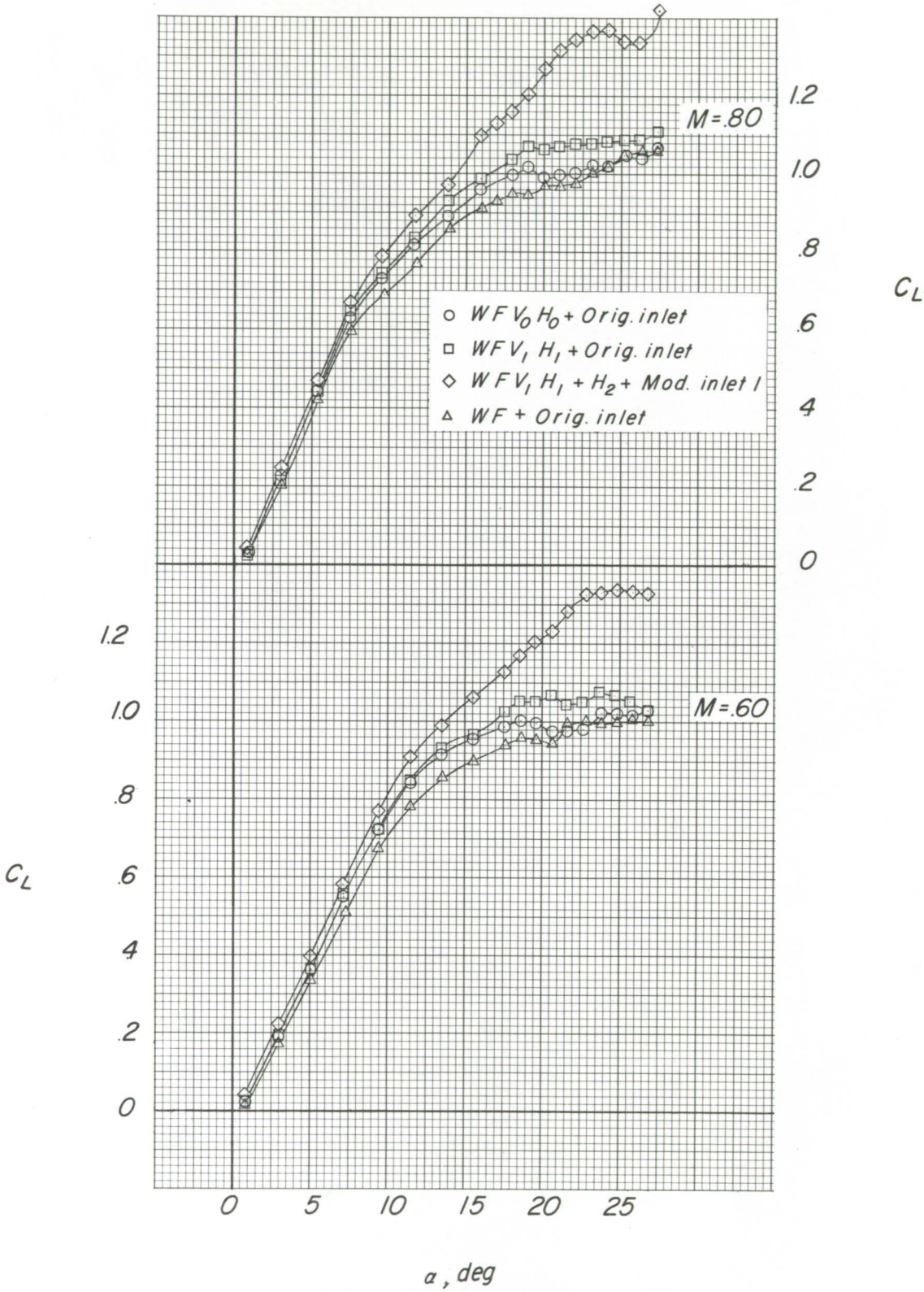

(c) C_L against α.

Figure 9.- Continued.

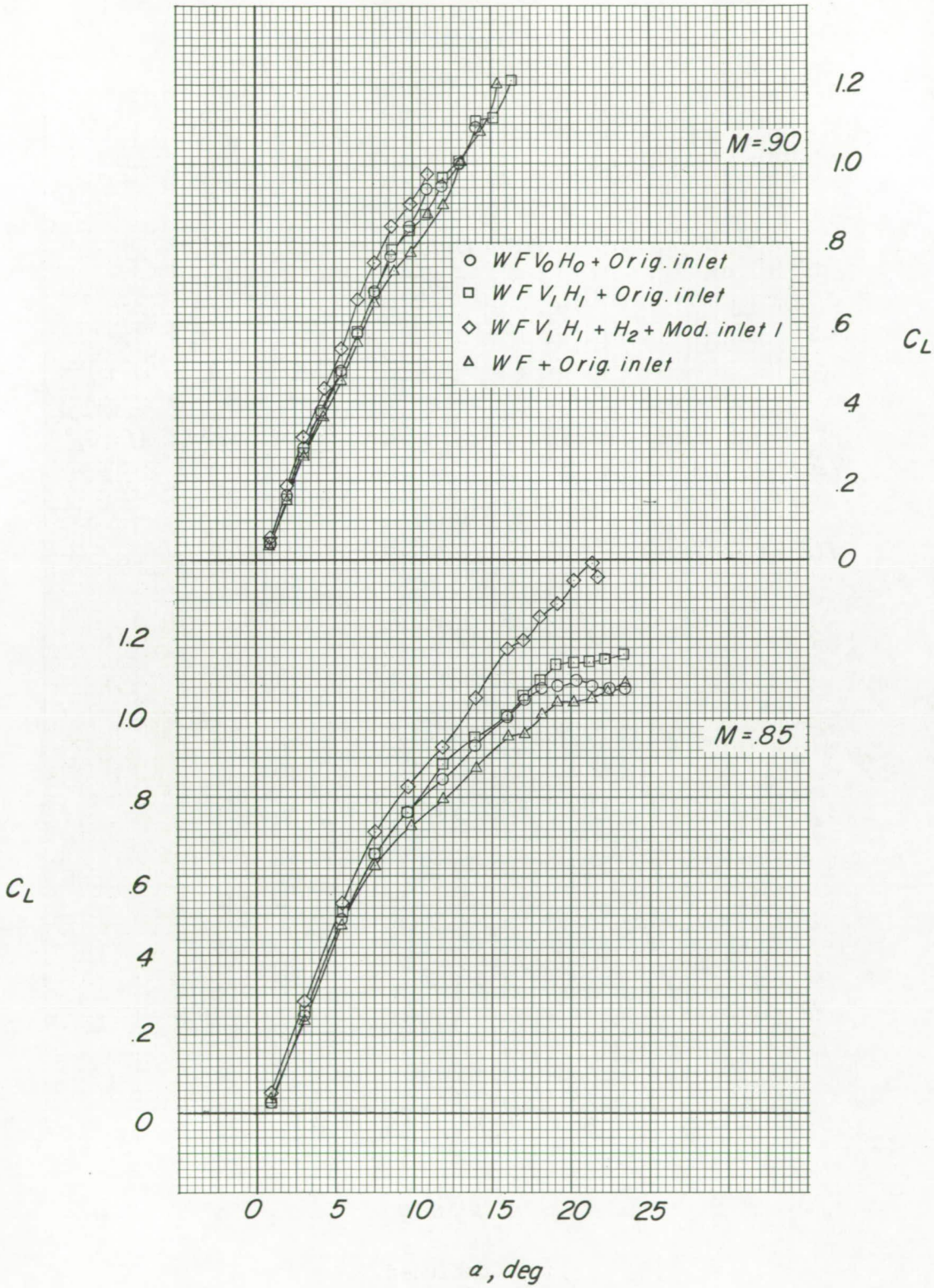

(c) Continued.

Figure 9.- Continued.

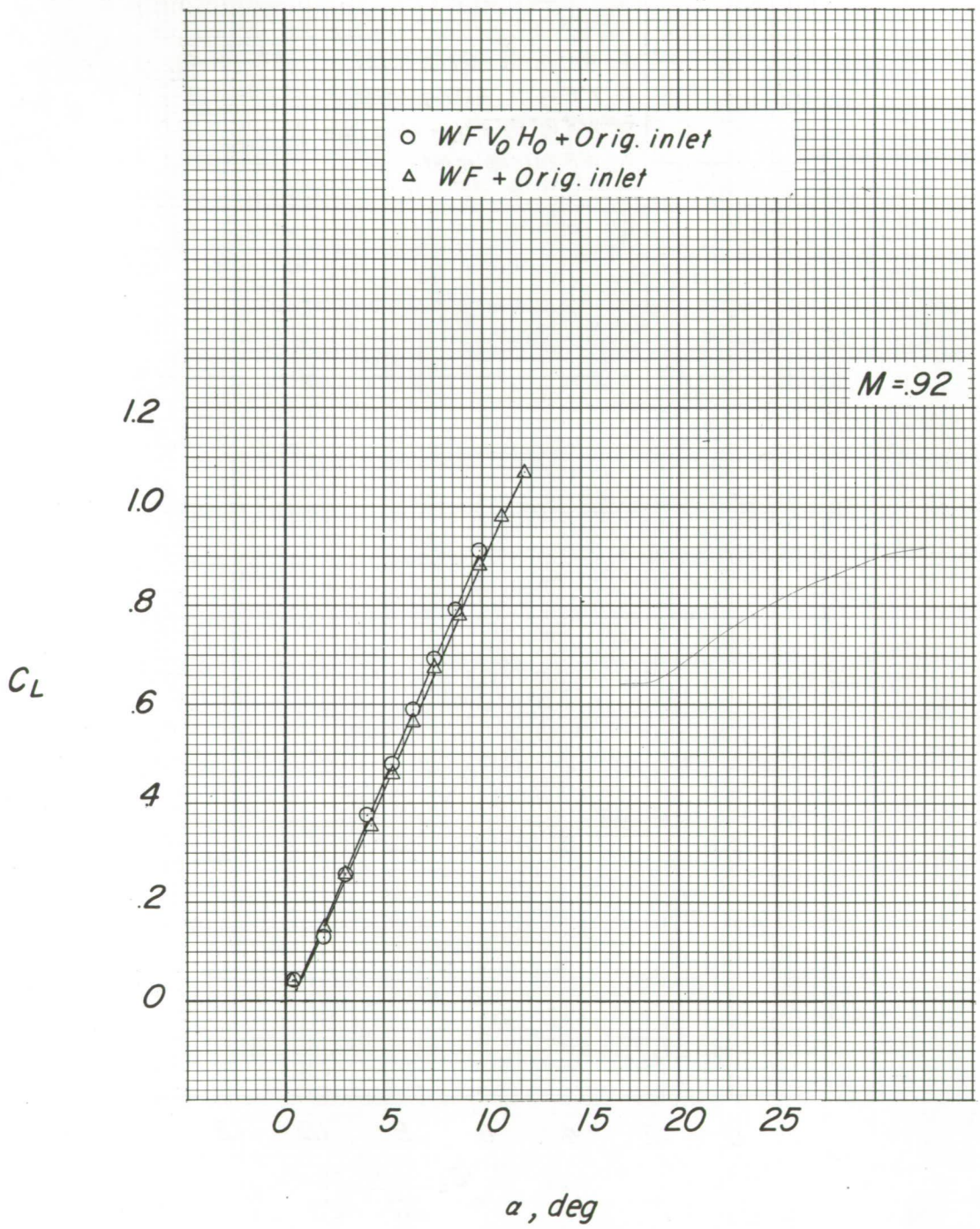

(c) Concluded.

Figure 9.- Continued.

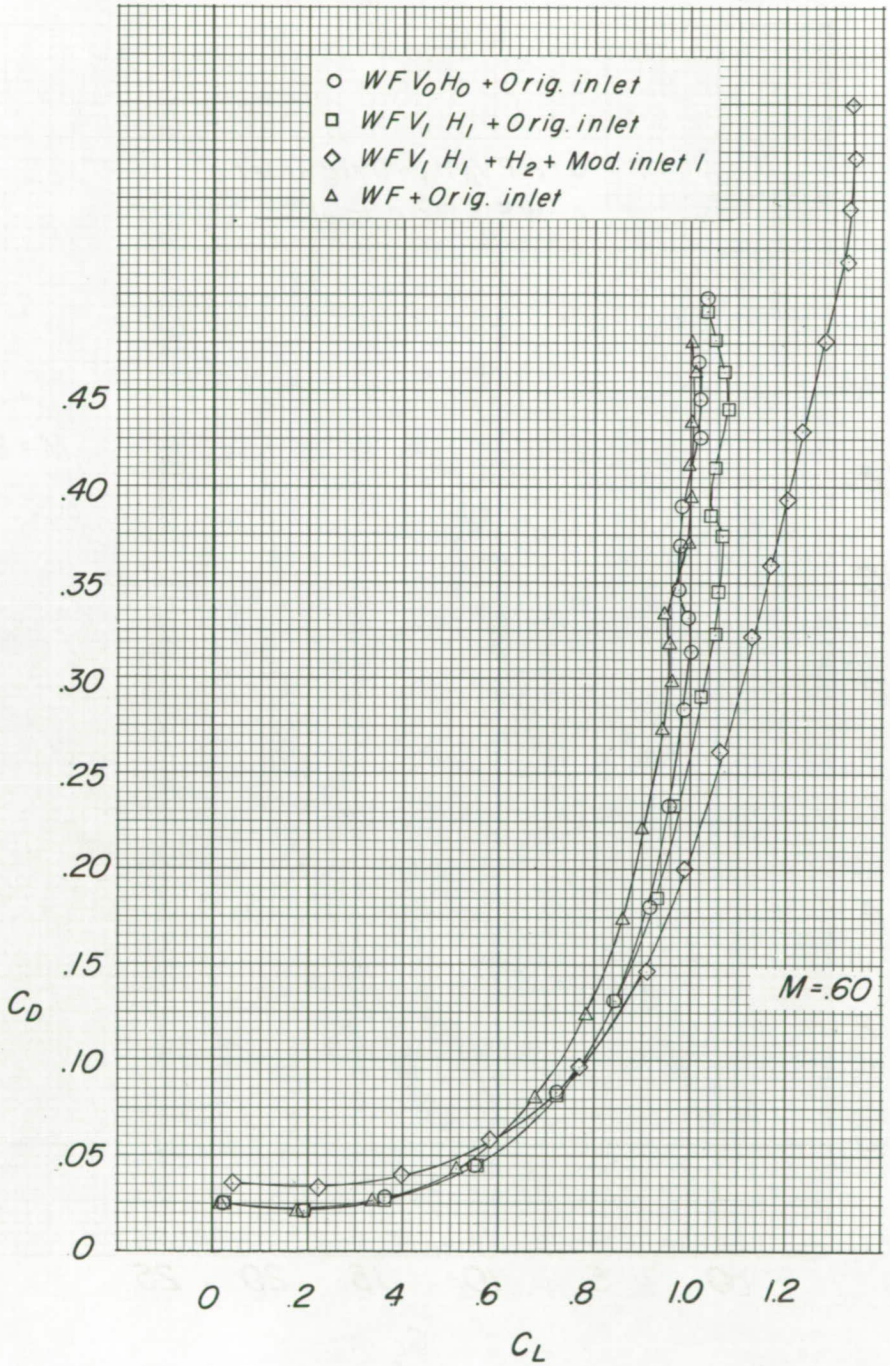

(d) C_D against C_L.

Figure 9.- Continued.

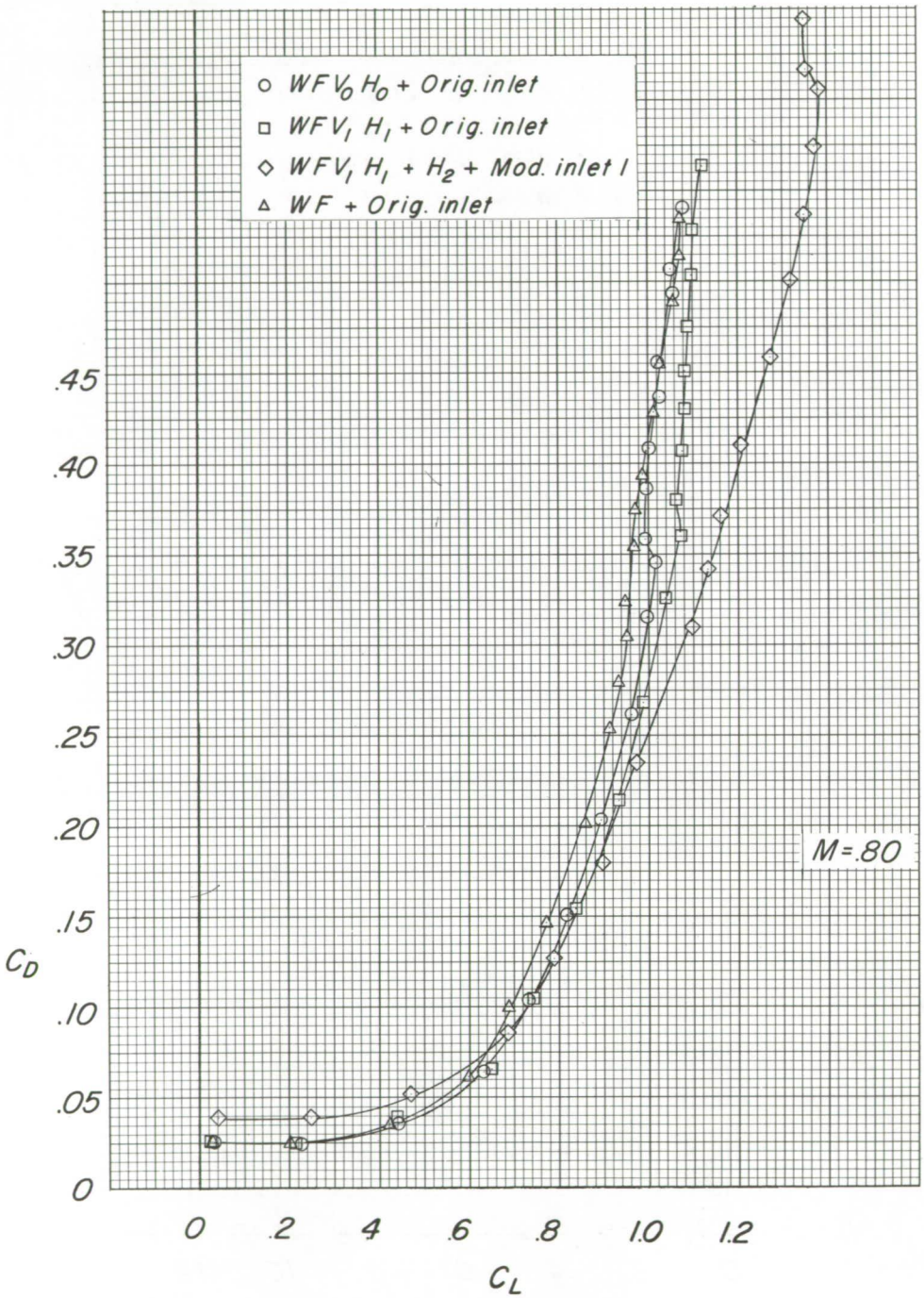

(d) Continued.

Figure 9.- Continued.

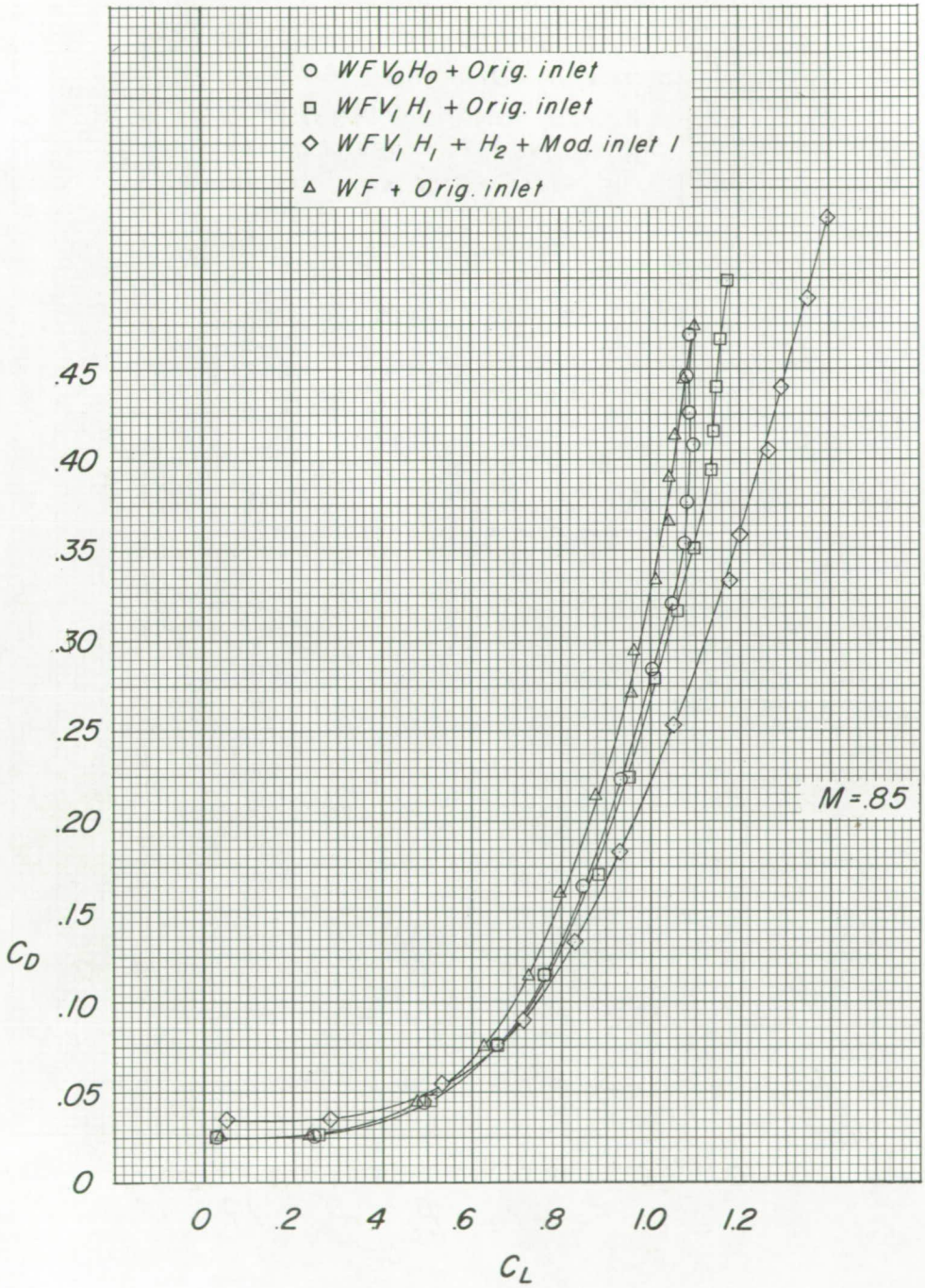

(d) Continued.

Figure 9.- Continued.

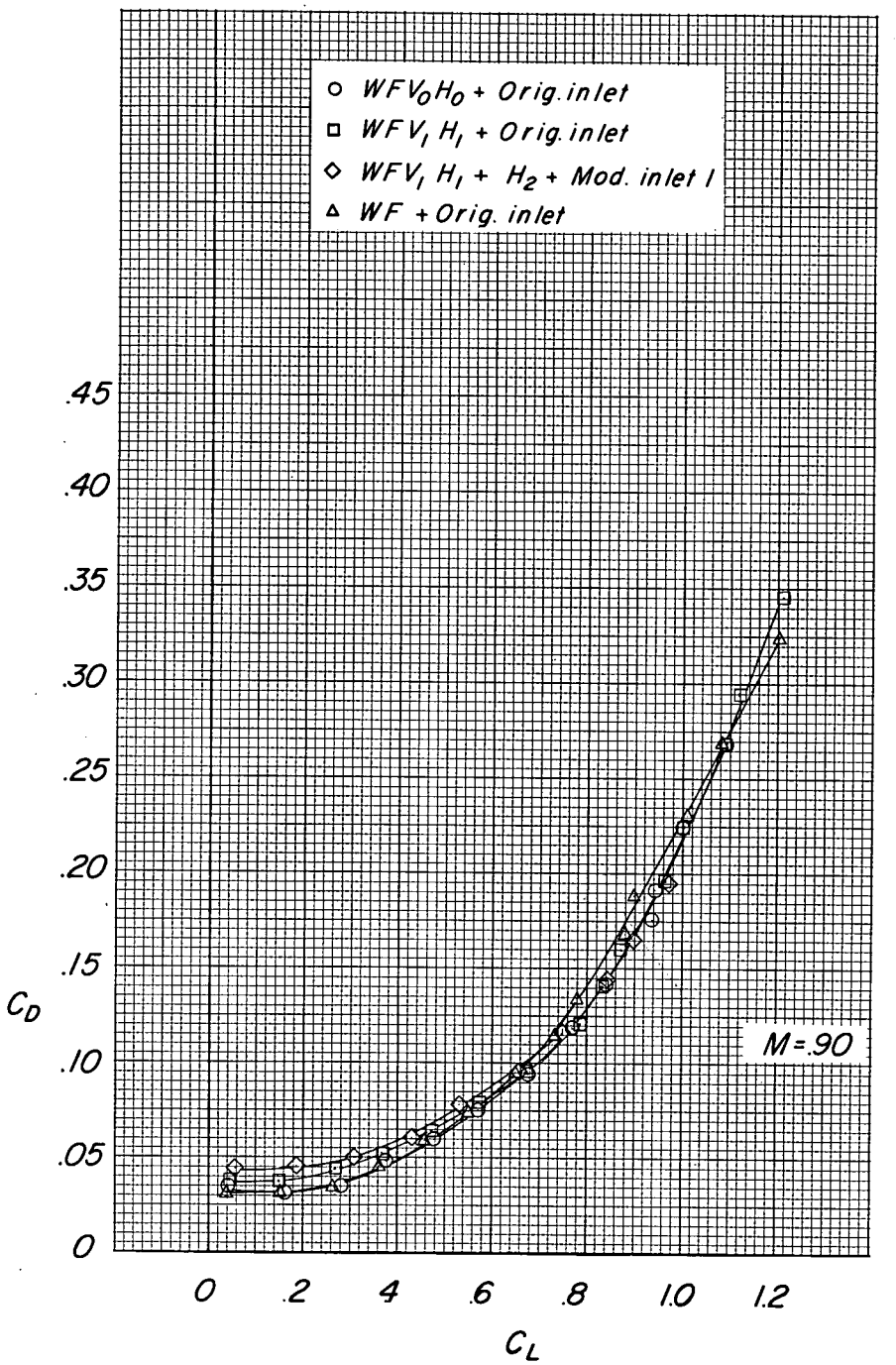

(d) Continued.

Figure 9.- Continued.

[redacted]

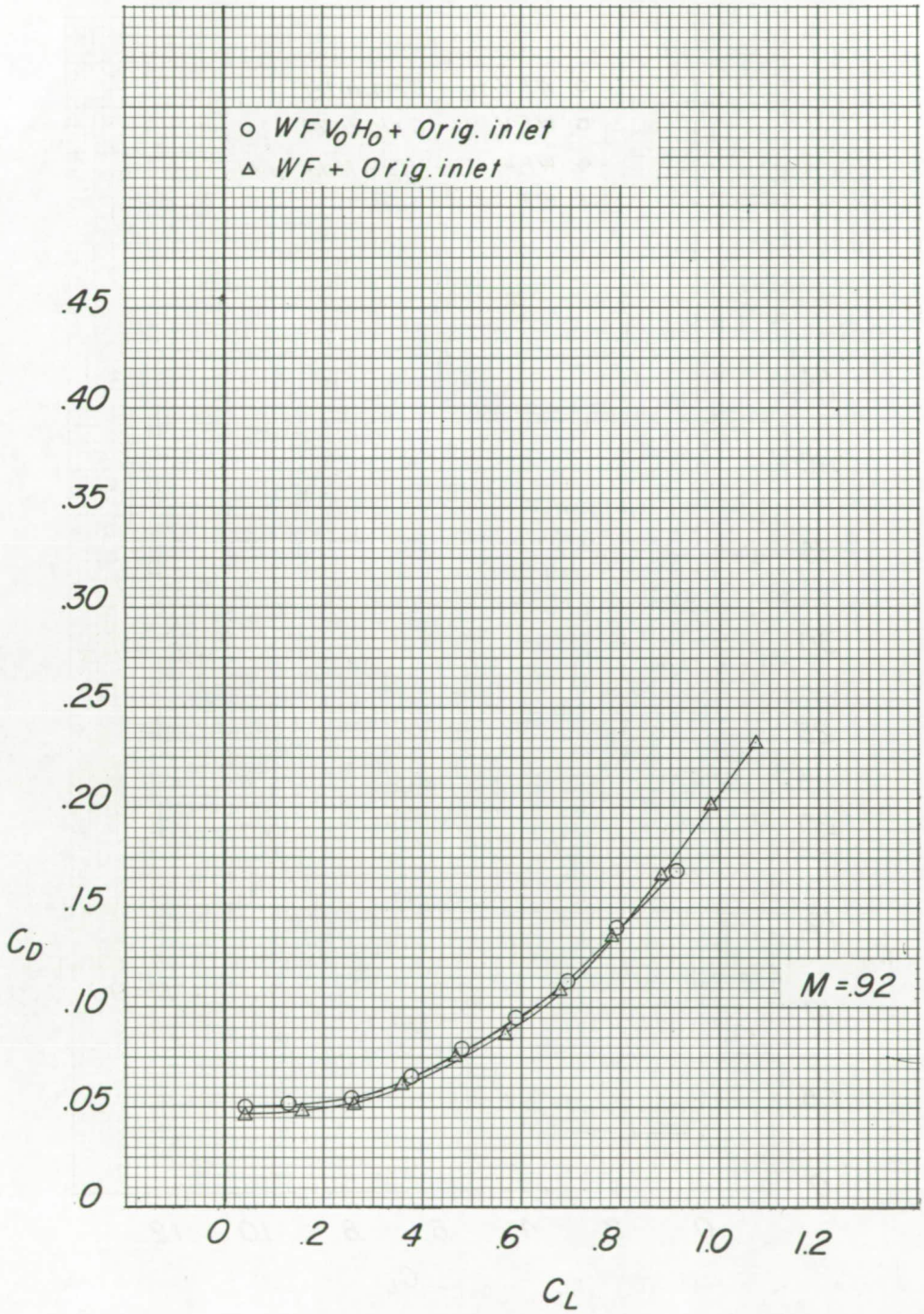

(d) Concluded.

Figure 9.- Concluded.

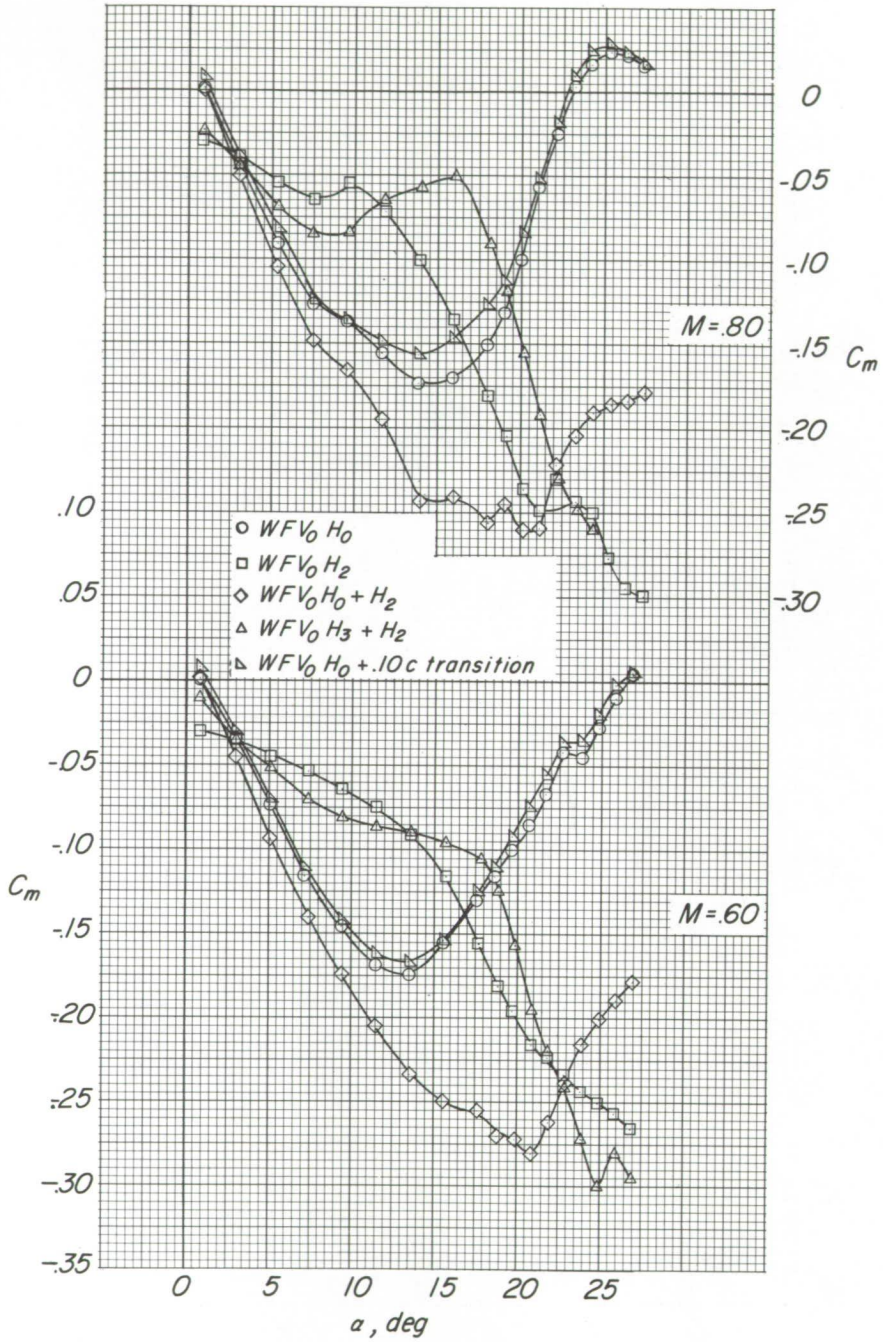

(a) C_m against α.

Figure 10.- Effect of several tail configurations on the longitudinal aerodynamic characteristics of the model. $i_t = 0^o$.

DECLASSIFIED

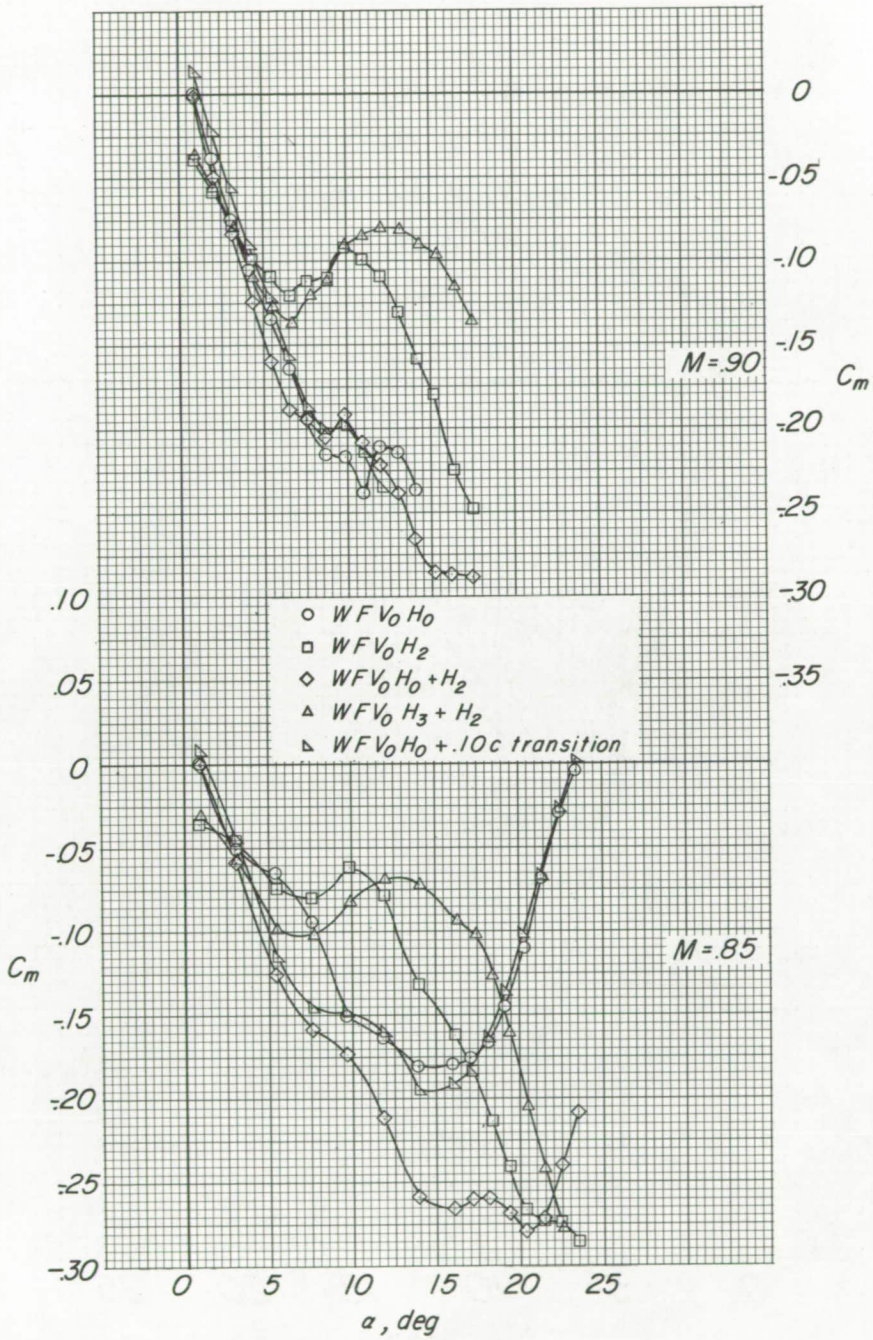

(a) Continued.

Figure 10.- Continued.

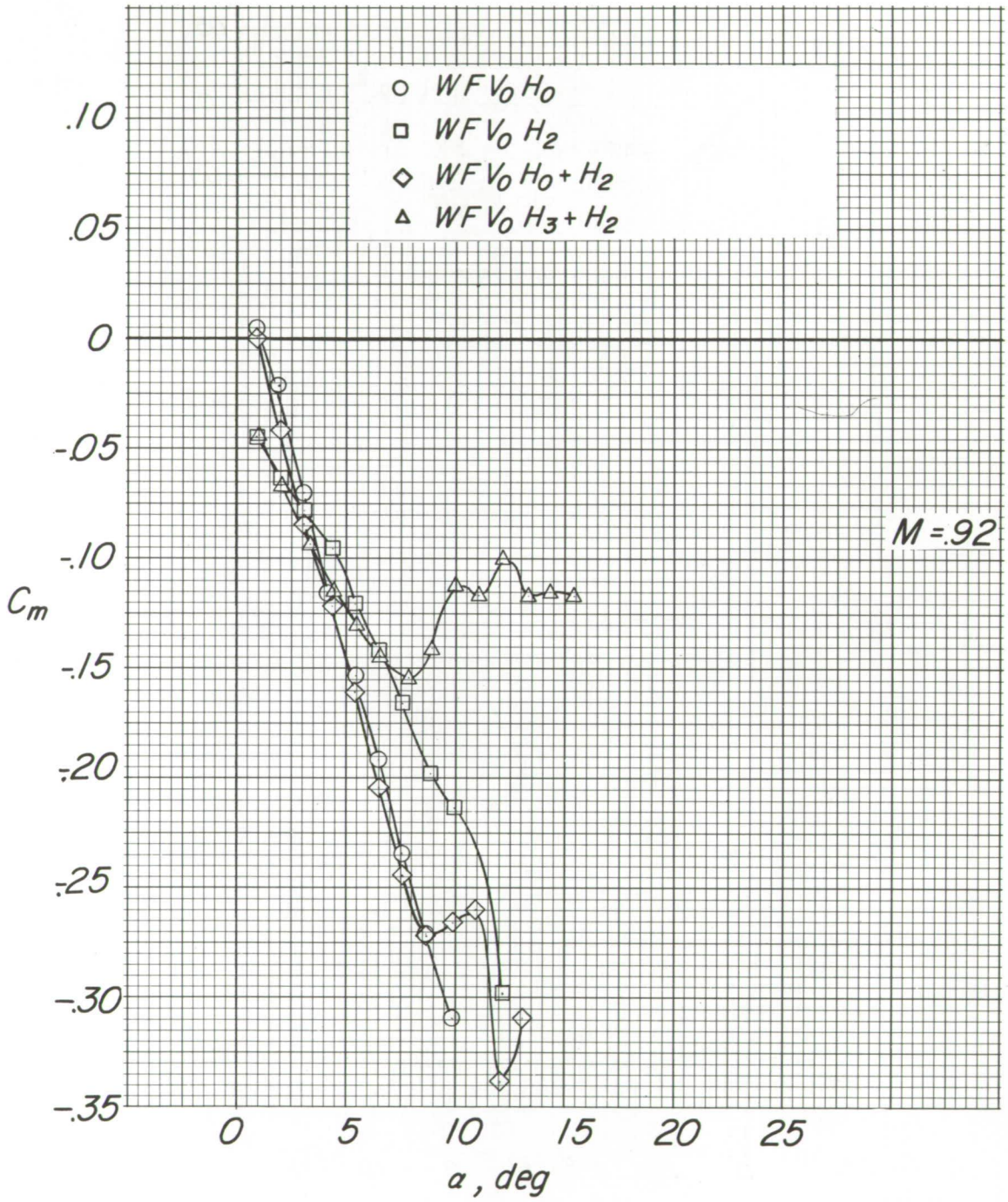

(a) Concluded.

Figure 10.- Continued.

DECLASSIFIED

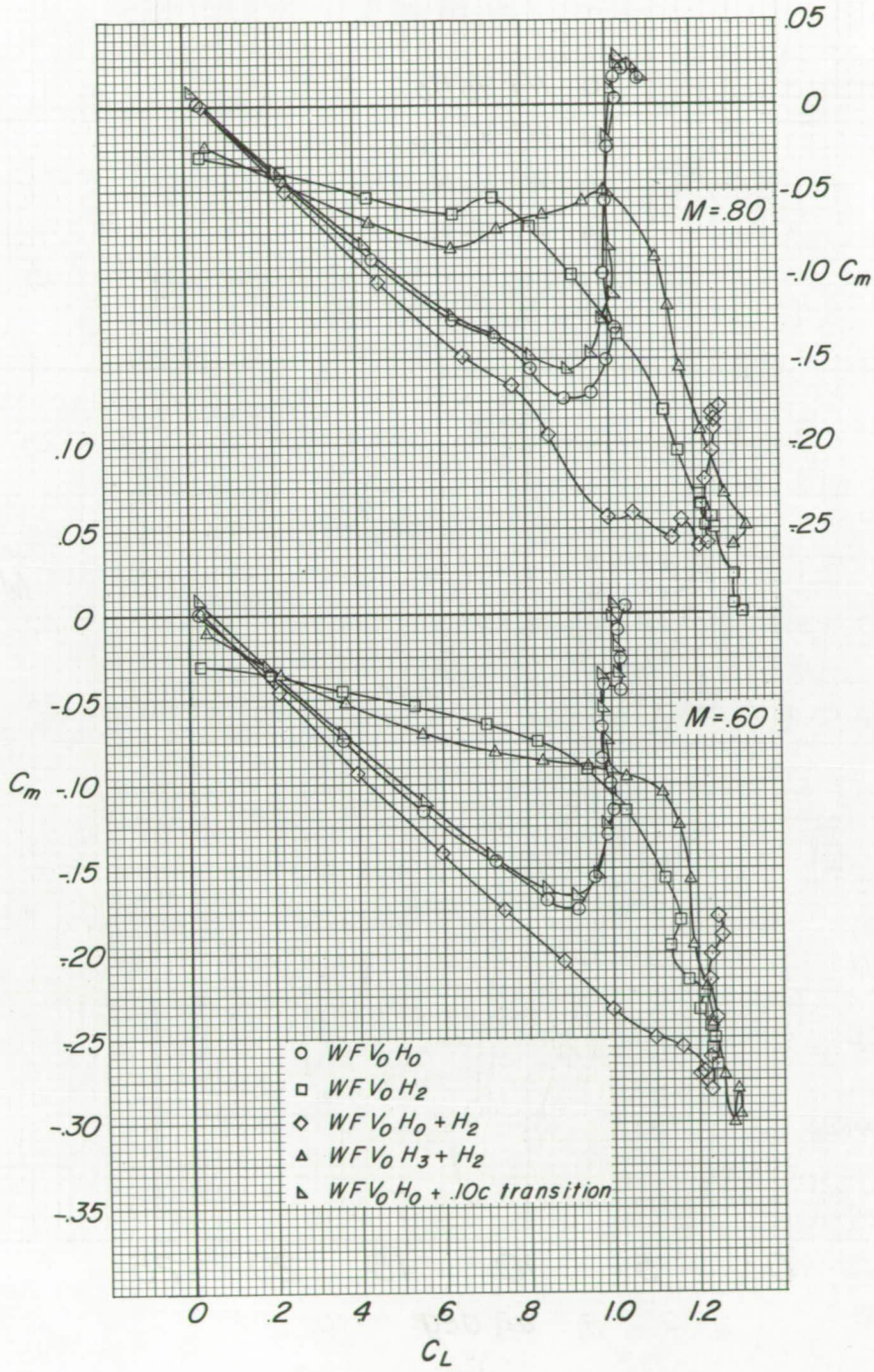

(b) C_m against C_L.

Figure 10.- Continued.

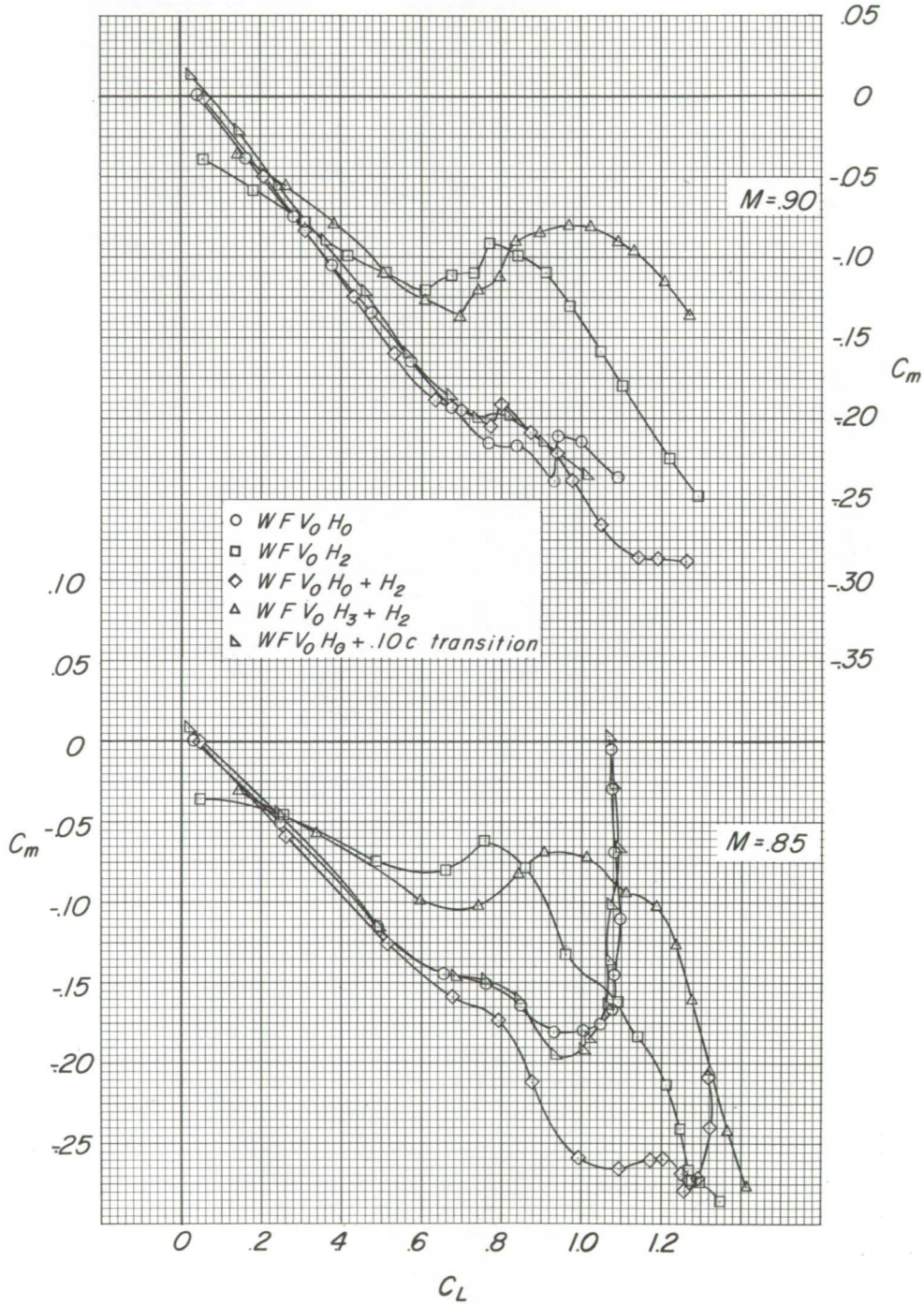

(b) Continued.

Figure 10.- Continued.

DECLASSIFIED

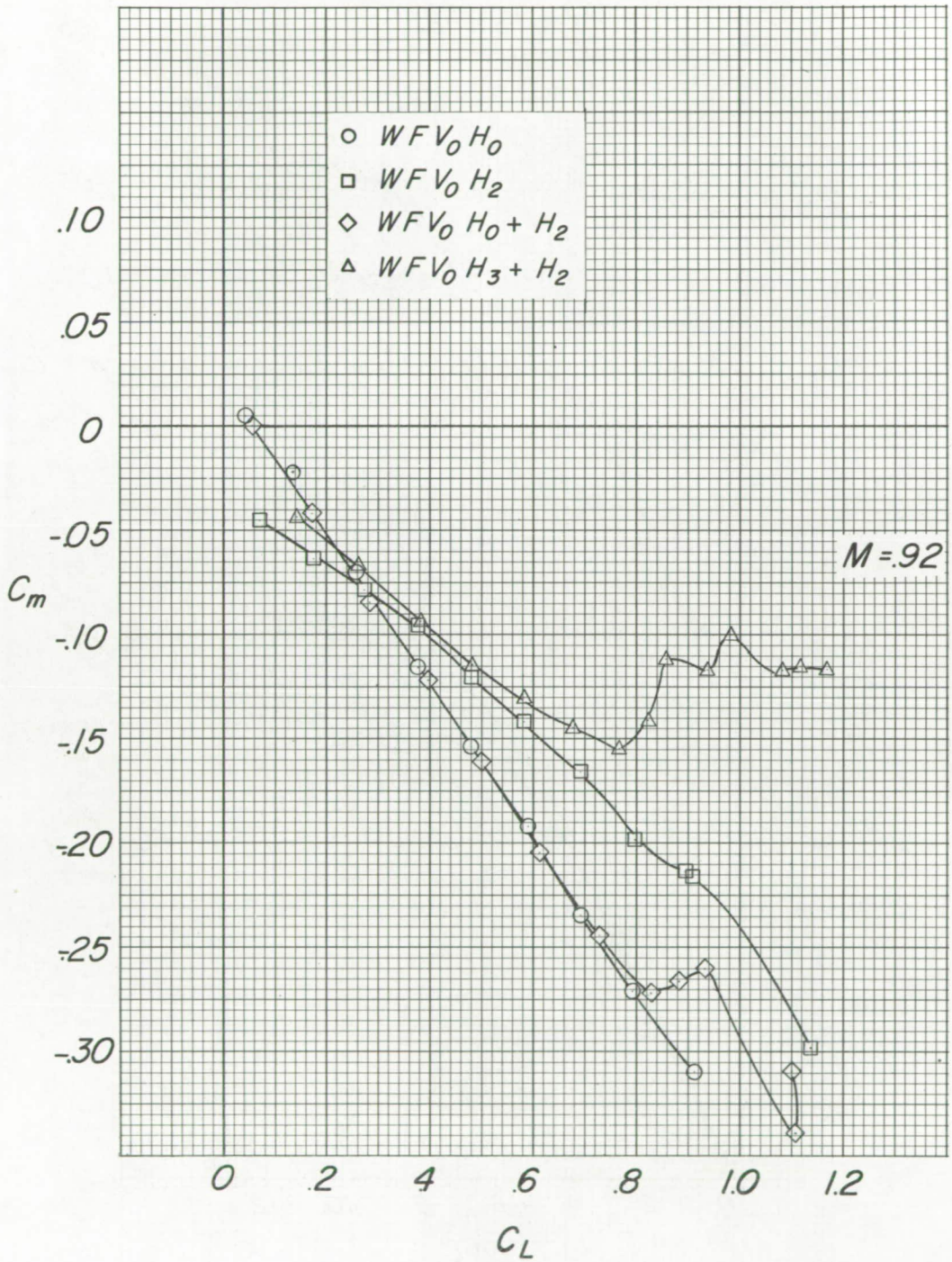

(b) Concluded.

Figure 10.- Continued.

(c) C_L against α.

Figure 10.- Continued.

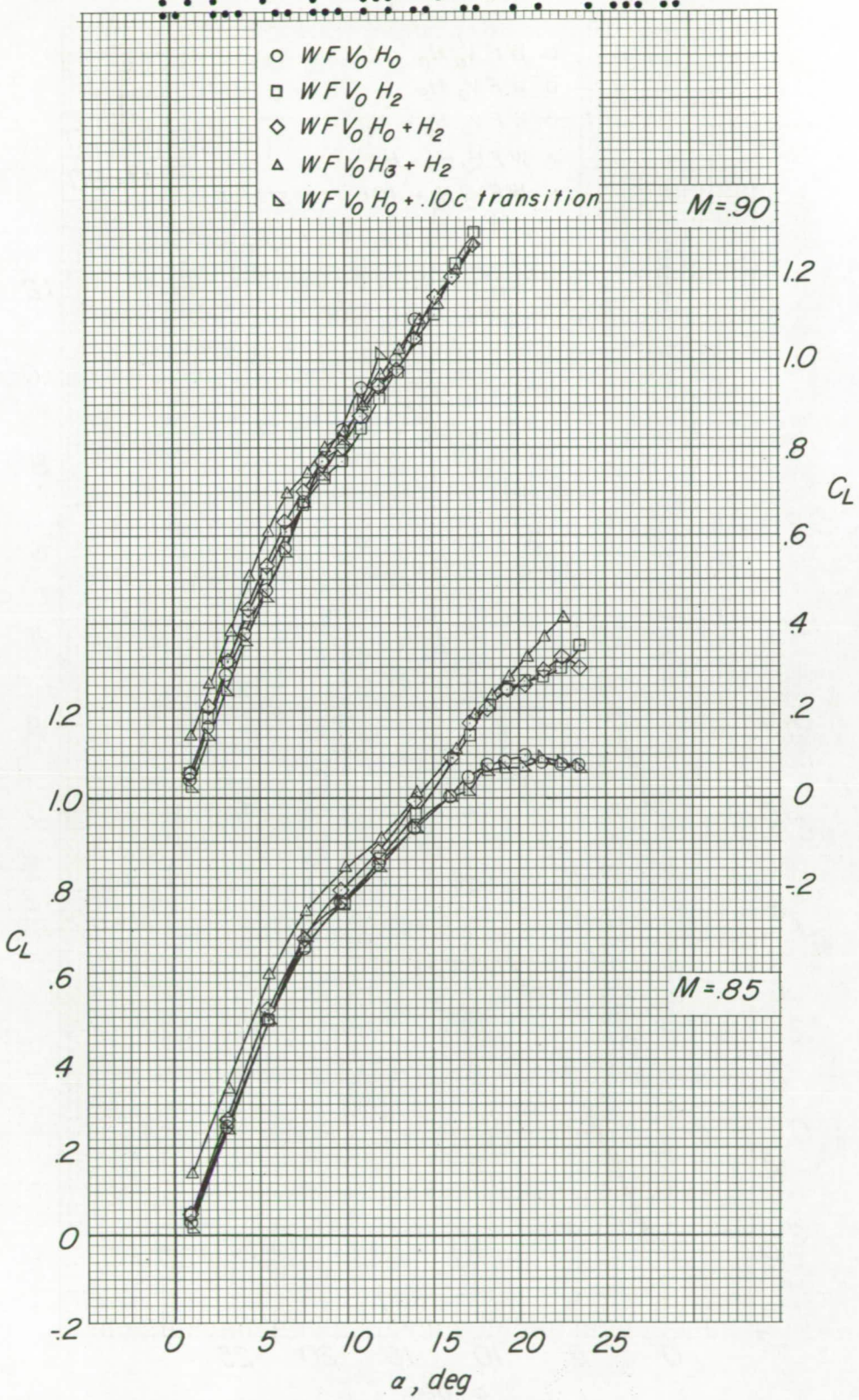

(c) Continued.

Figure 10.- Continued.

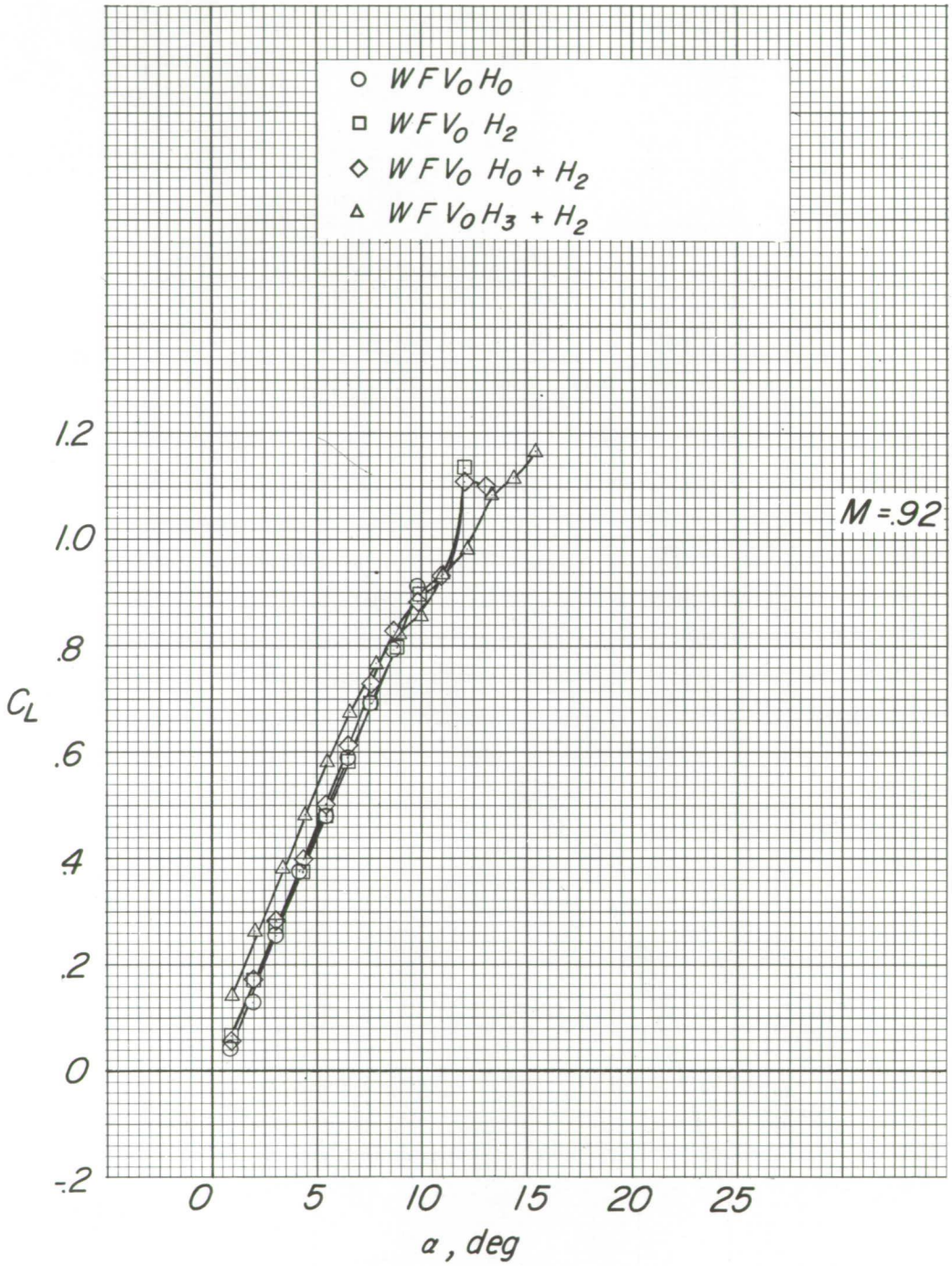

(c) Concluded.

Figure 10.- Continued.

DECLASSIFIED

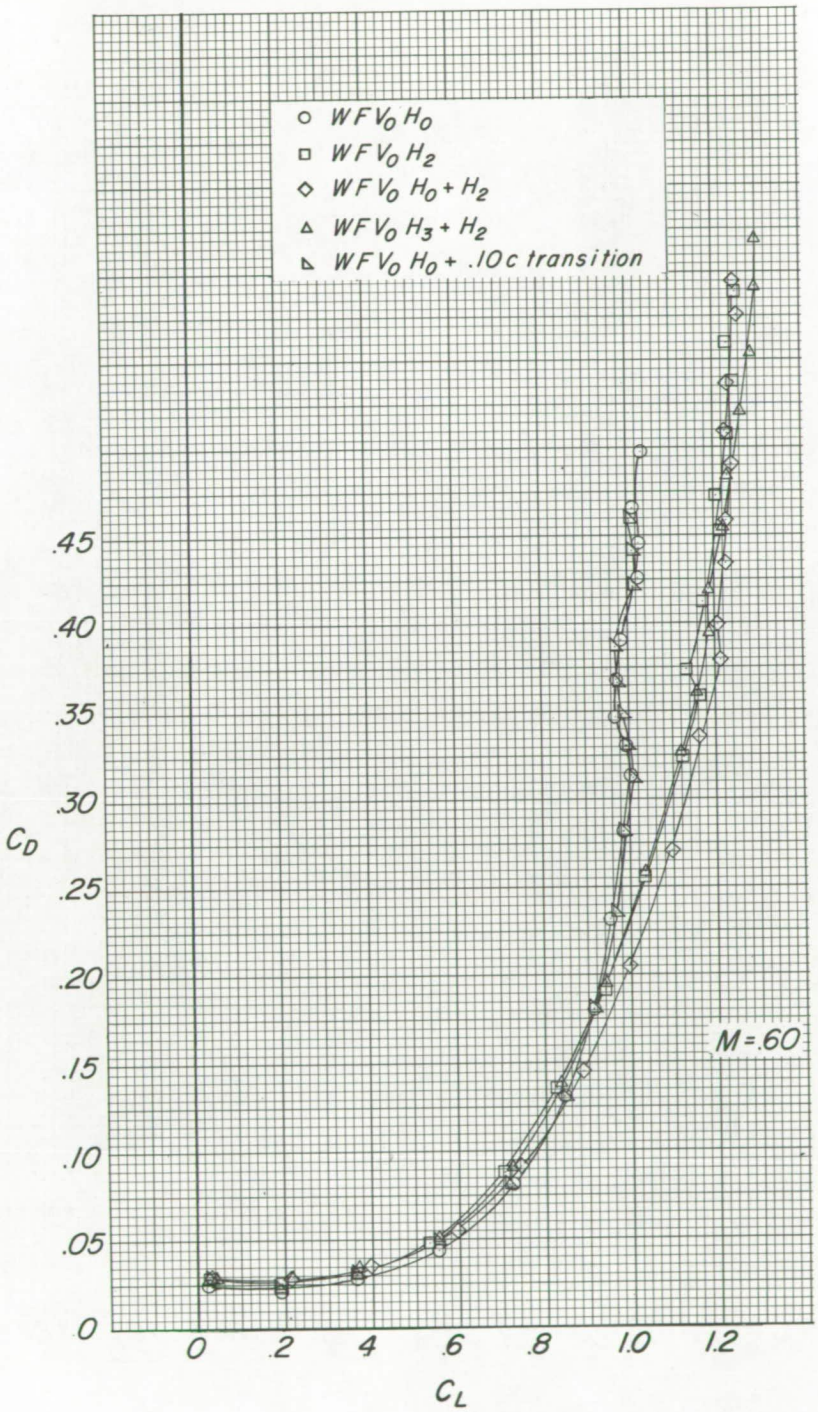

(d) C_D against C_L.

Figure 10.- Continued.

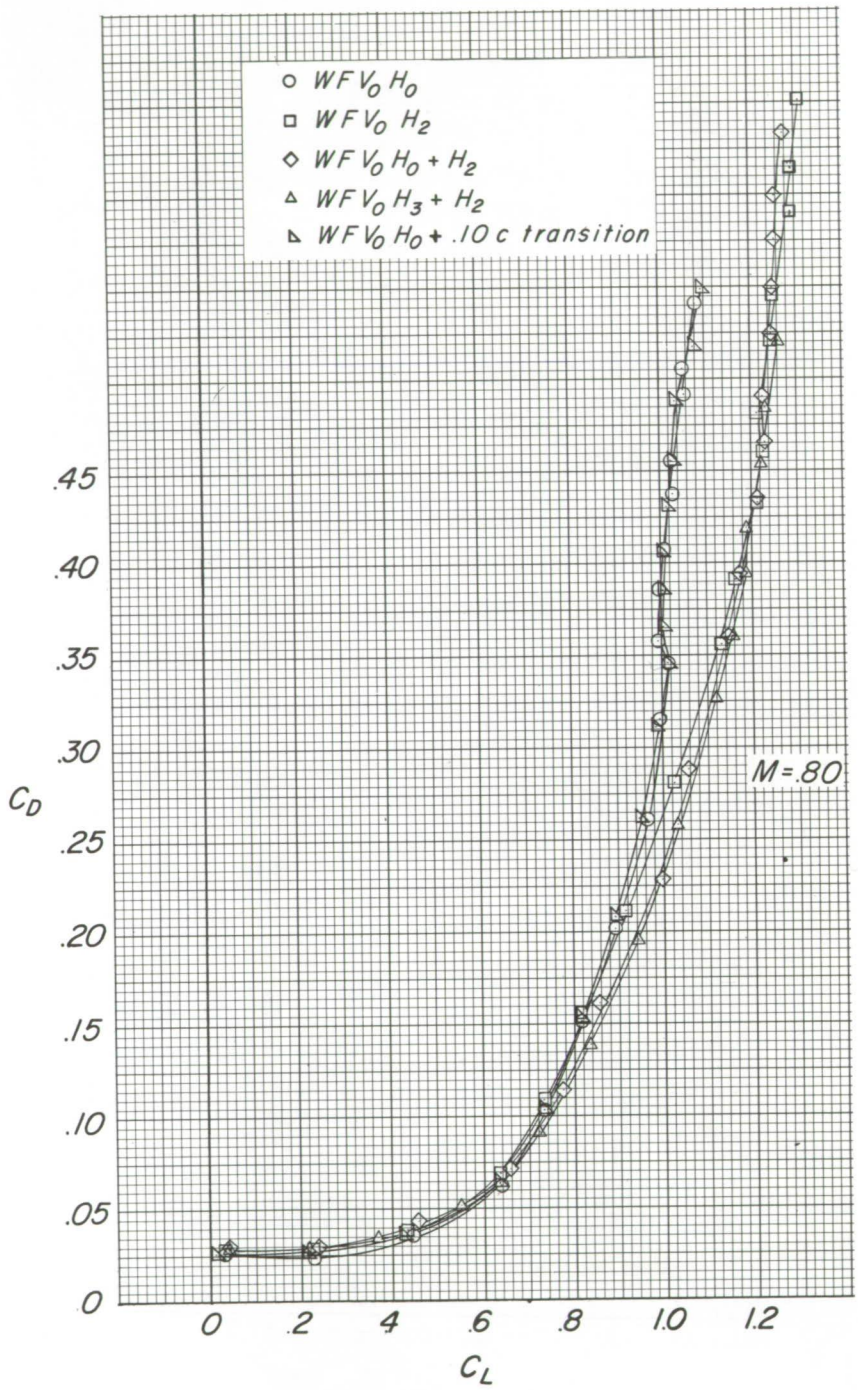

(d) Continued.

Figure 10.- Continued.

DECLASSIFIED

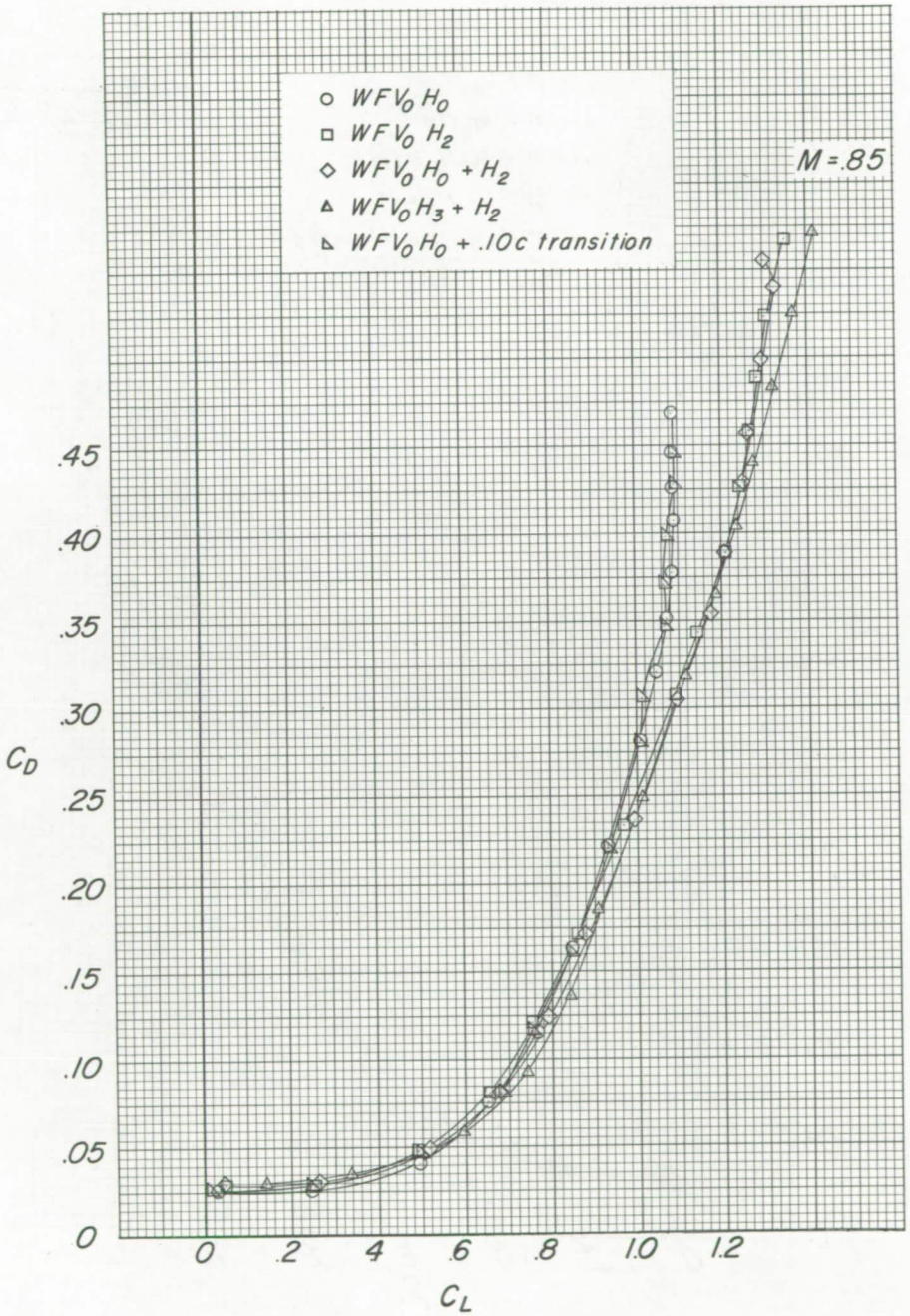

(d) Continued.

Figure 10.- Continued.

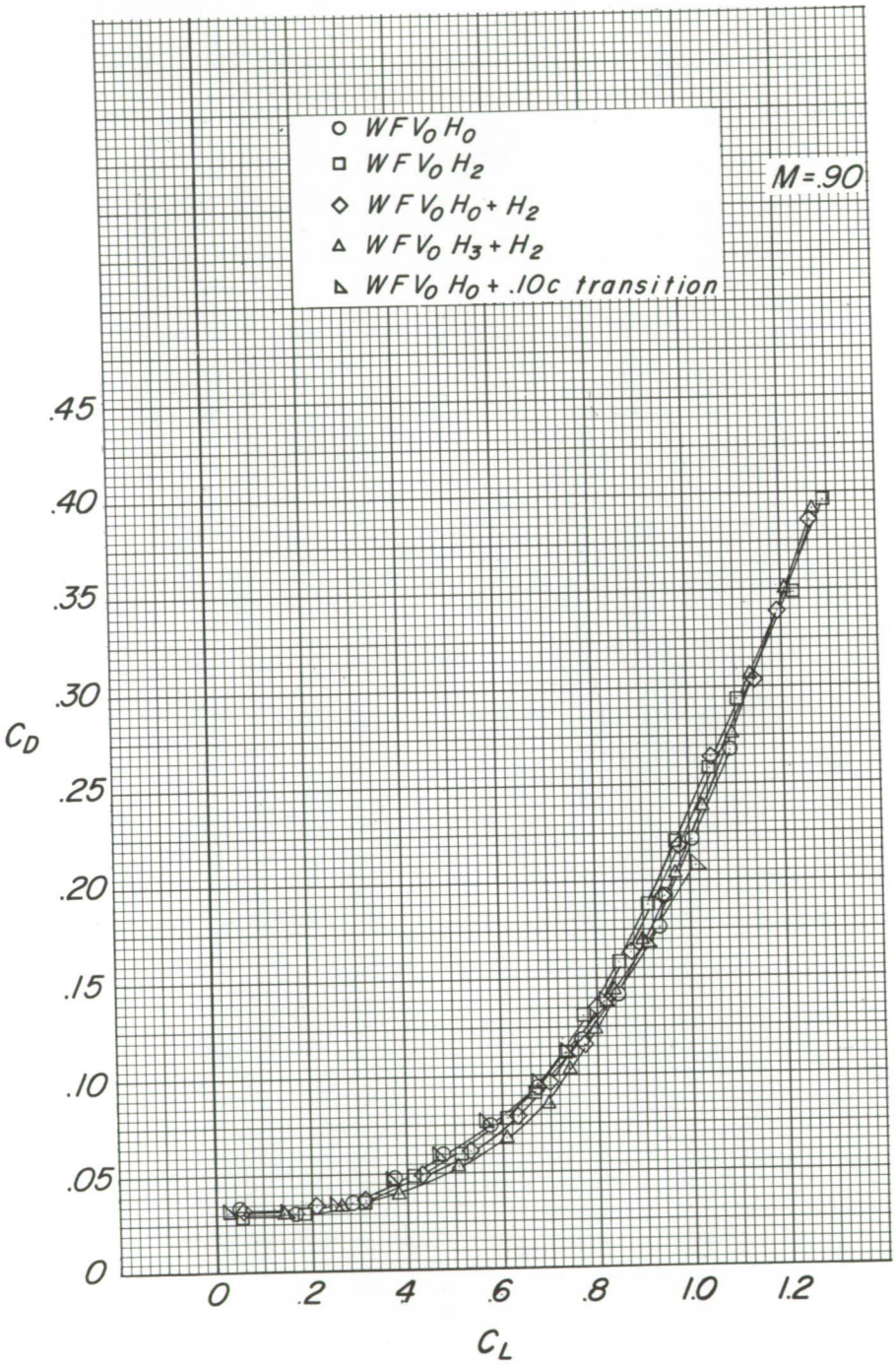

(d) Continued.

Figure 10.- Continued.

DECLASSIFIED

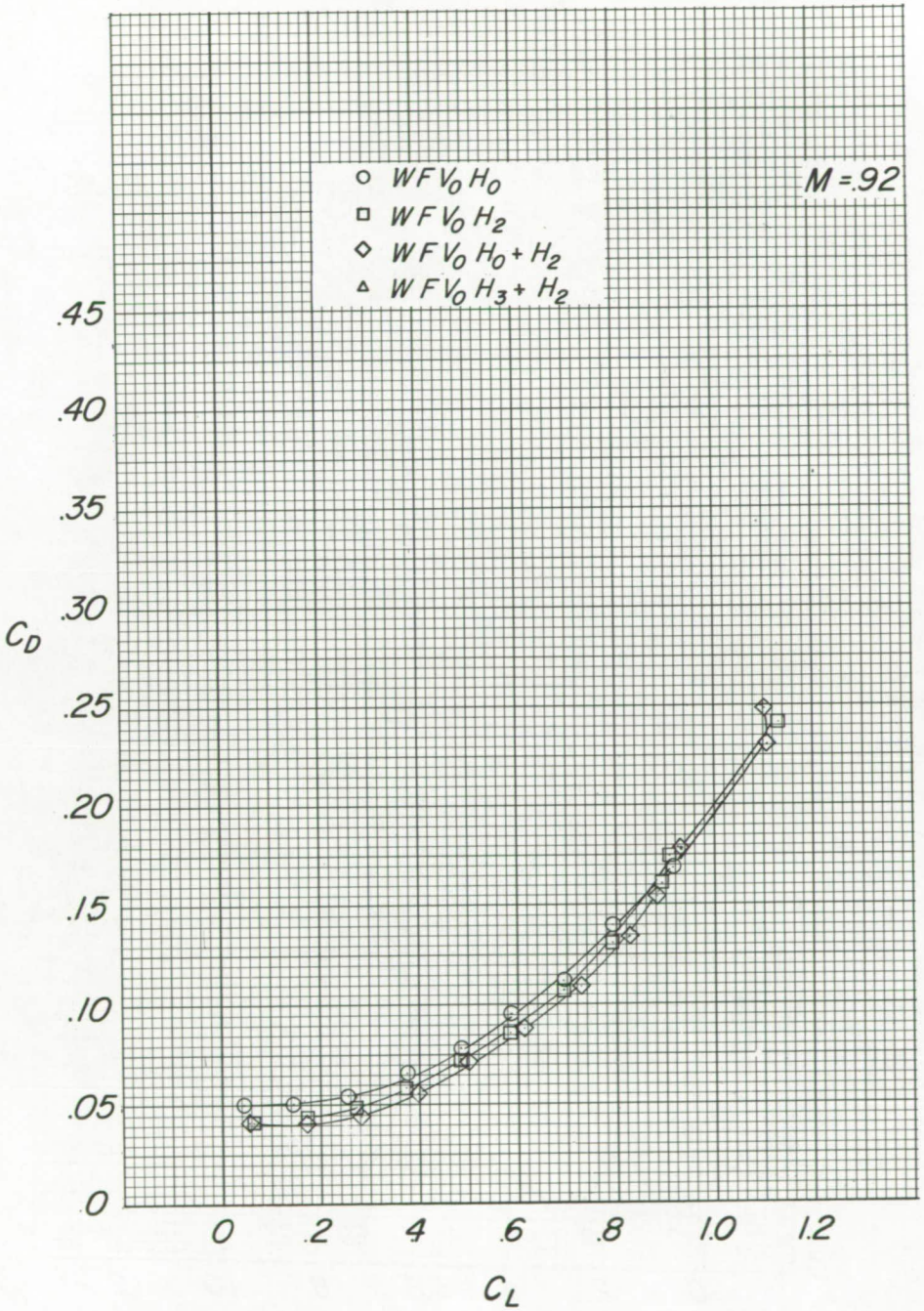

(d) Concluded.

Figure 10.- Concluded.

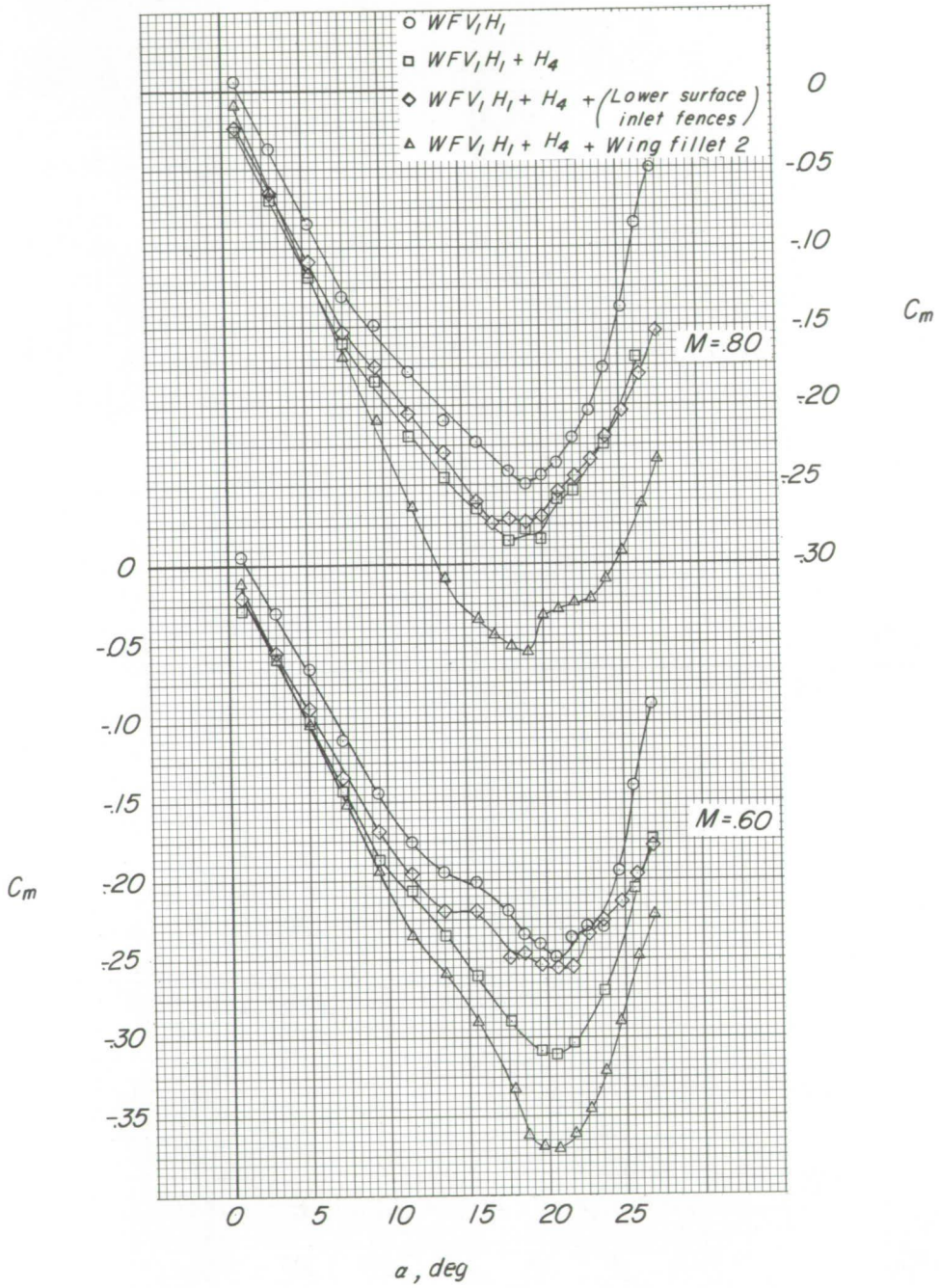

(a) C_m against α.

Figure 11.- Effect of several tail and wing modifications on the longitudinal aerodynamic characteristics of the model. $i_t = 0^\circ$.

DECLASSIFIED

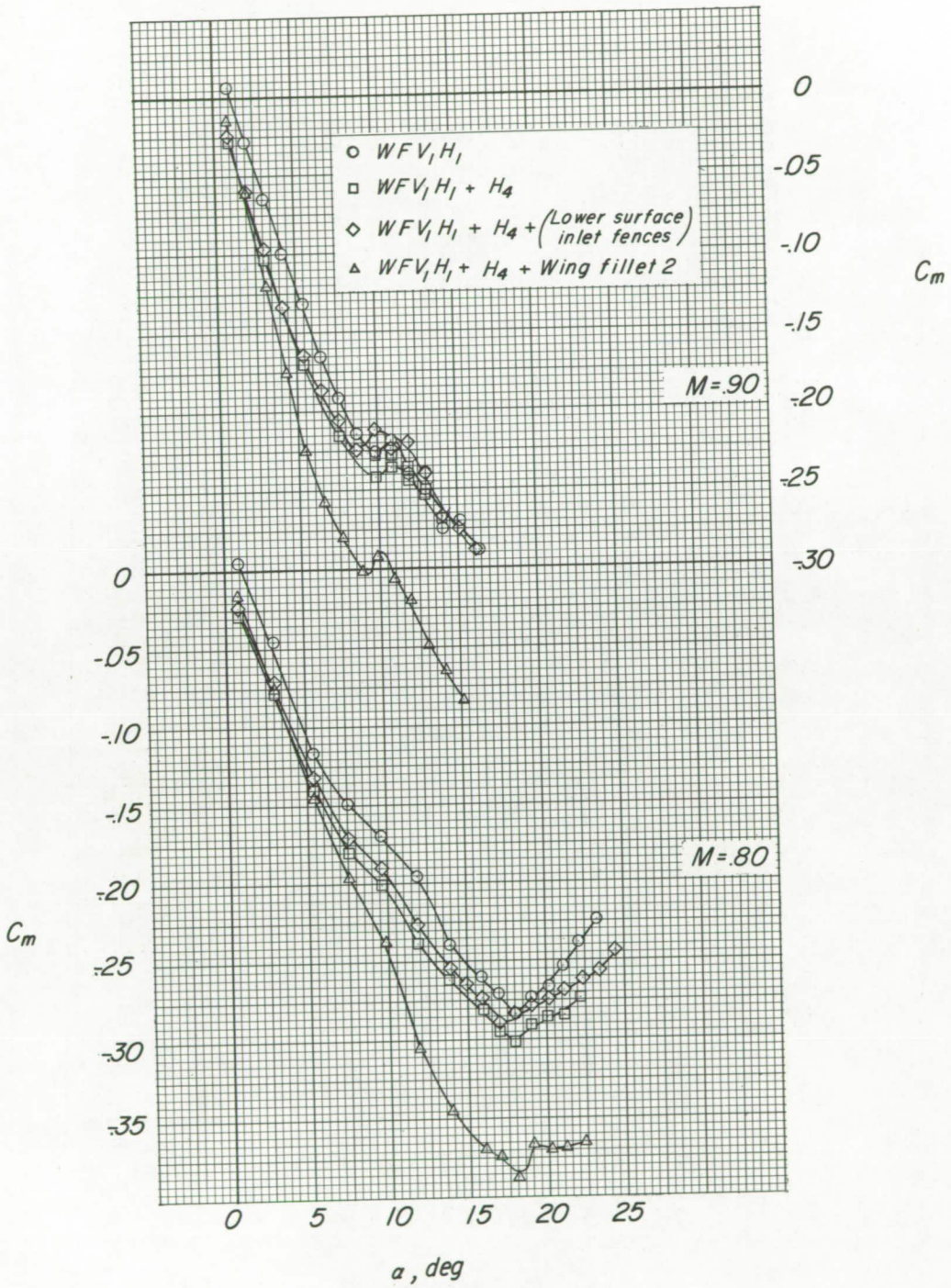

(a) Continued.

Figure 11.- Continued.

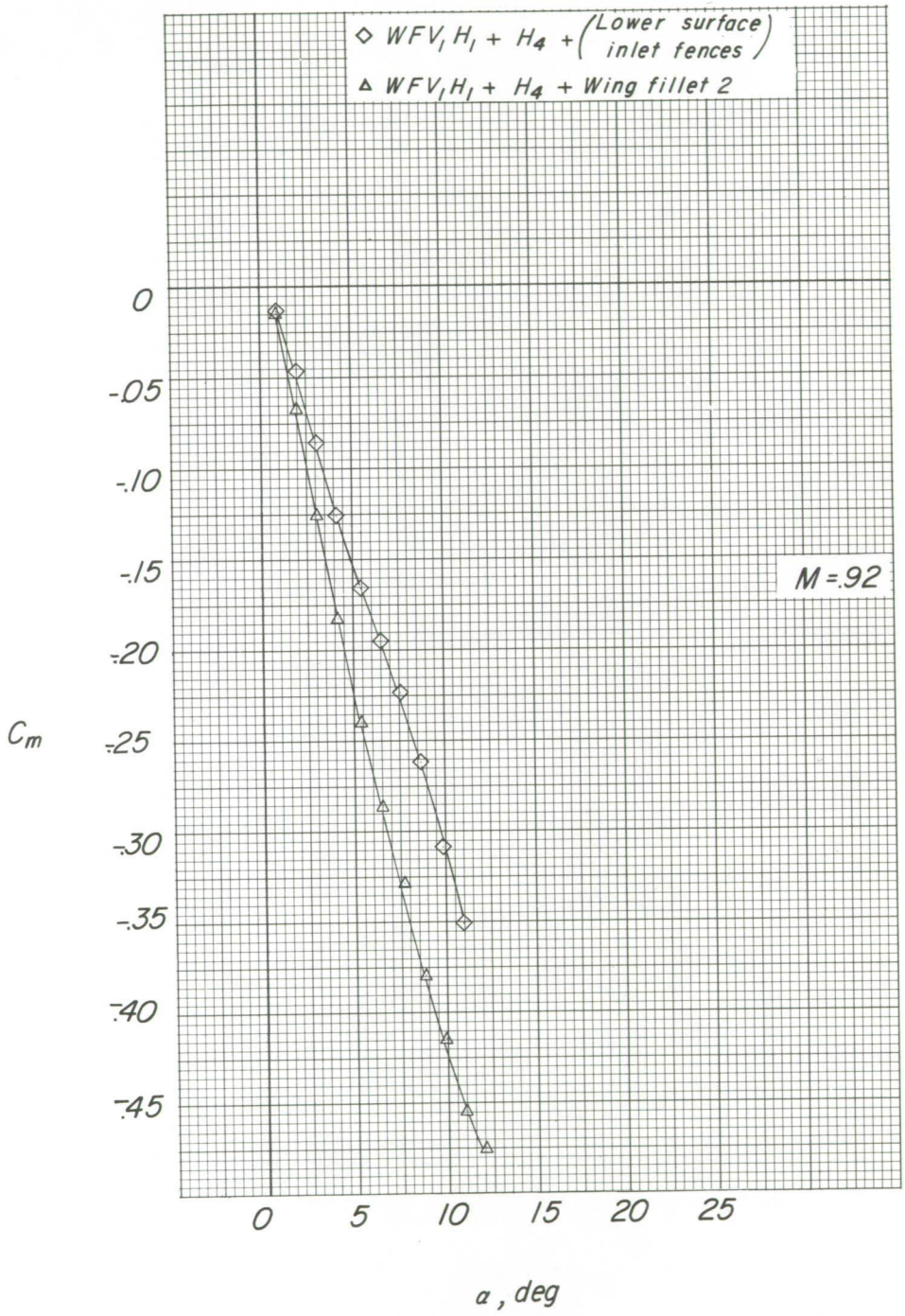

(a) Concluded.

Figure 11.- Continued.

DECLASSIFIED

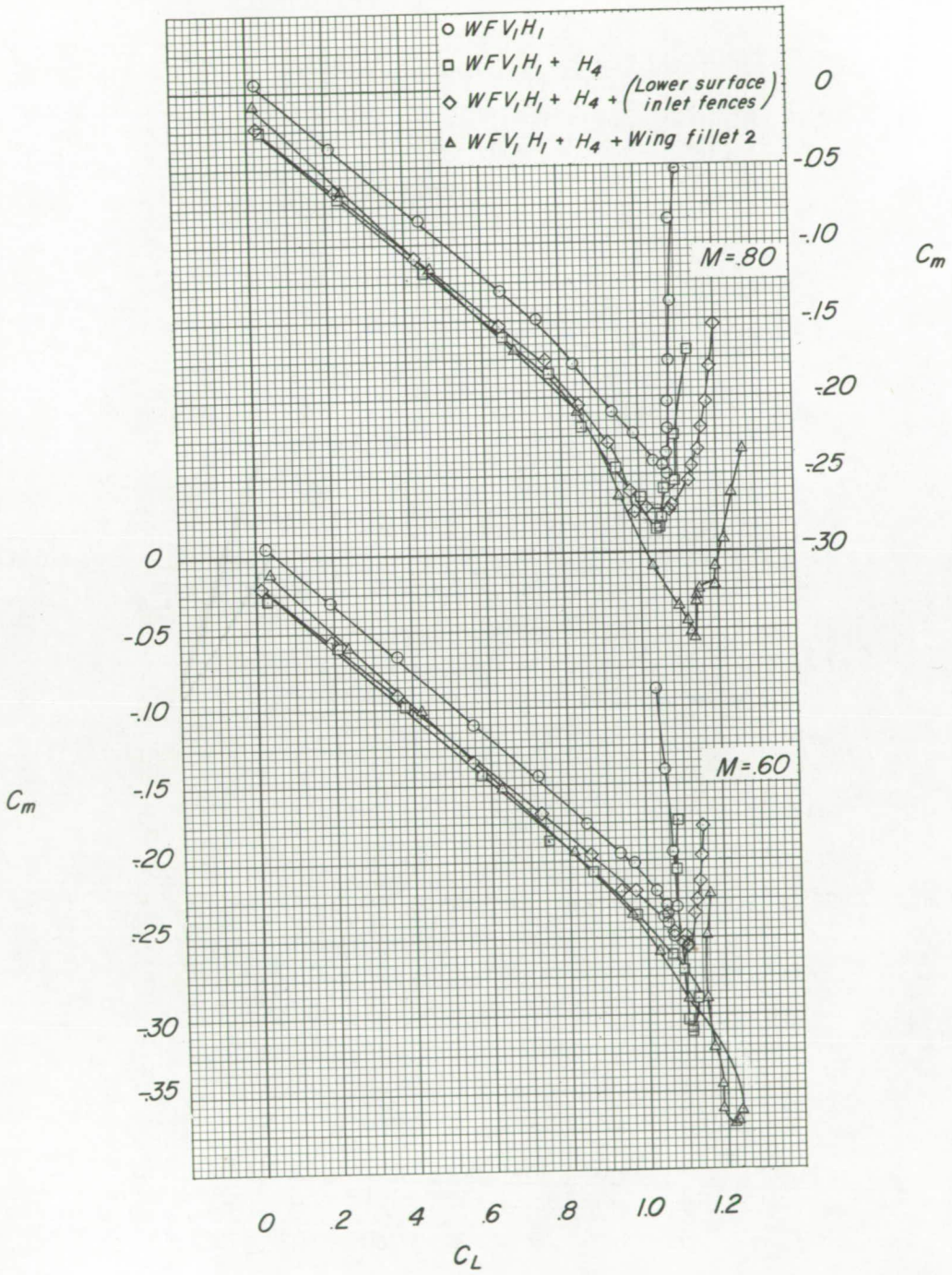

(b) C_m against C_L.

Figure 11.- Continued.

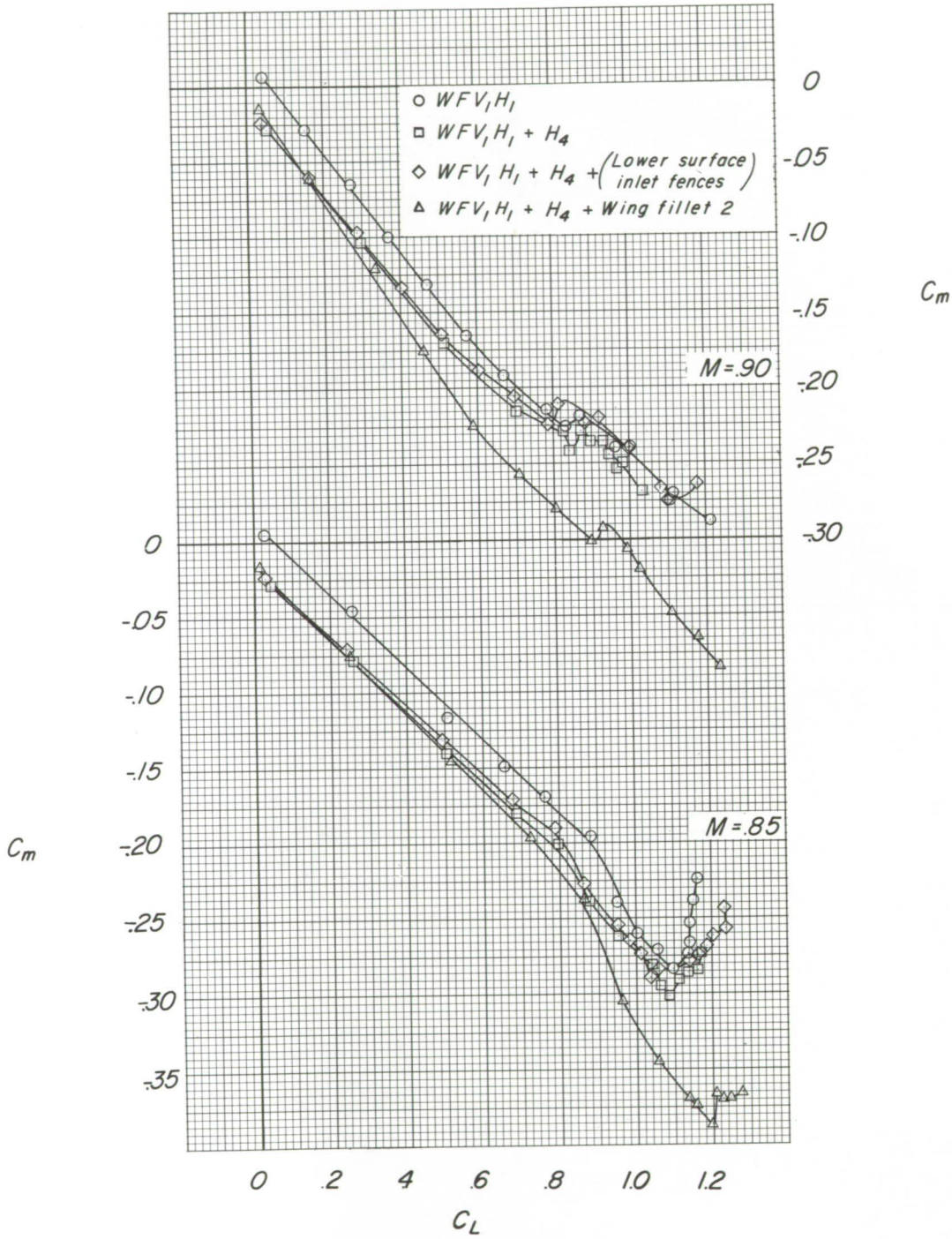

(b) Continued.

Figure 11.- Continued.

DECLASSIFIED

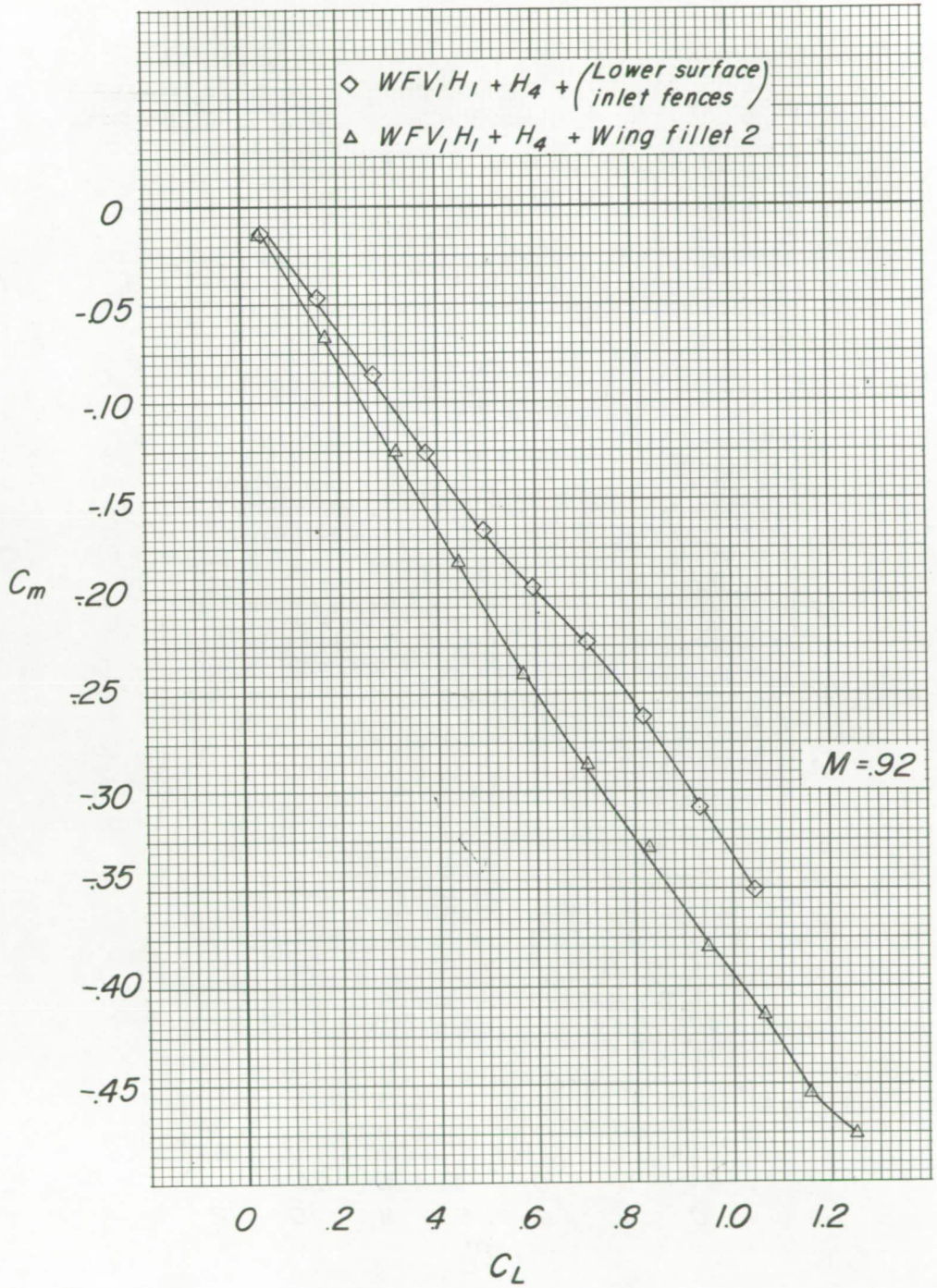

(b) Concluded.

Figure 11.- Continued.

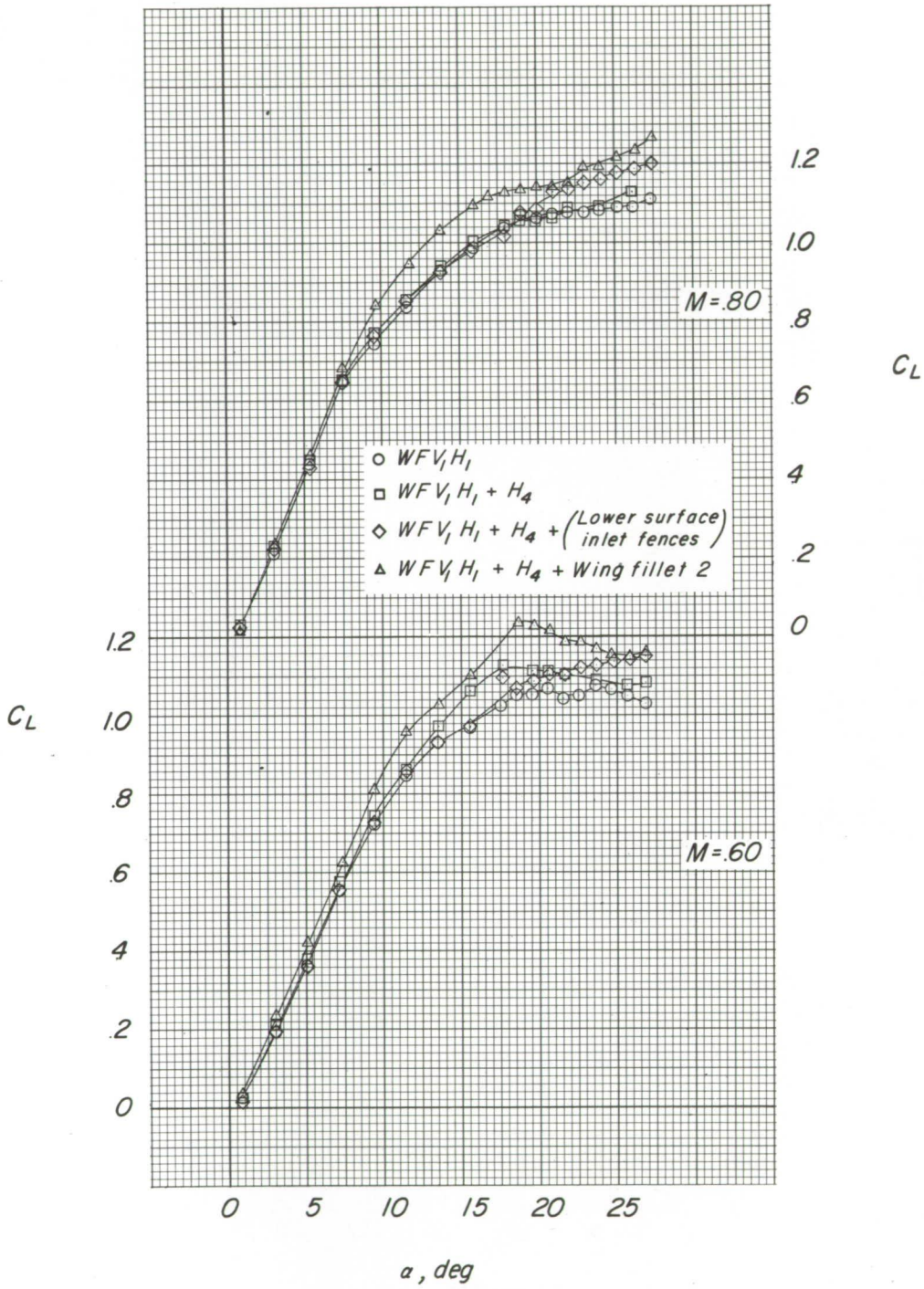

(c) C_L against α.

Figure 11.- Continued.

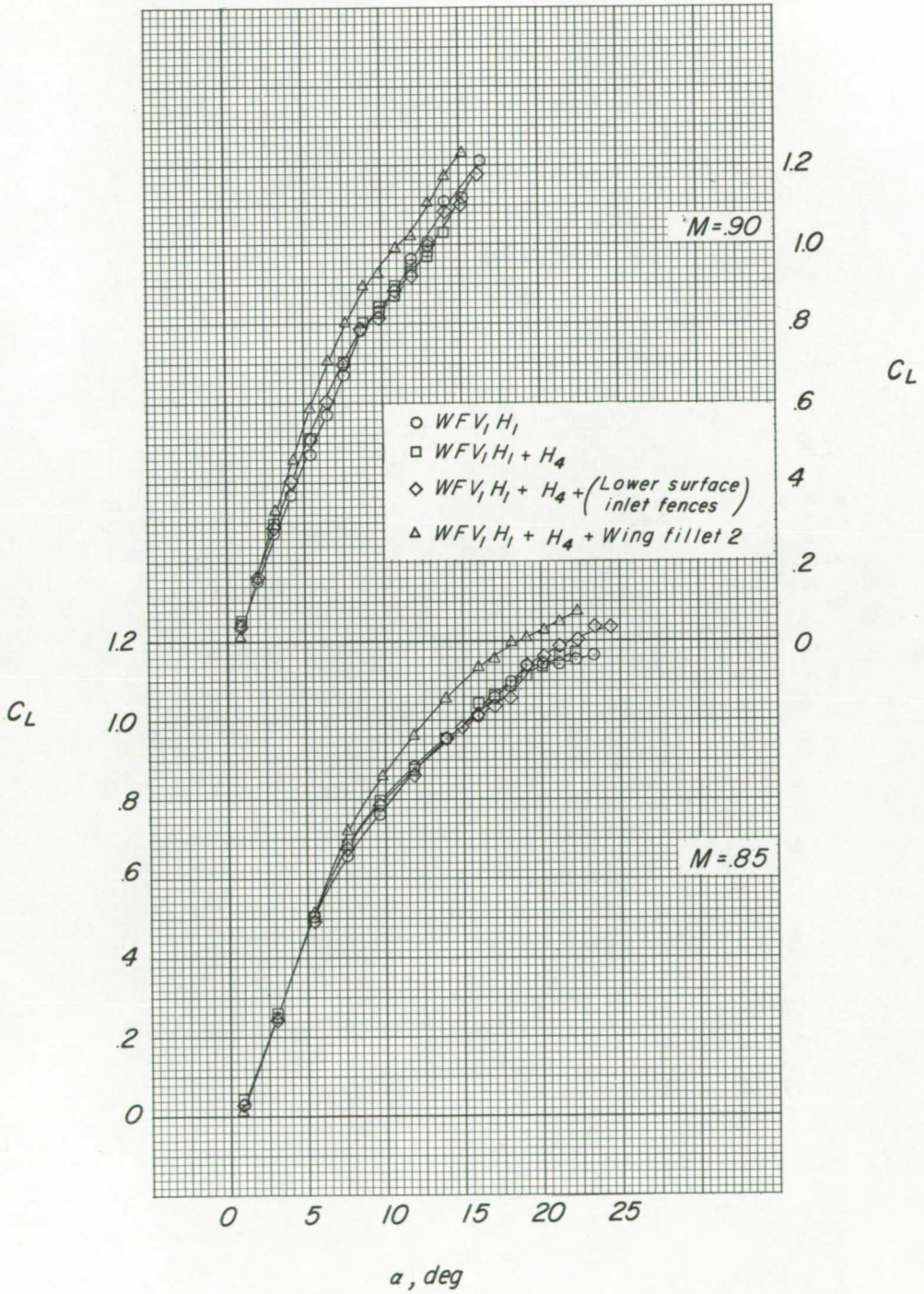

(c) Continued.

Figure 11.- Continued.

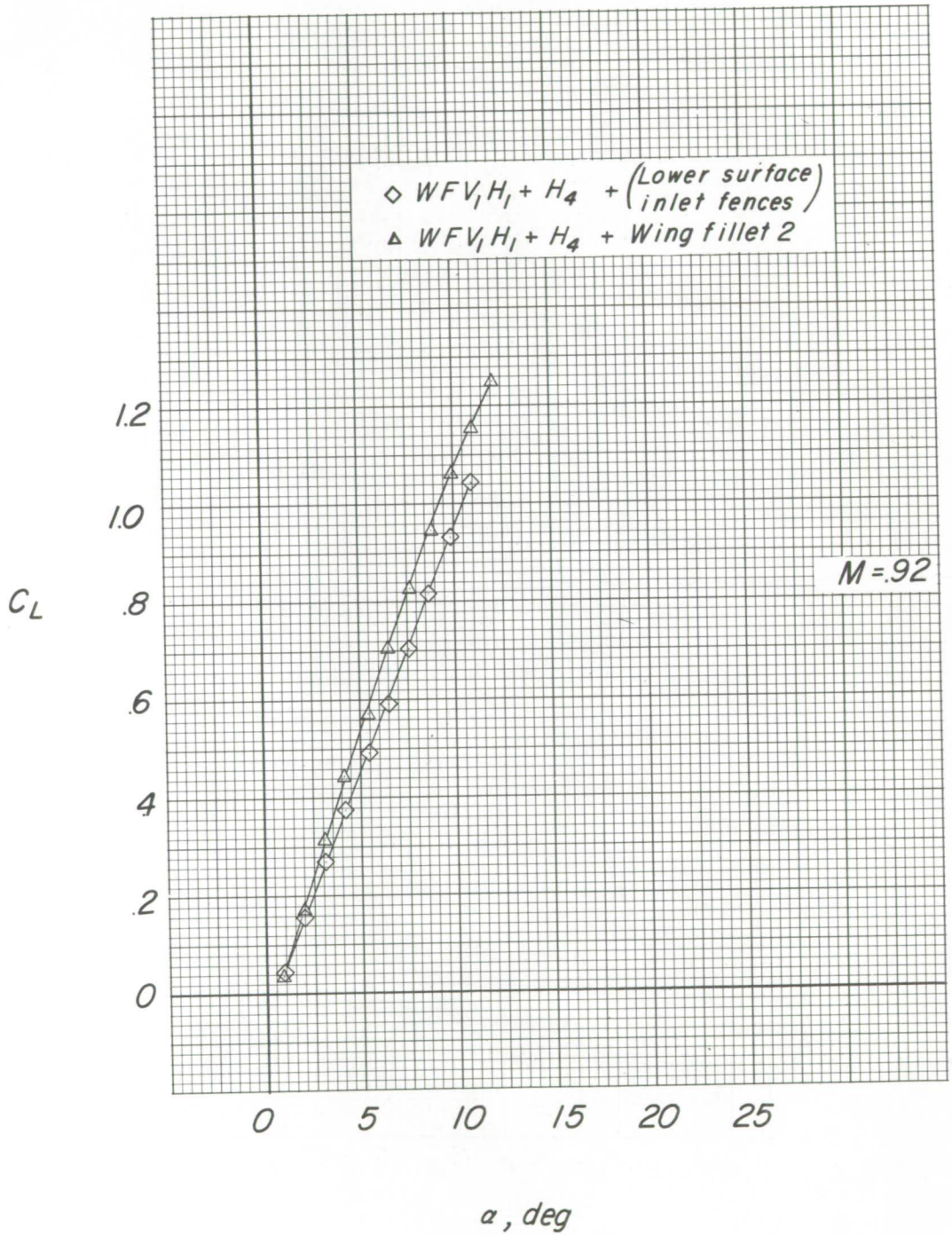

(c) Concluded.

Figure 11.- Continued.

DECLASSIFIED

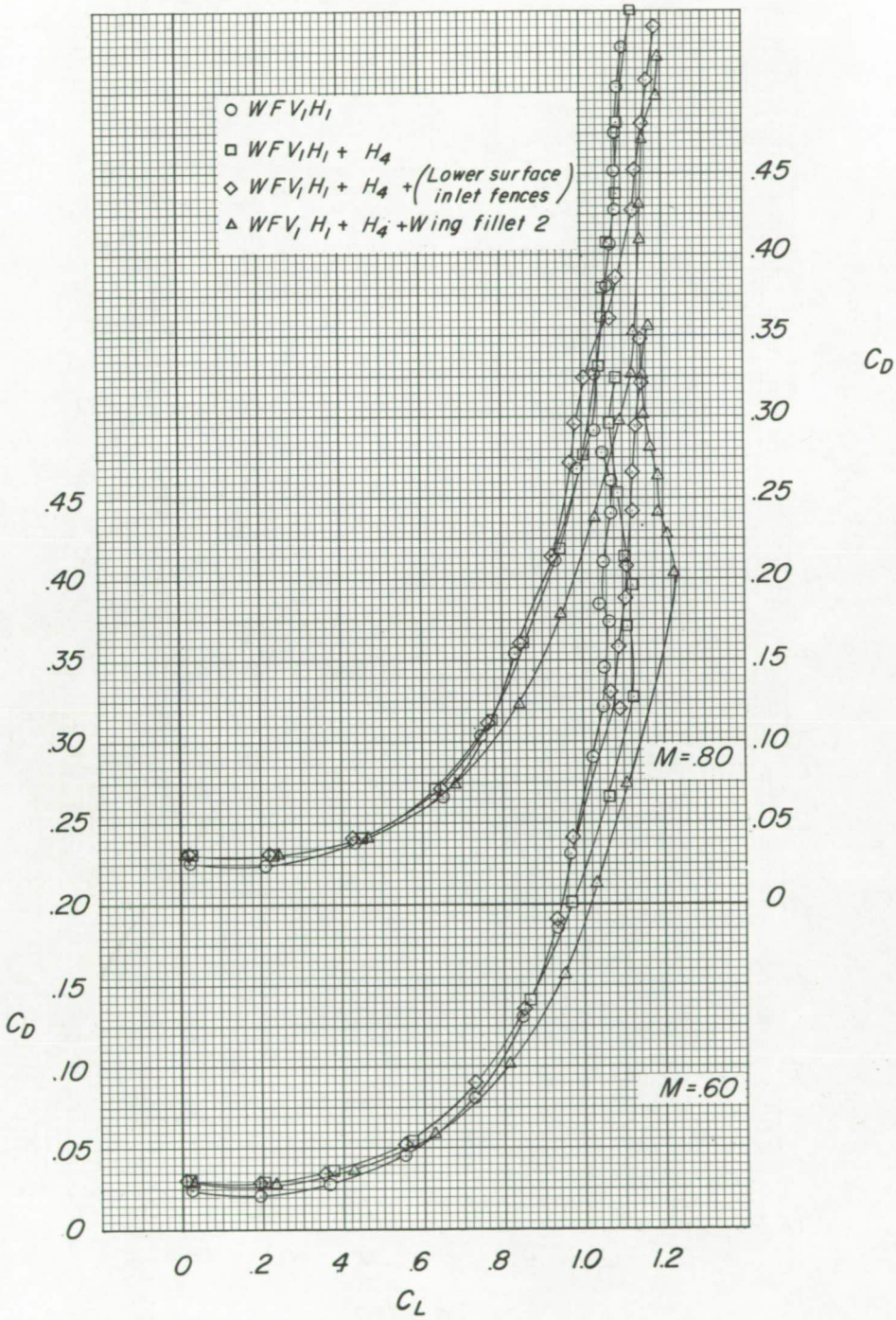

(d) C_D against C_L.

Figure 11.- Continued.

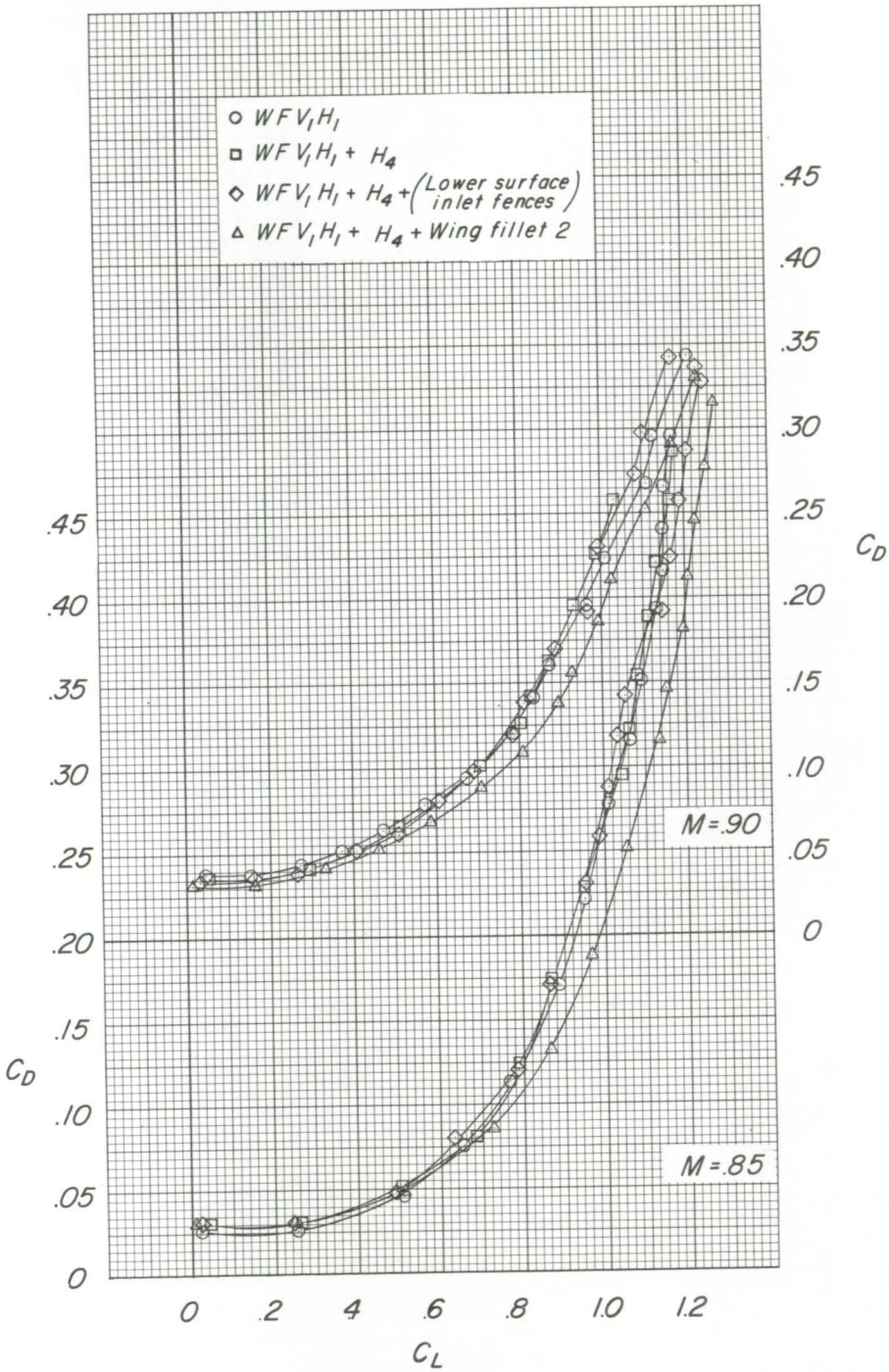

(d) Continued.

Figure 11.- Continued.

DECLASSIFIED

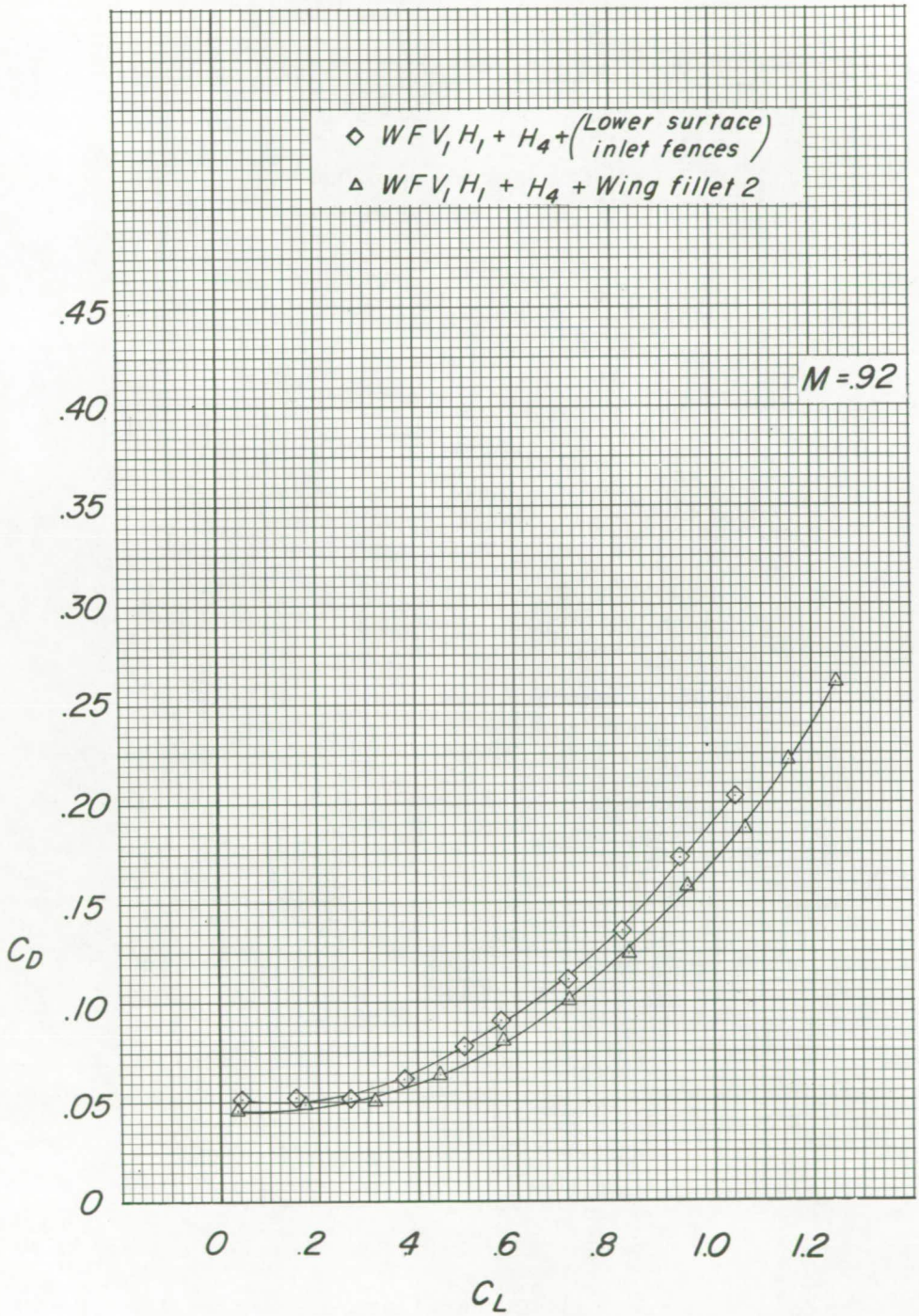

(d) Concluded.

Figure 11.- Concluded.

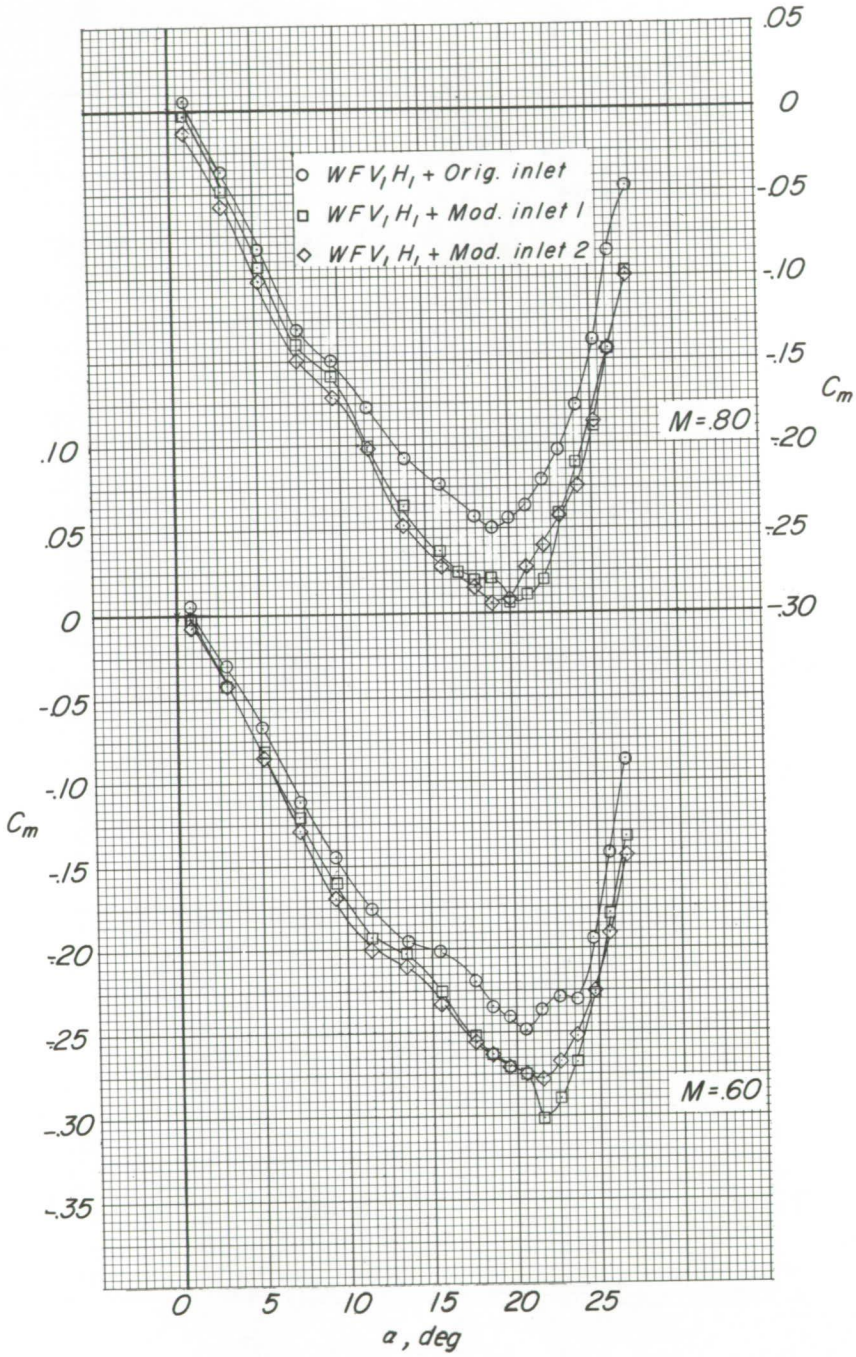

(a) C_m against α.

Figure 12.- Effect of duct-inlet modifications on the longitudinal aerodynamic characteristics of the model. $i_t = 0^{\circ}$.

DECLASSIFIED

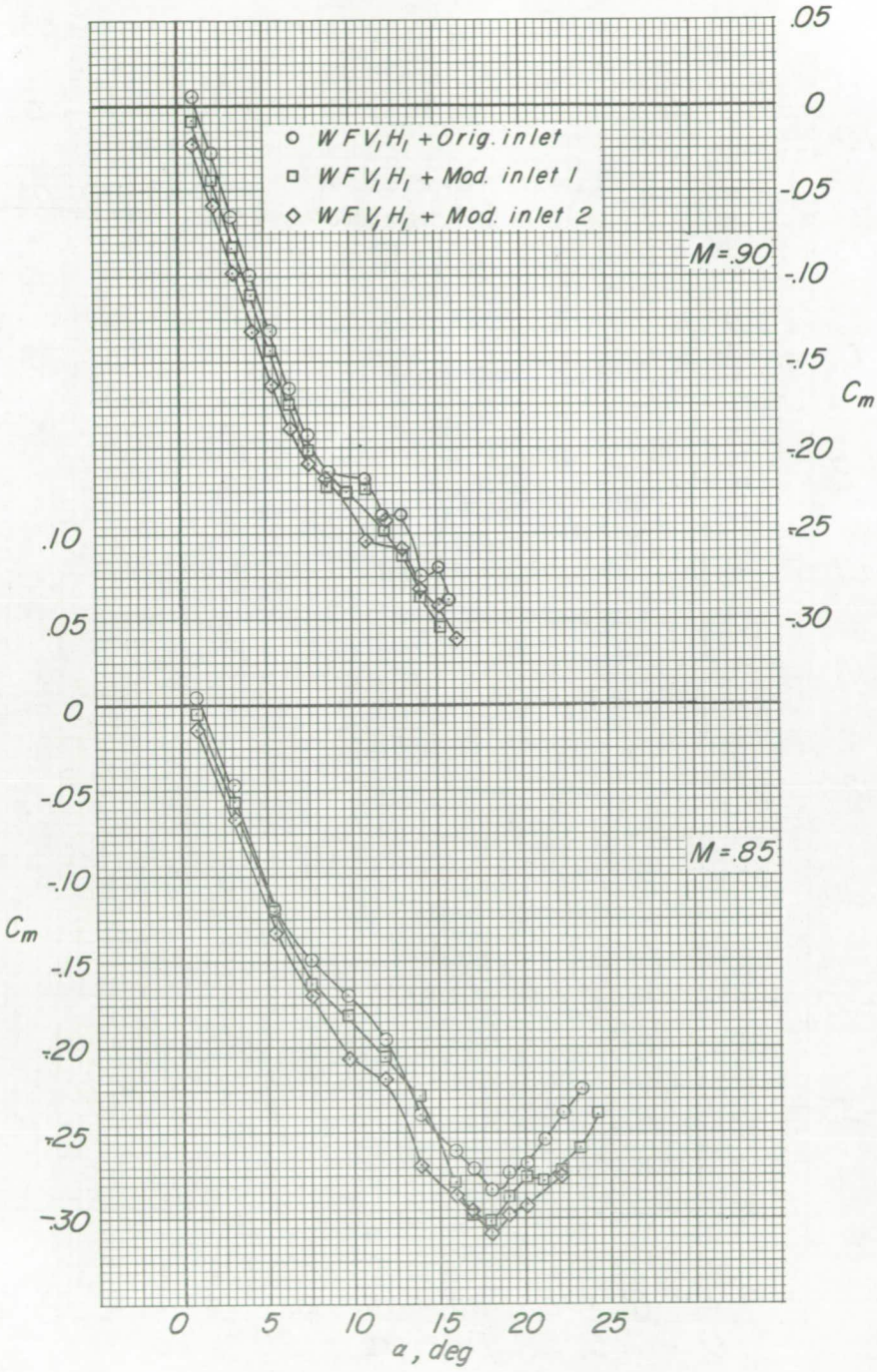

(a) Continued.

Figure 12.- Continued.

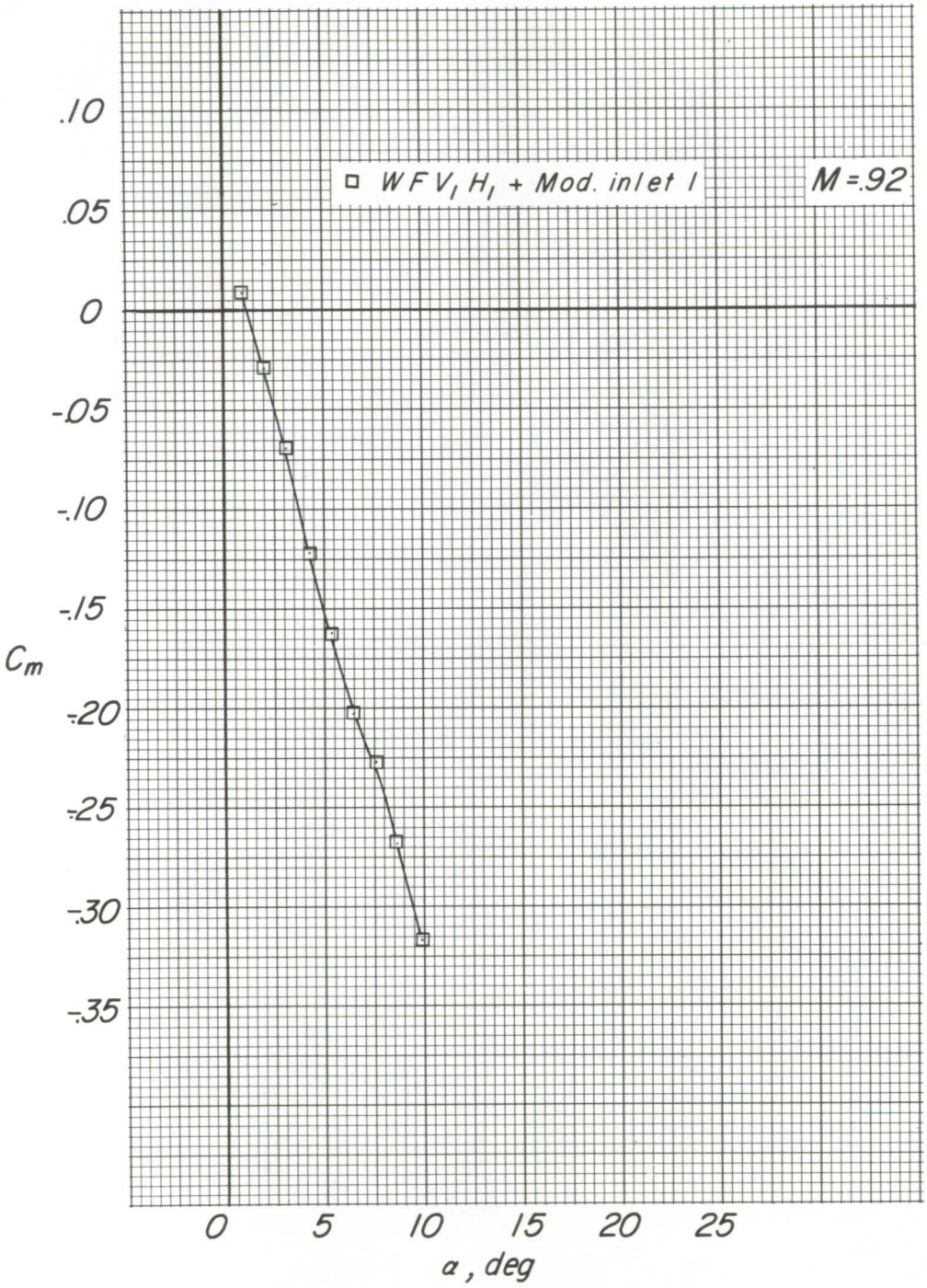

(a) Concluded.

Figure 12.- Continued.

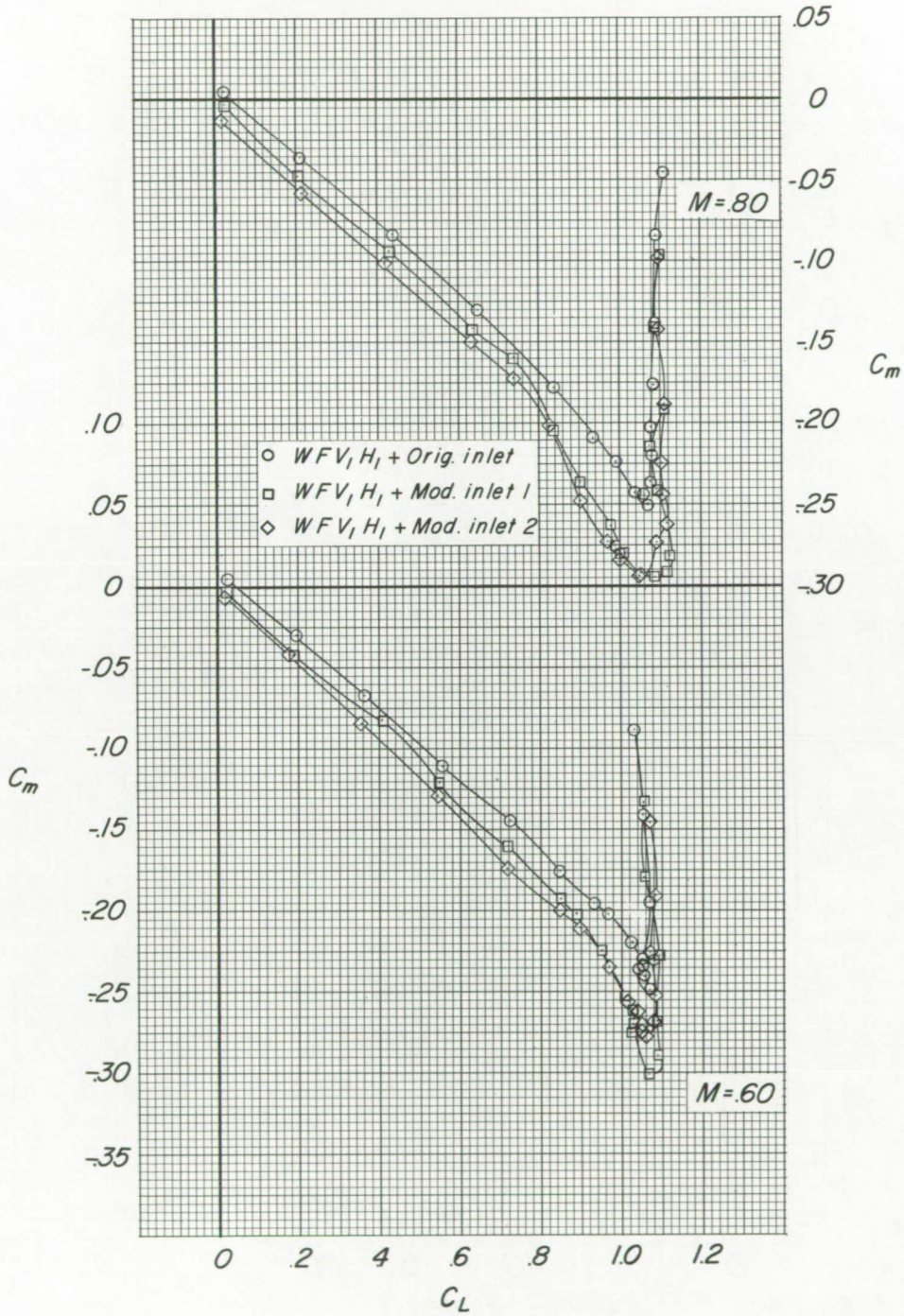

(b) C_m against C_L.

Figure 12.- Continued.

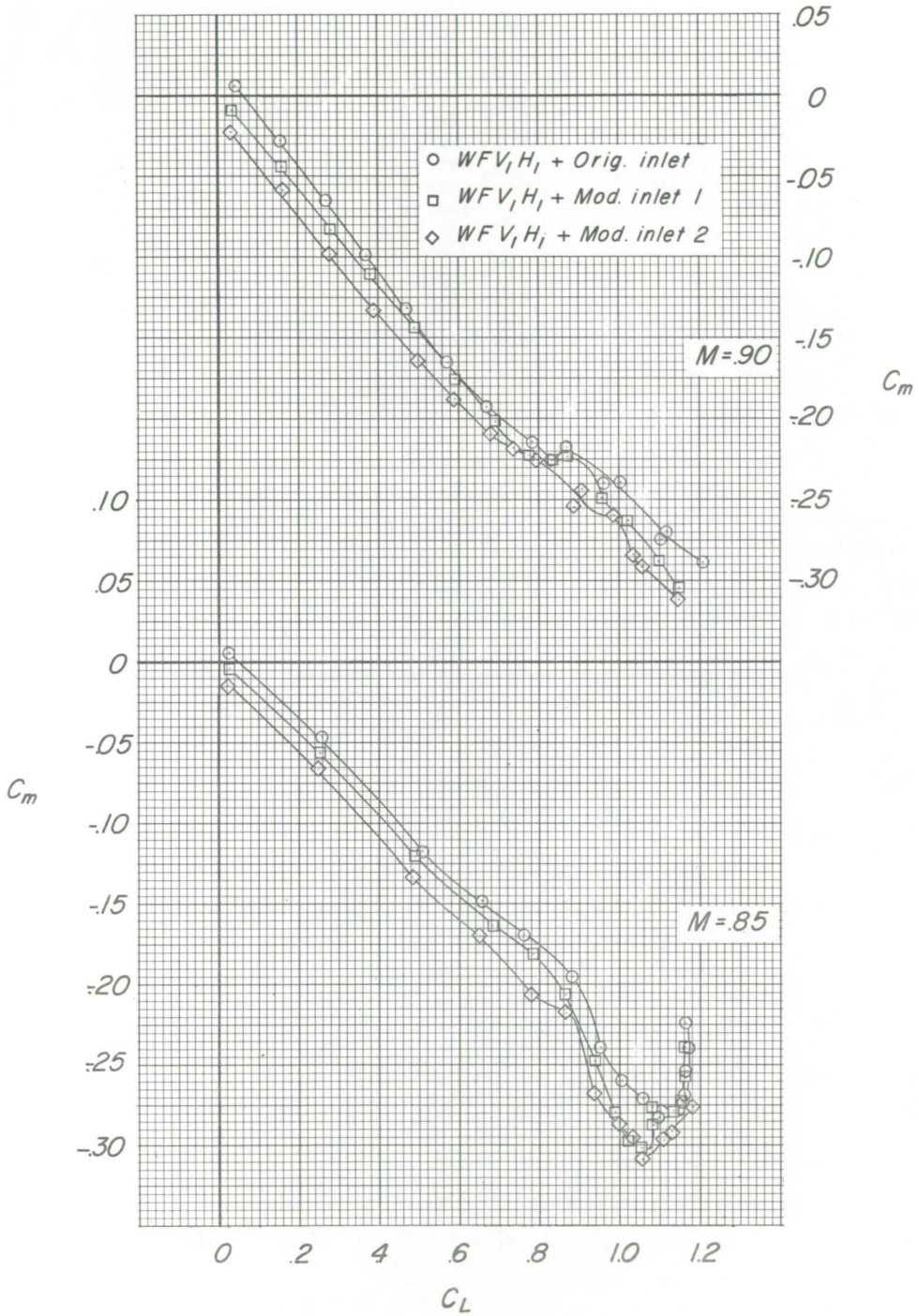

(b) Continued.

Figure 12.- Continued.

DECLASSIFIED

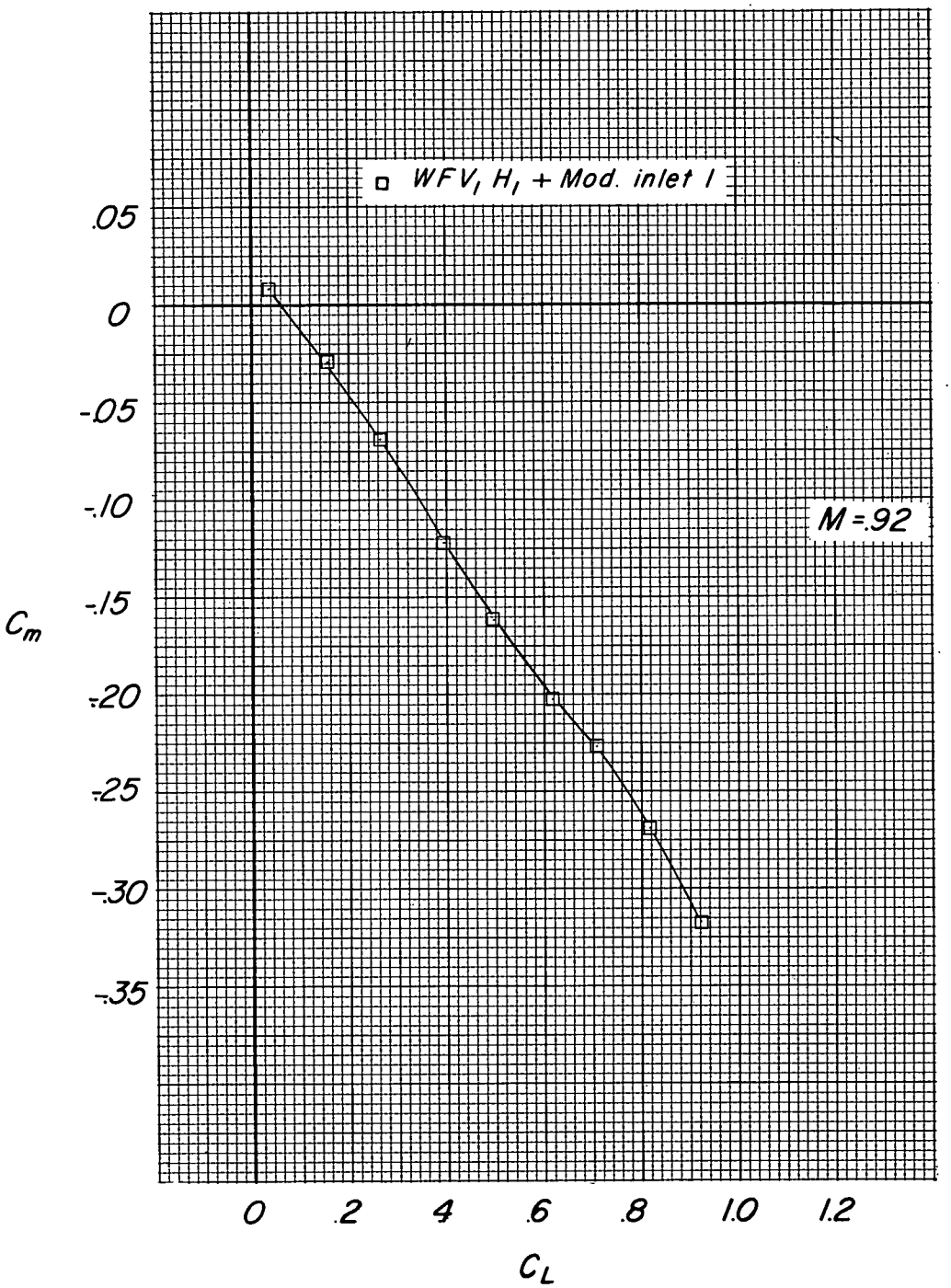

(b) Concluded.

Figure 12.- Continued.

[redacted]

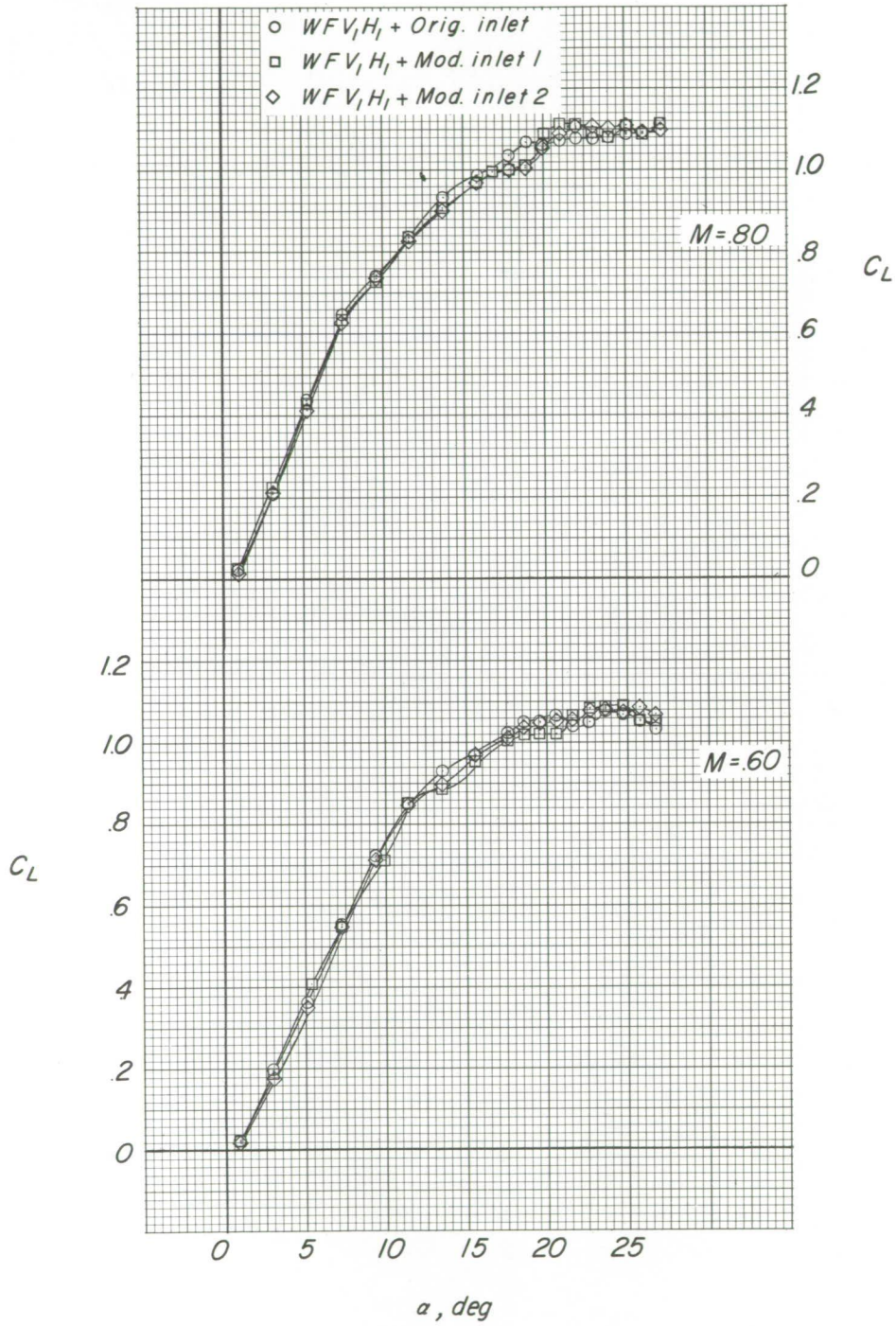

(c) C_L against α.

Figure 12.- Continued.

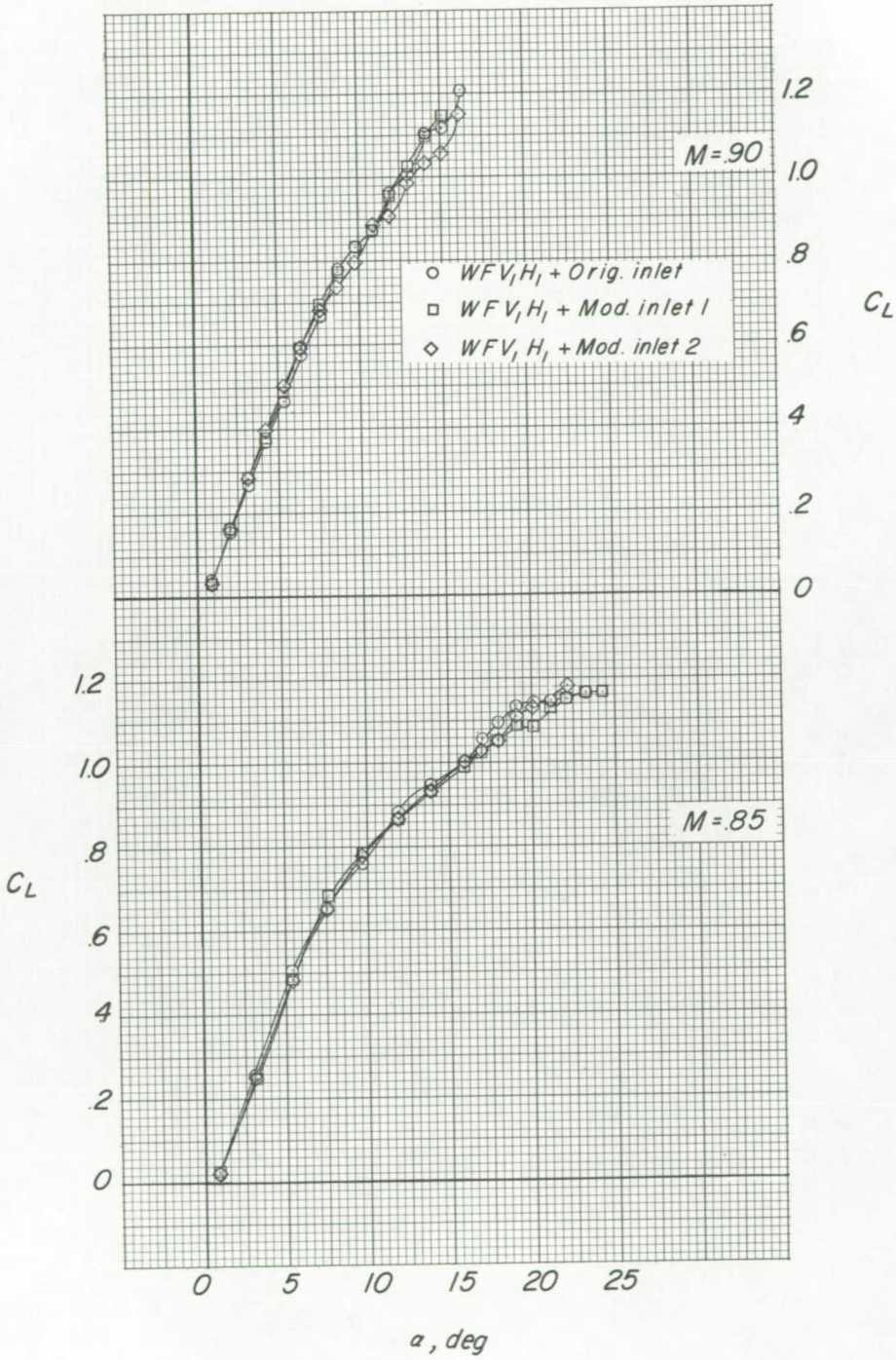

(c) Continued.

Figure 12.- Continued.

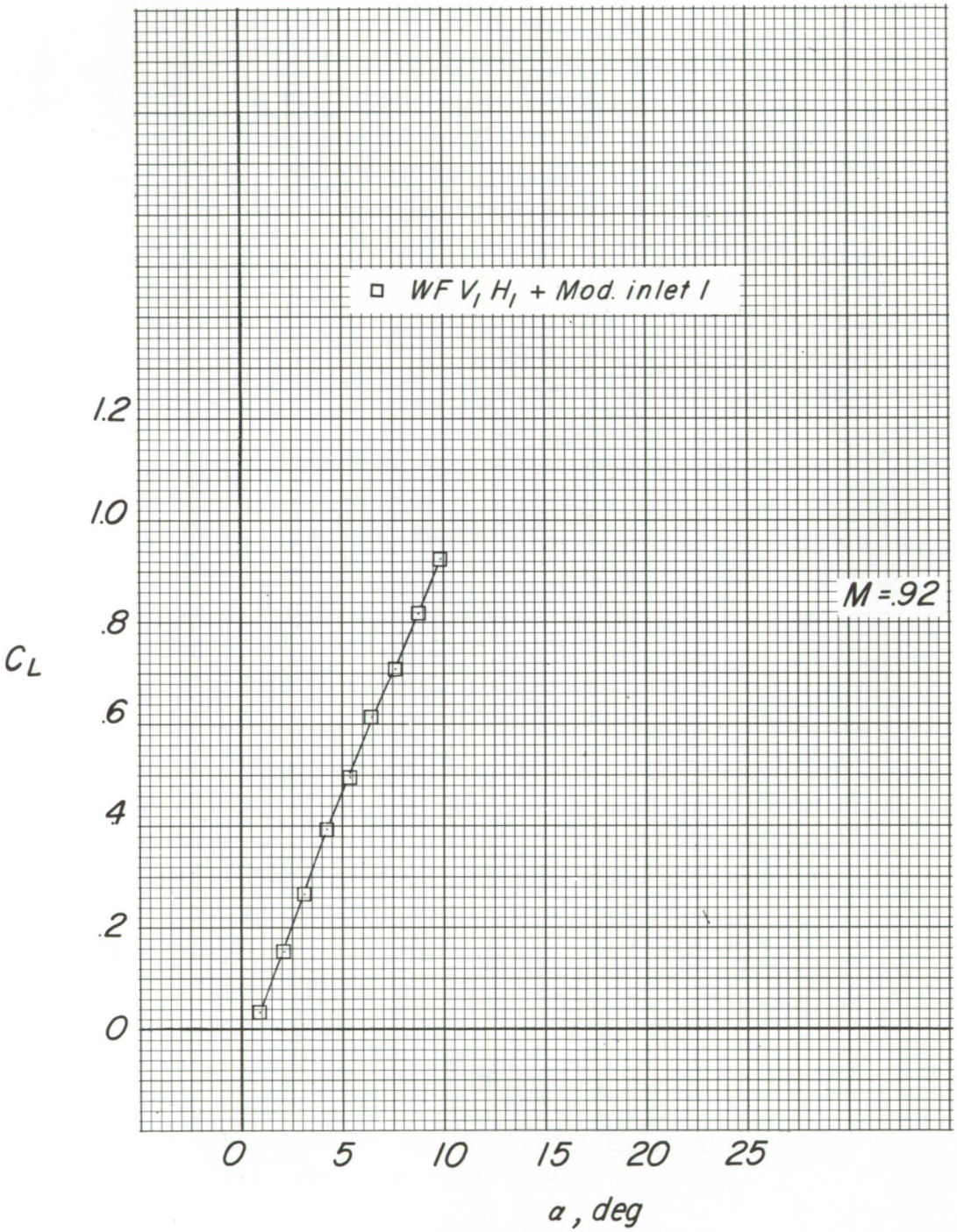

(c) Concluded.

Figure 12.- Continued.

DECLASSIFIED

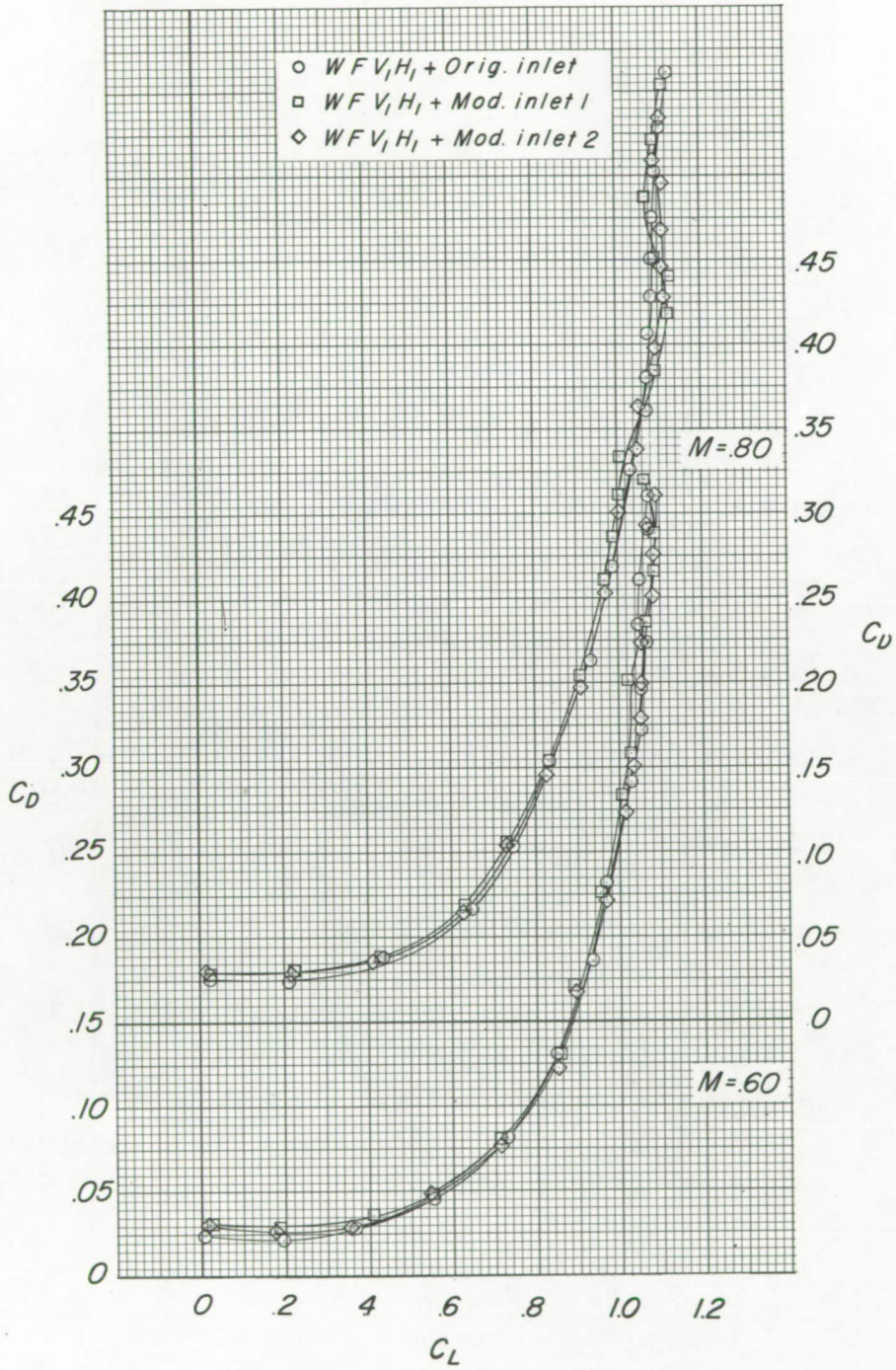

(d) C_D against C_L.

Figure 12.- Continued.

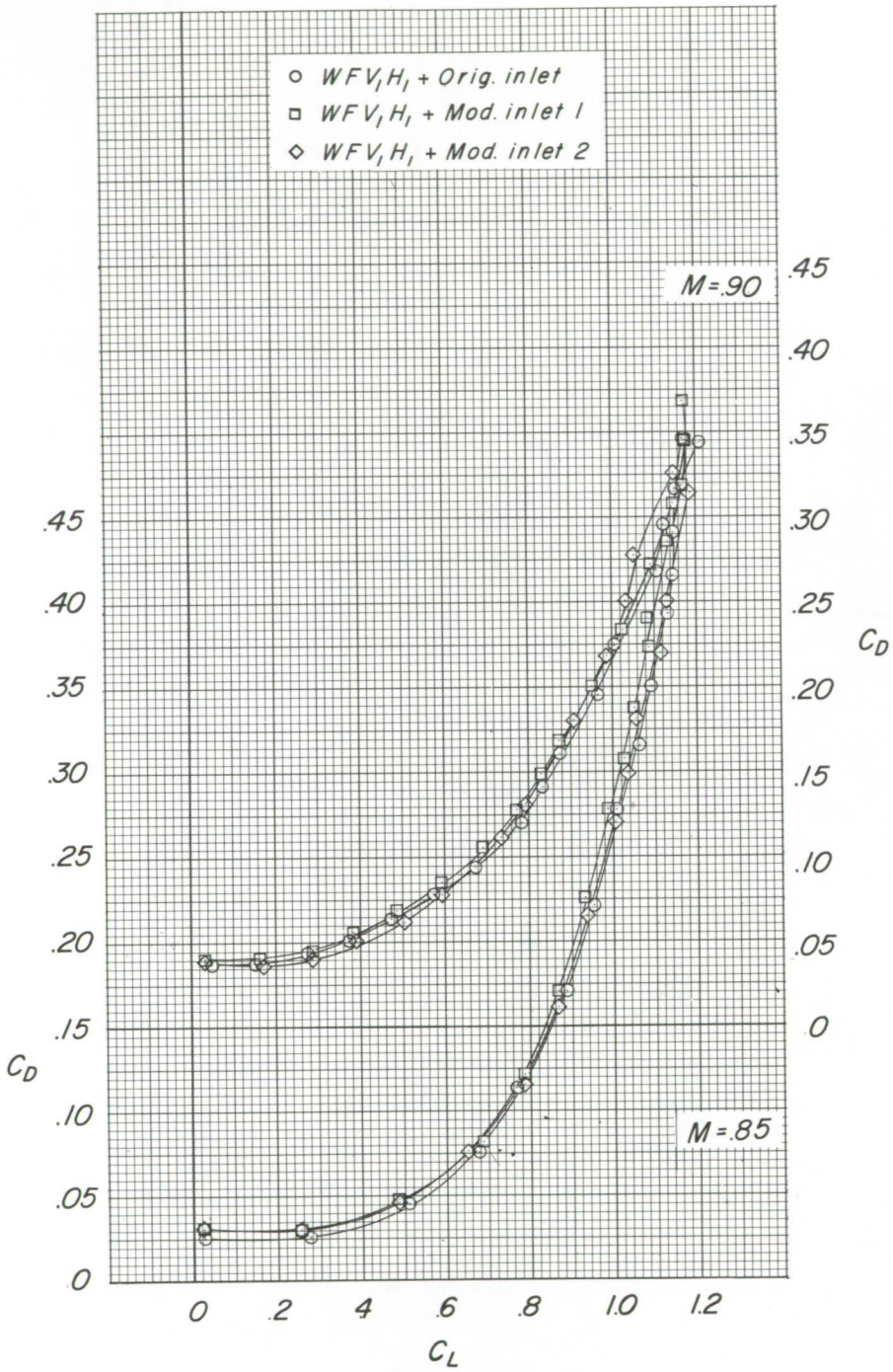

(d) Continued.

Figure 12.- Continued.

DECLASSIFIED

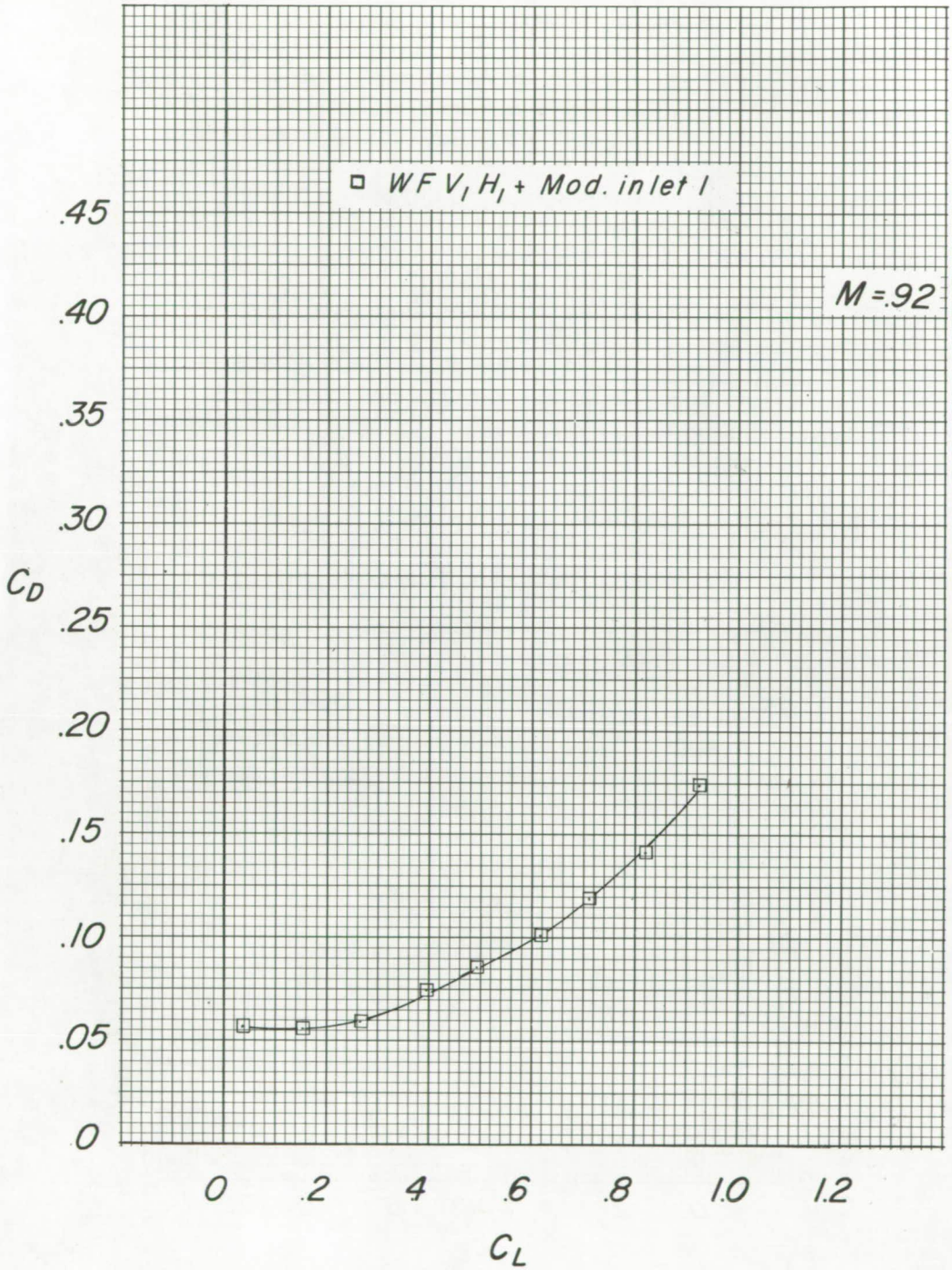

(d) Concluded.

Figure 12.- Concluded.

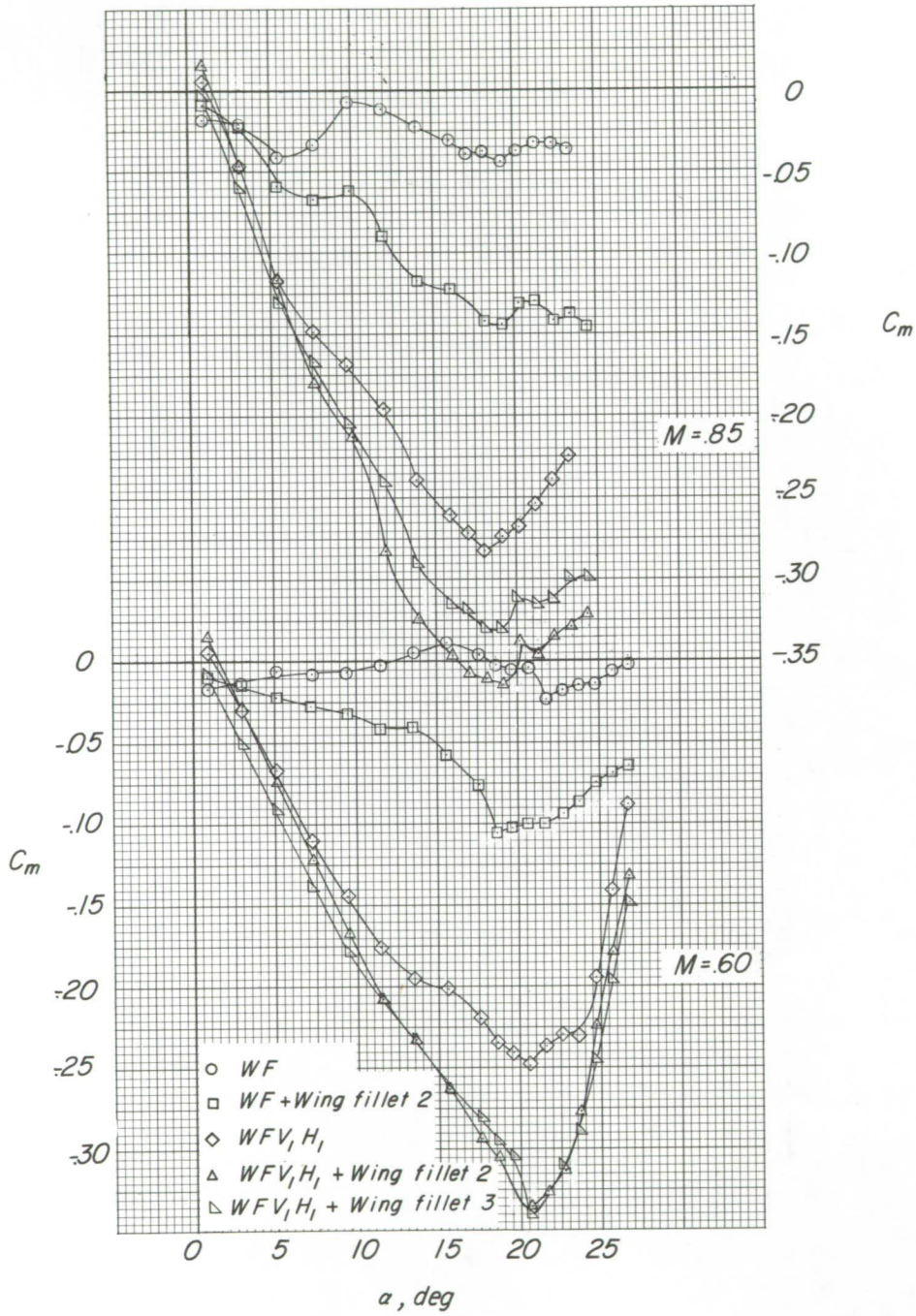

(a) C_m against α.

Figure 13.- Effect of wing-trailing-edge fillets on the longitudinal aerodynamic characteristics of the model.

DECLASSIFIED

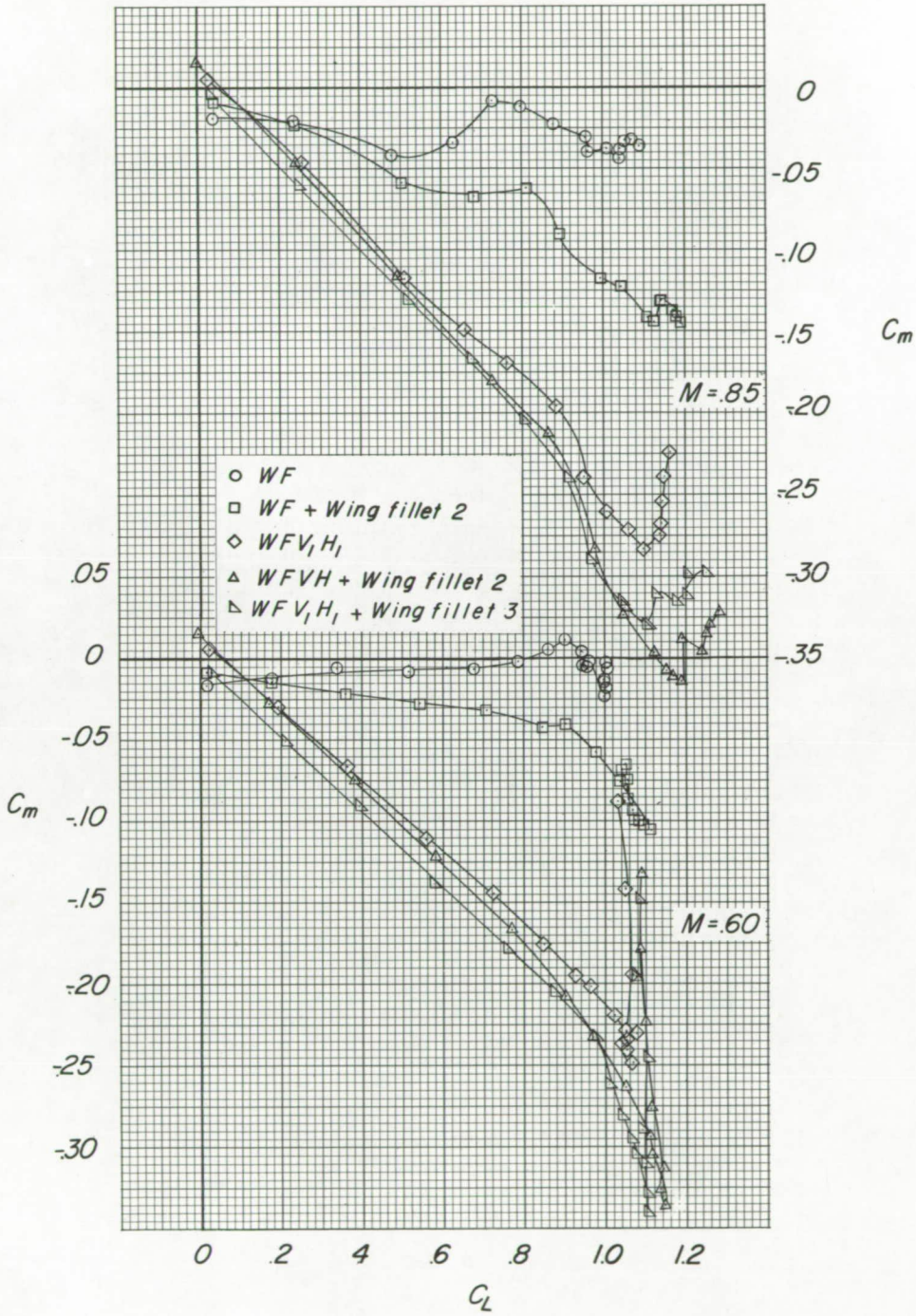

(b) C_m against C_L.

Figure 13.- Continued.

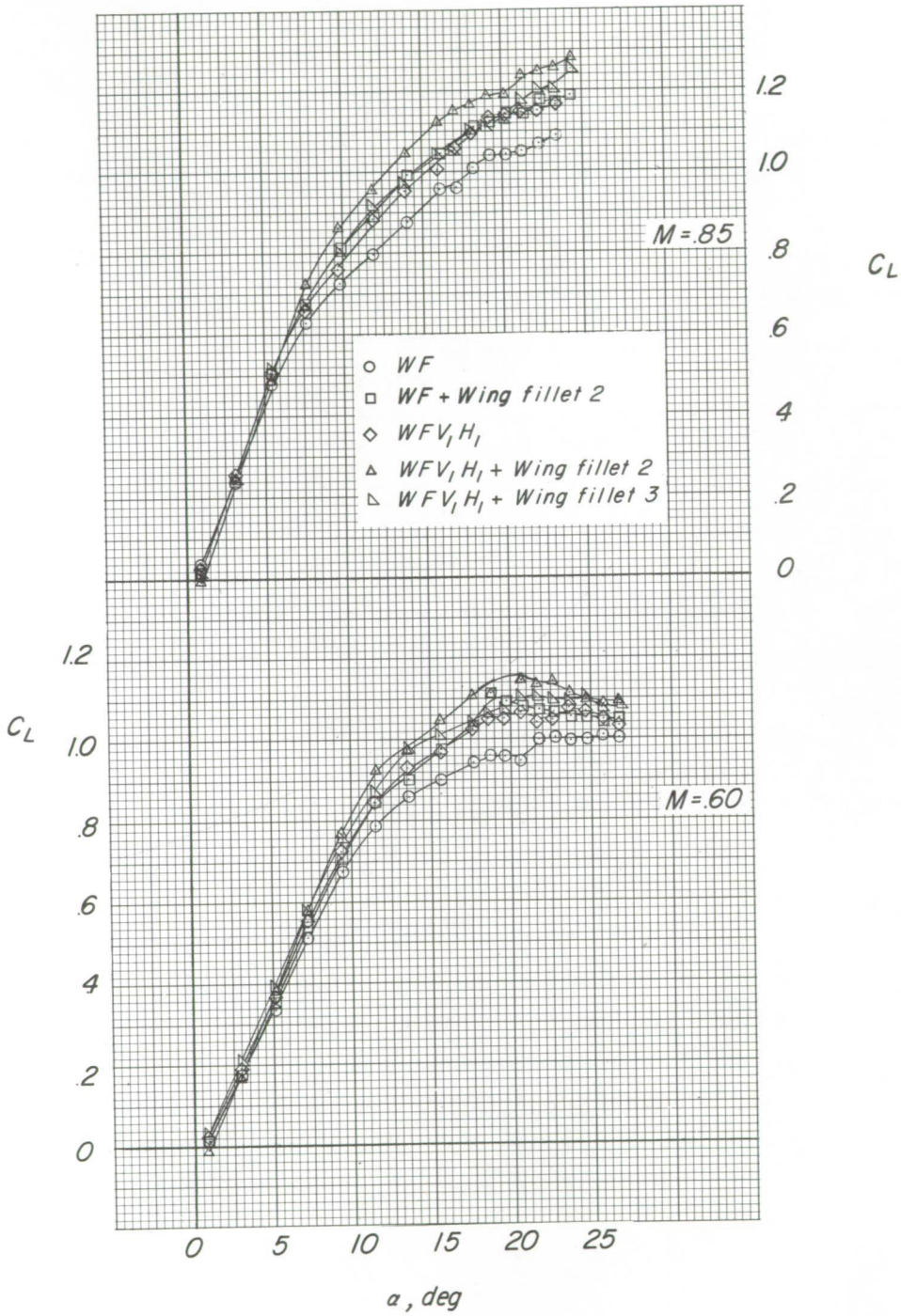

(c) C_L against α.

Figure 13.- Continued.

DECLASSIFIED

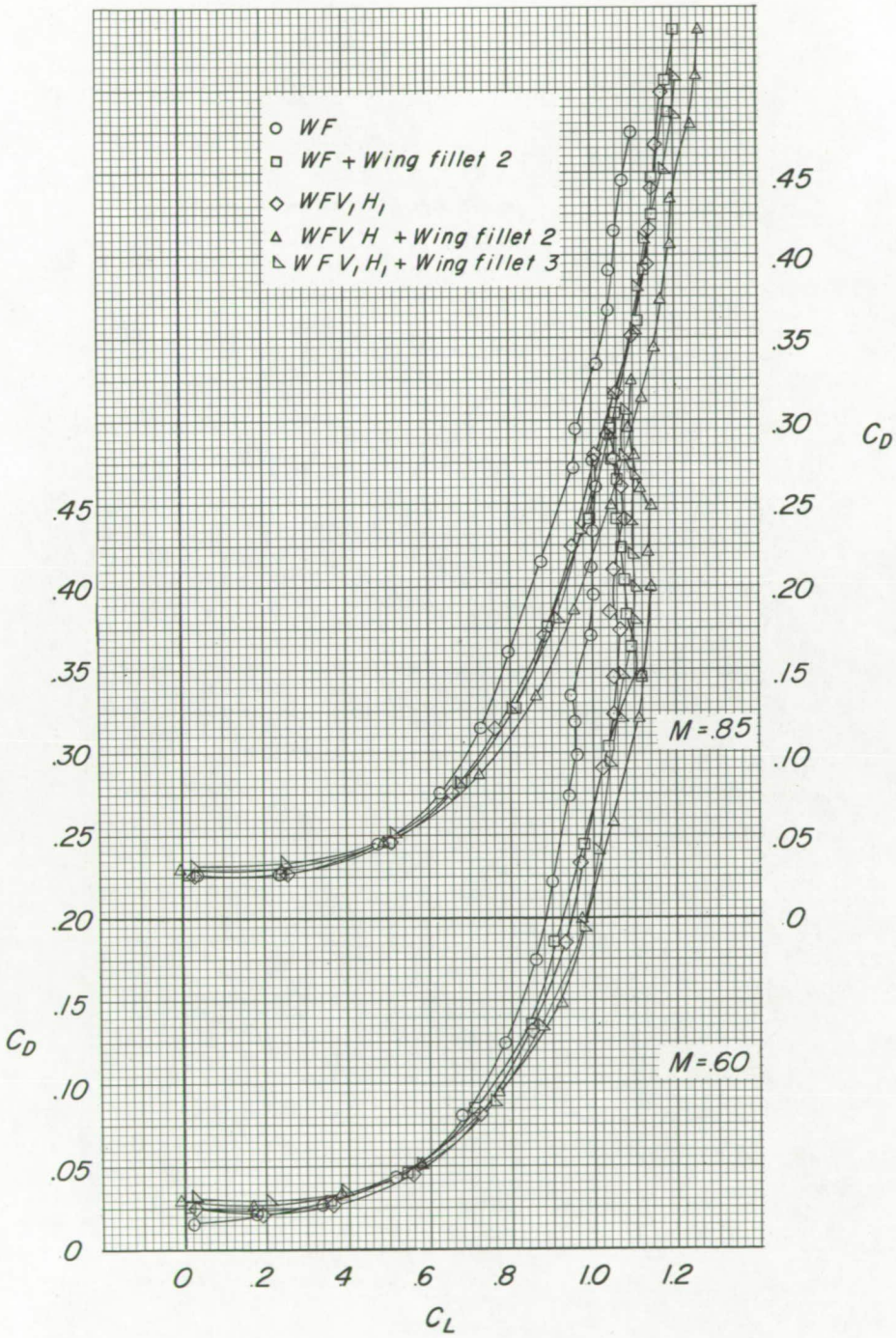

(d) C_D against C_L.

Figure 13.- Concluded.

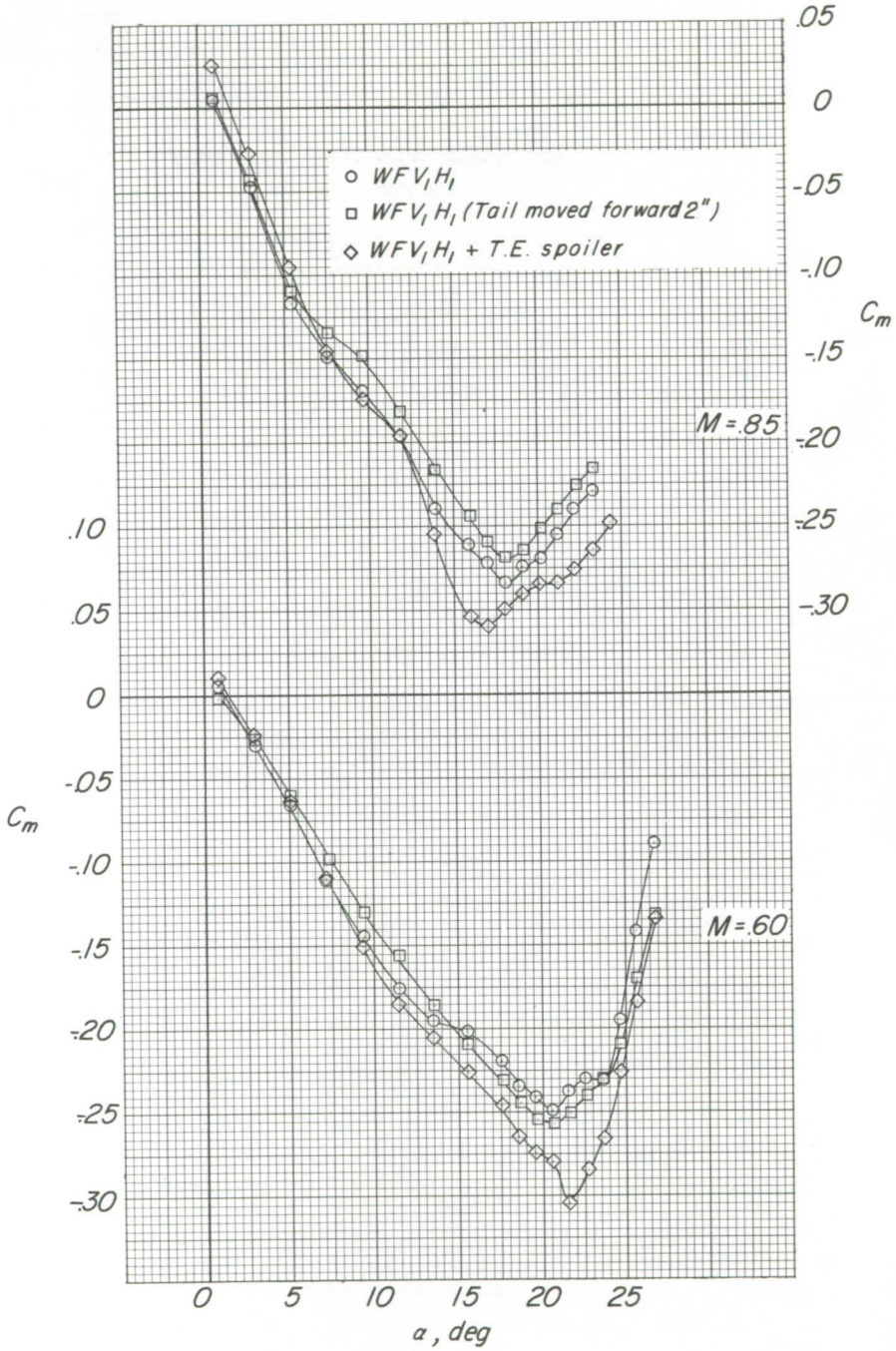

(a) C_m against α.

Figure 14.- Effect of tail position and spoilers on the longitudinal aerodynamic characteristics of the model.

DECLASSIFIED

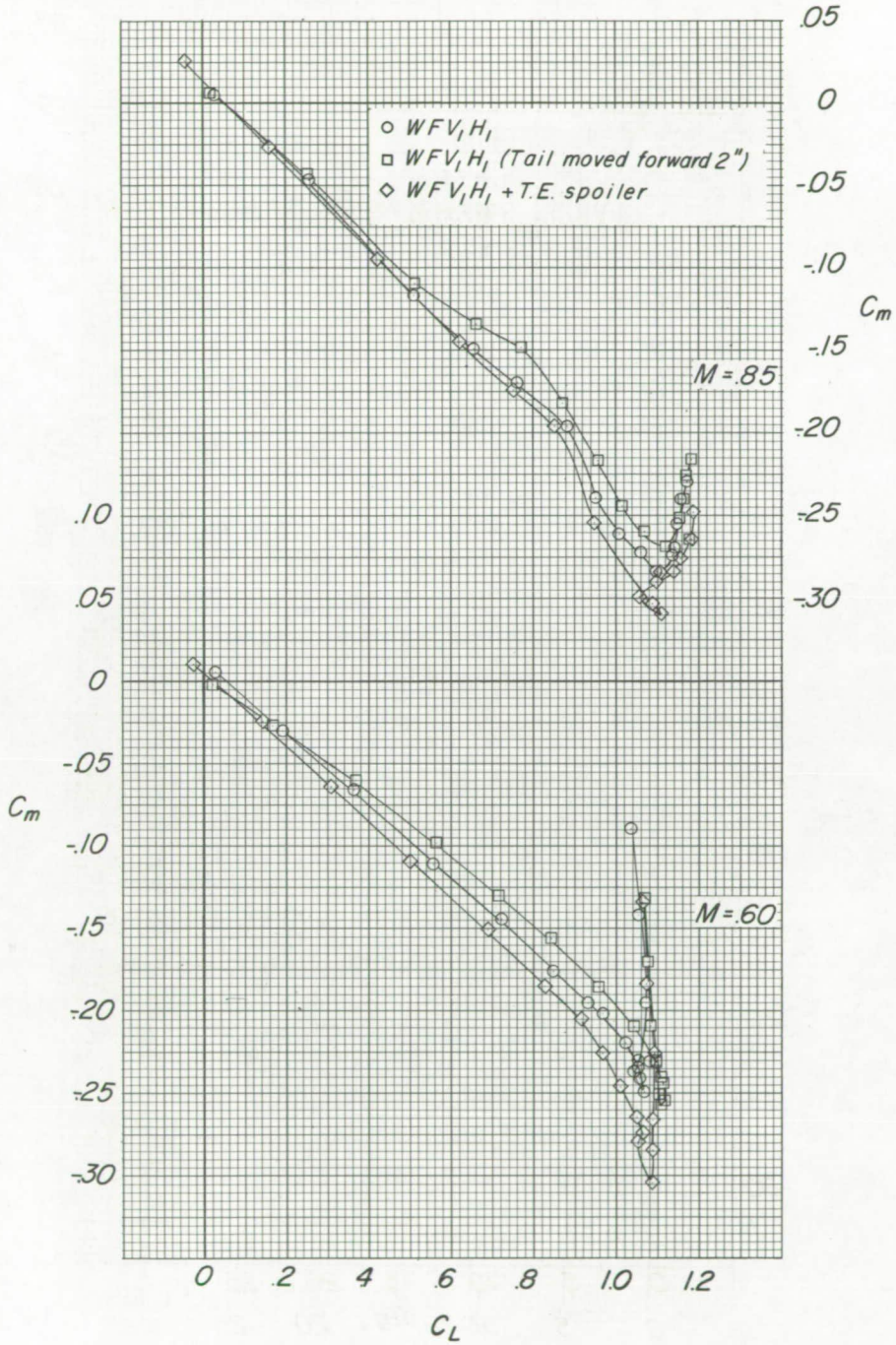

(b) C_m against C_L.

Figure 14.- Continued.

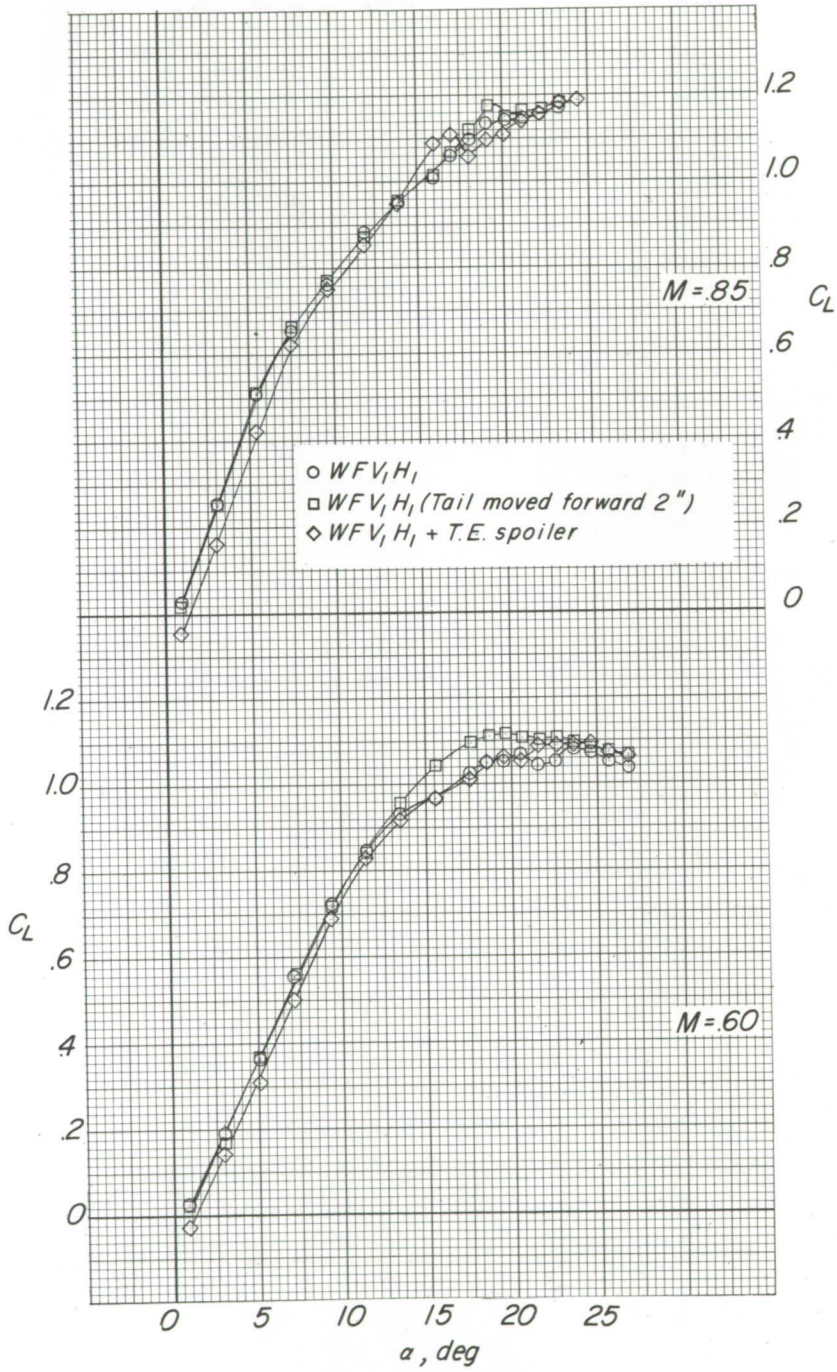

(c) C_L against α.

Figure 14.- Continued.

DECLASSIFIED

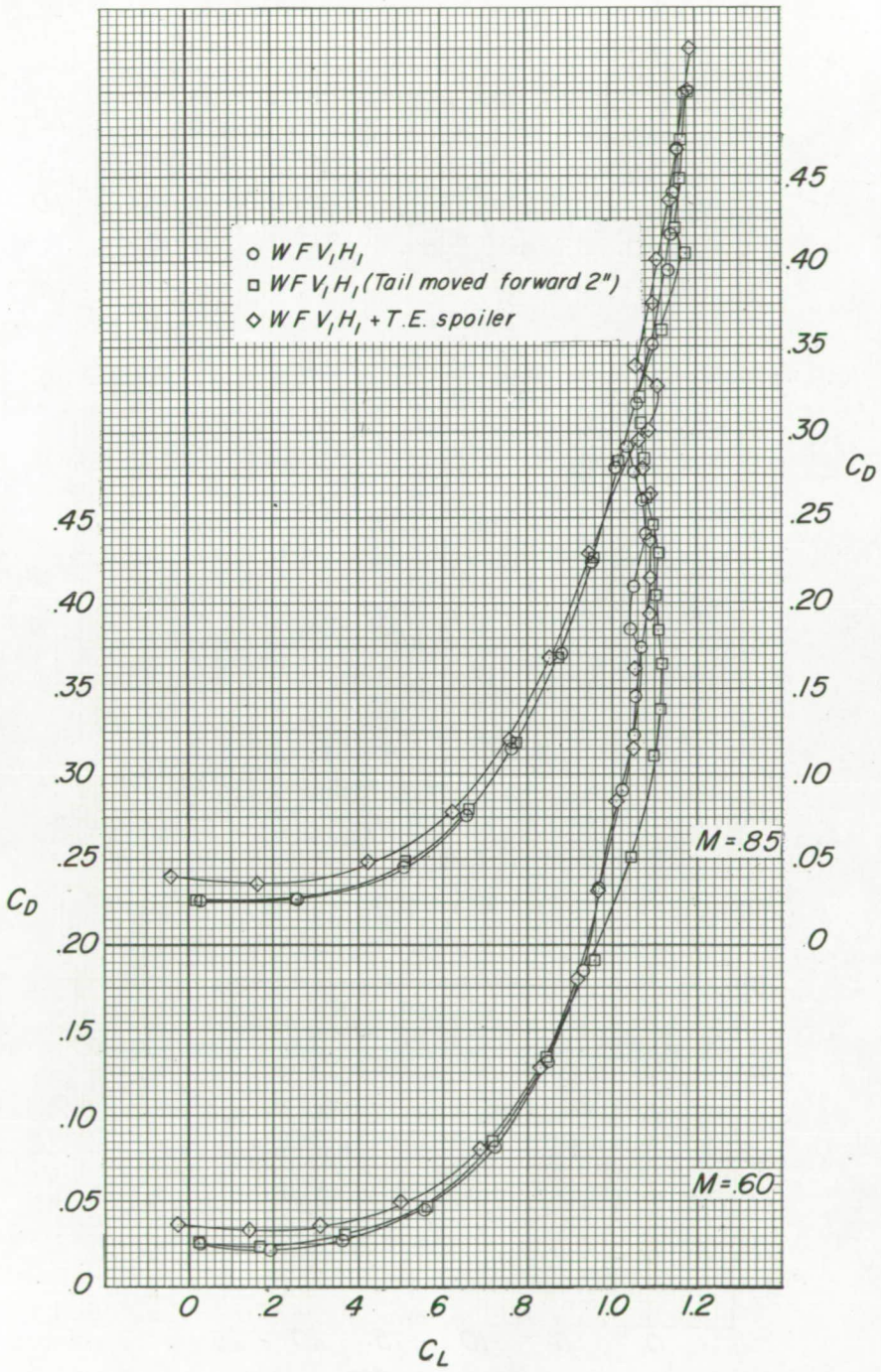

(d) C_D against C_L.

Figure 14.- Concluded.

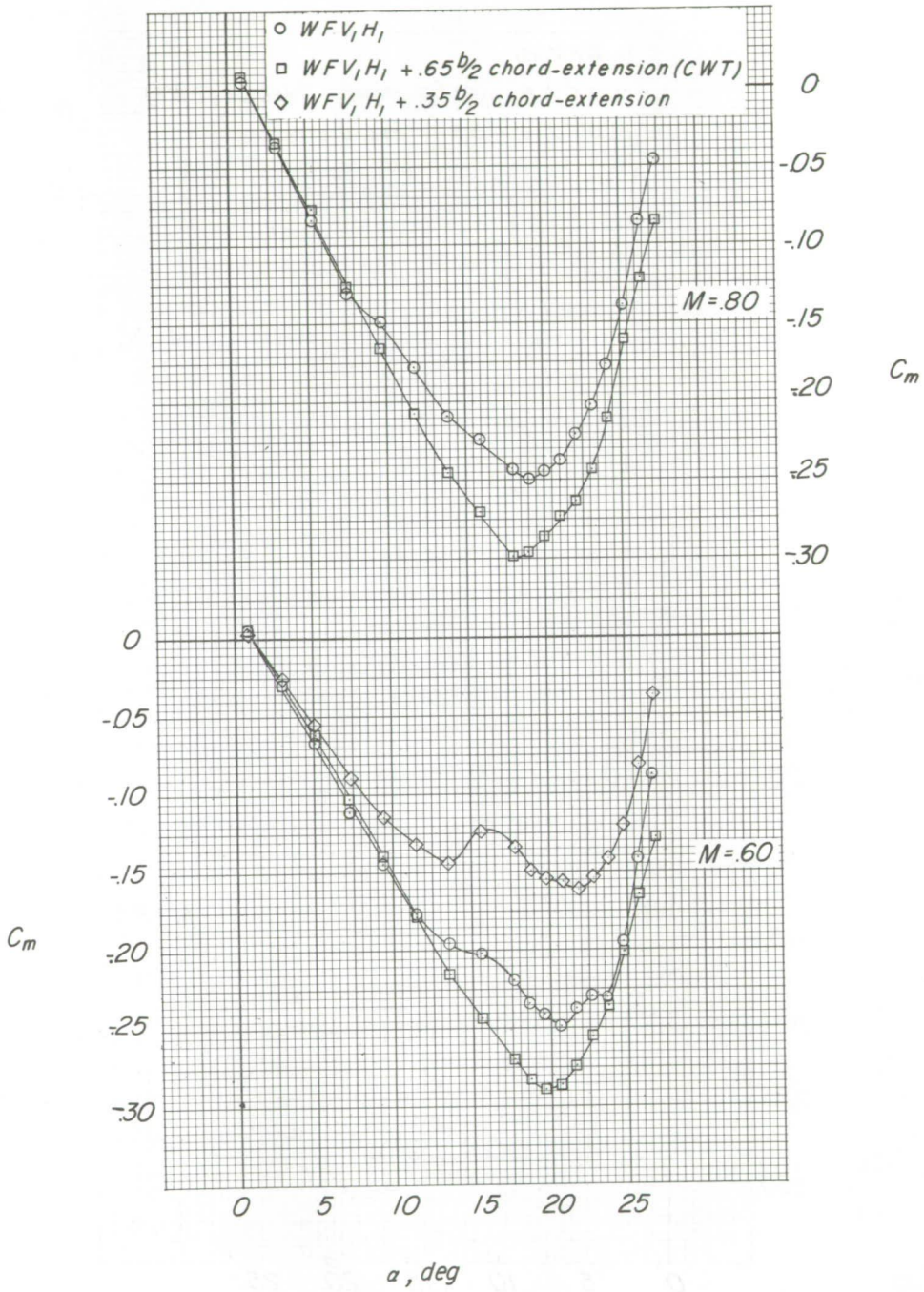

(a) C_m against α.

Figure 15.- Effect of chord-extensions on the longitudinal aerodynamic characteristics of the model.

DECLASSIFIED

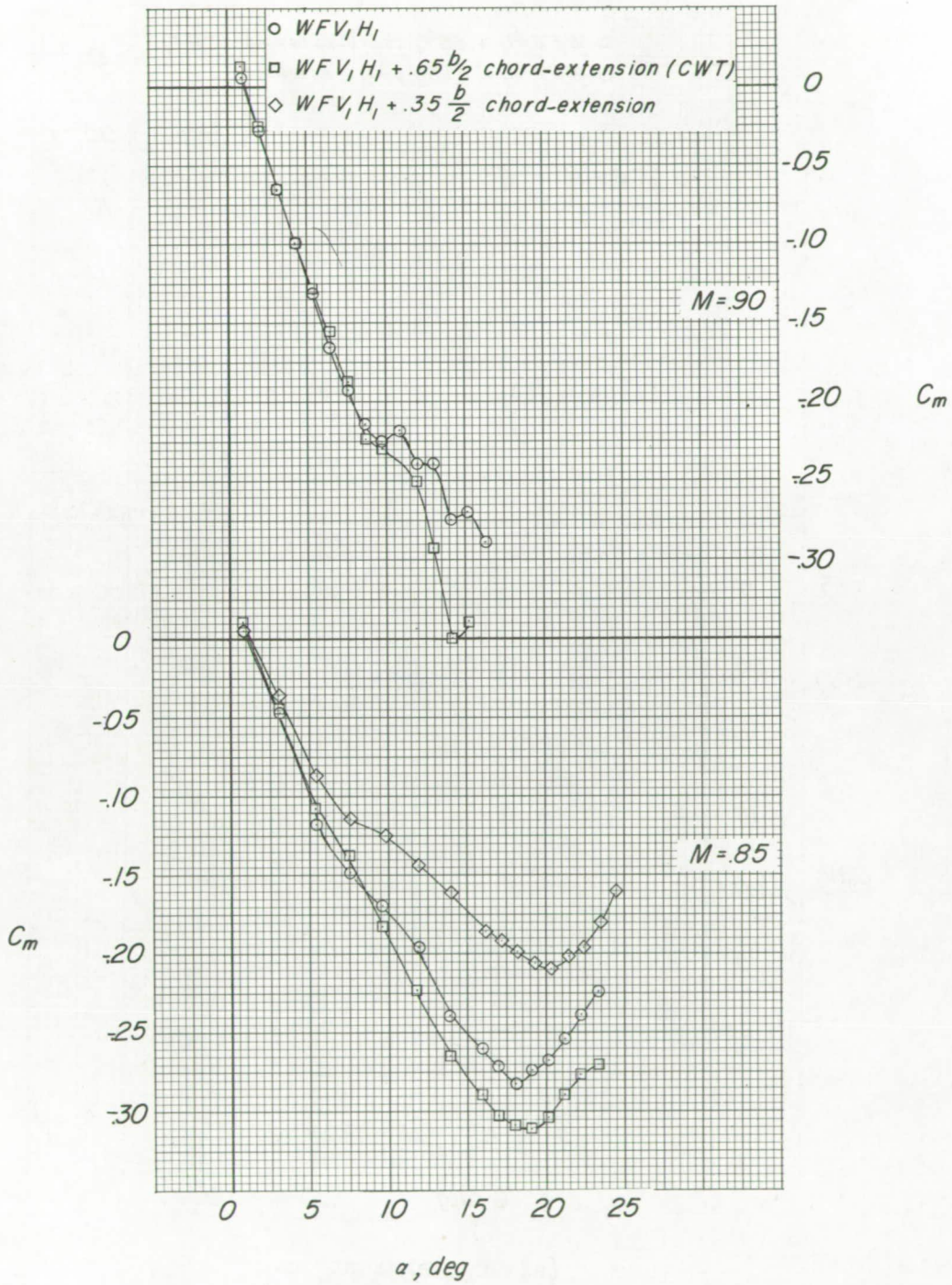

(a) Continued.

Figure 15.- Continued.

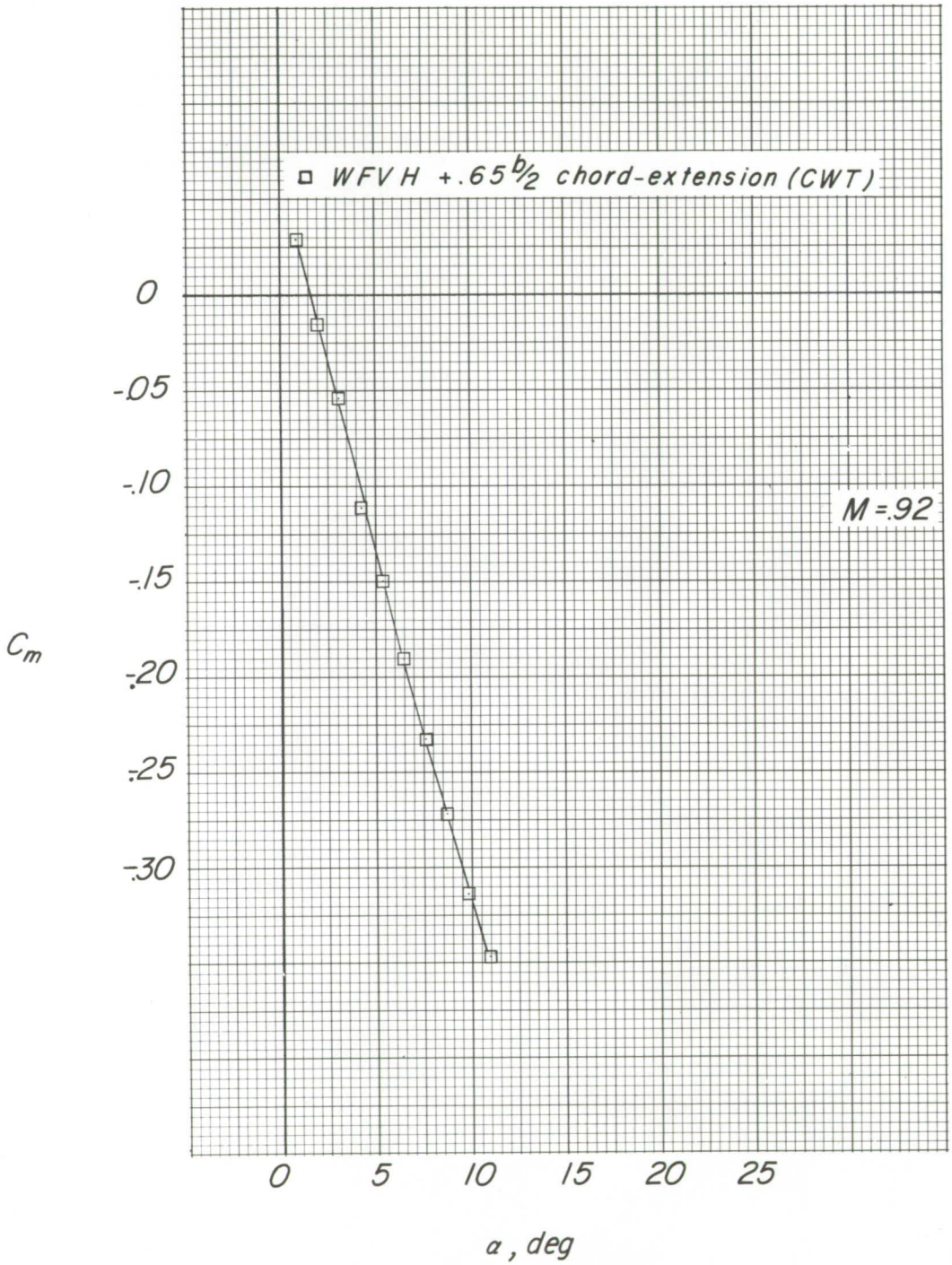

(a) Concluded.

Figure 15.- Continued.

DECLASSIFIED

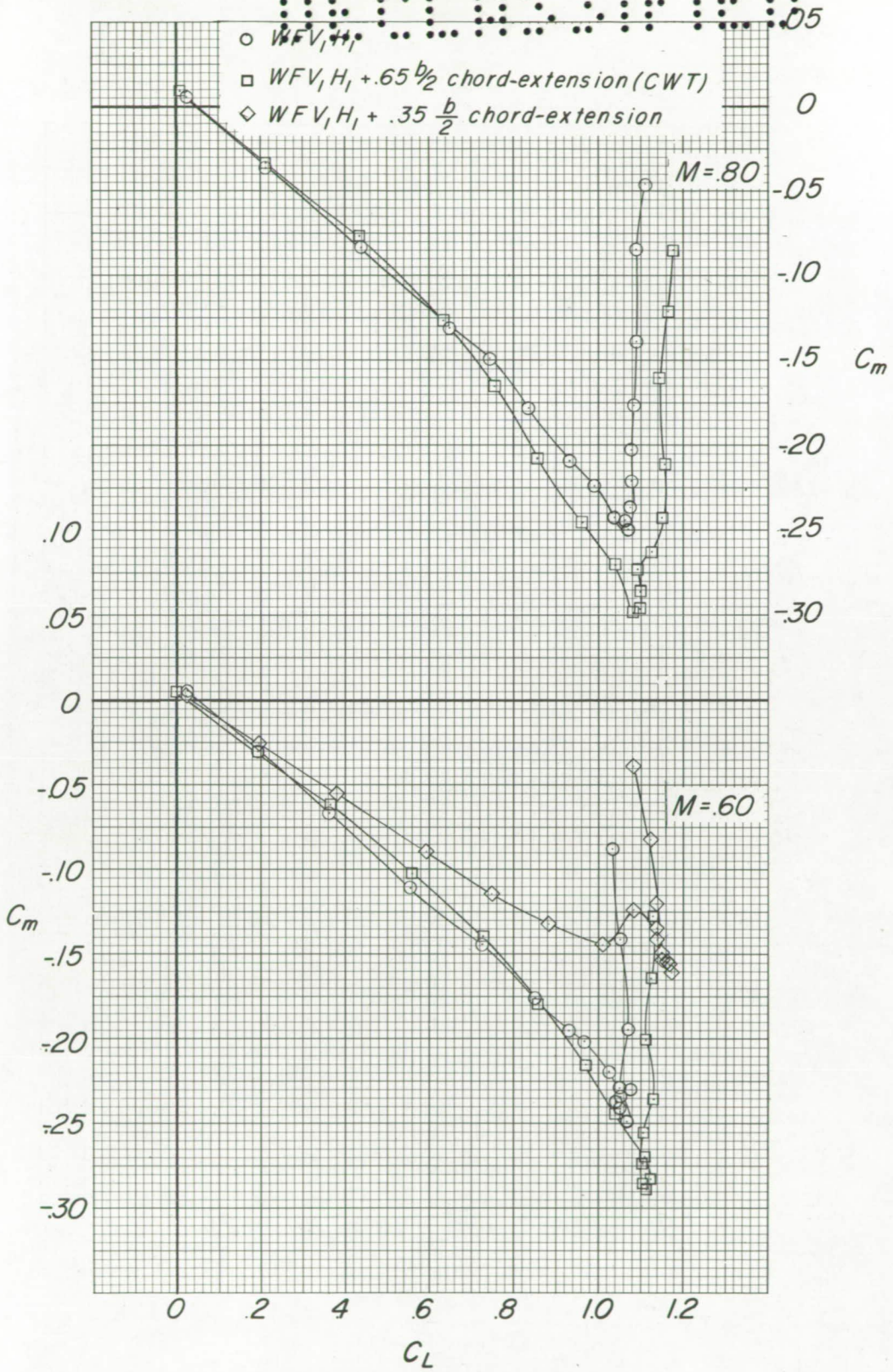

(b) C_m against C_L.

Figure 15.- Continued.

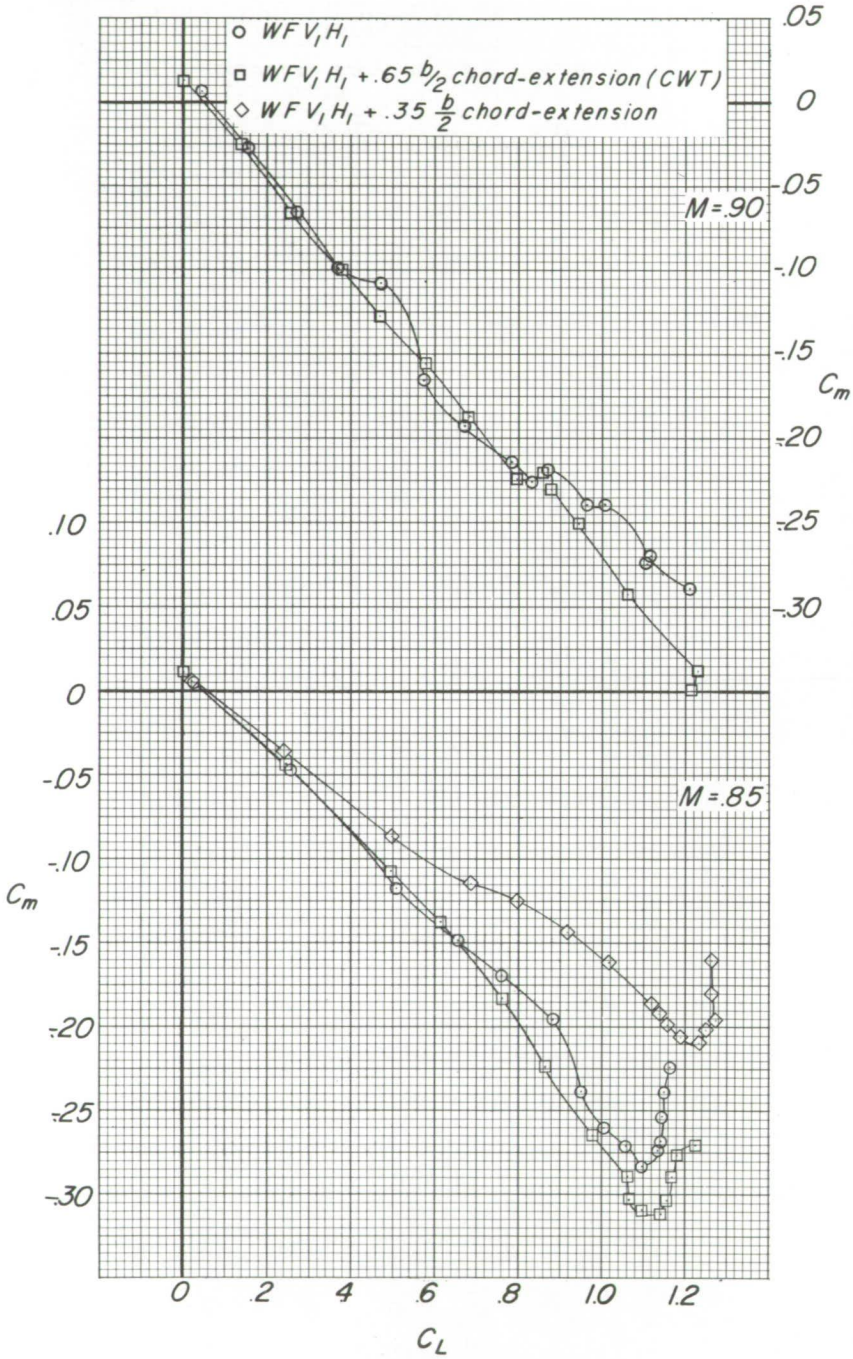

(b) Continued.

Figure 15.- Continued.

DECLASSIFIED

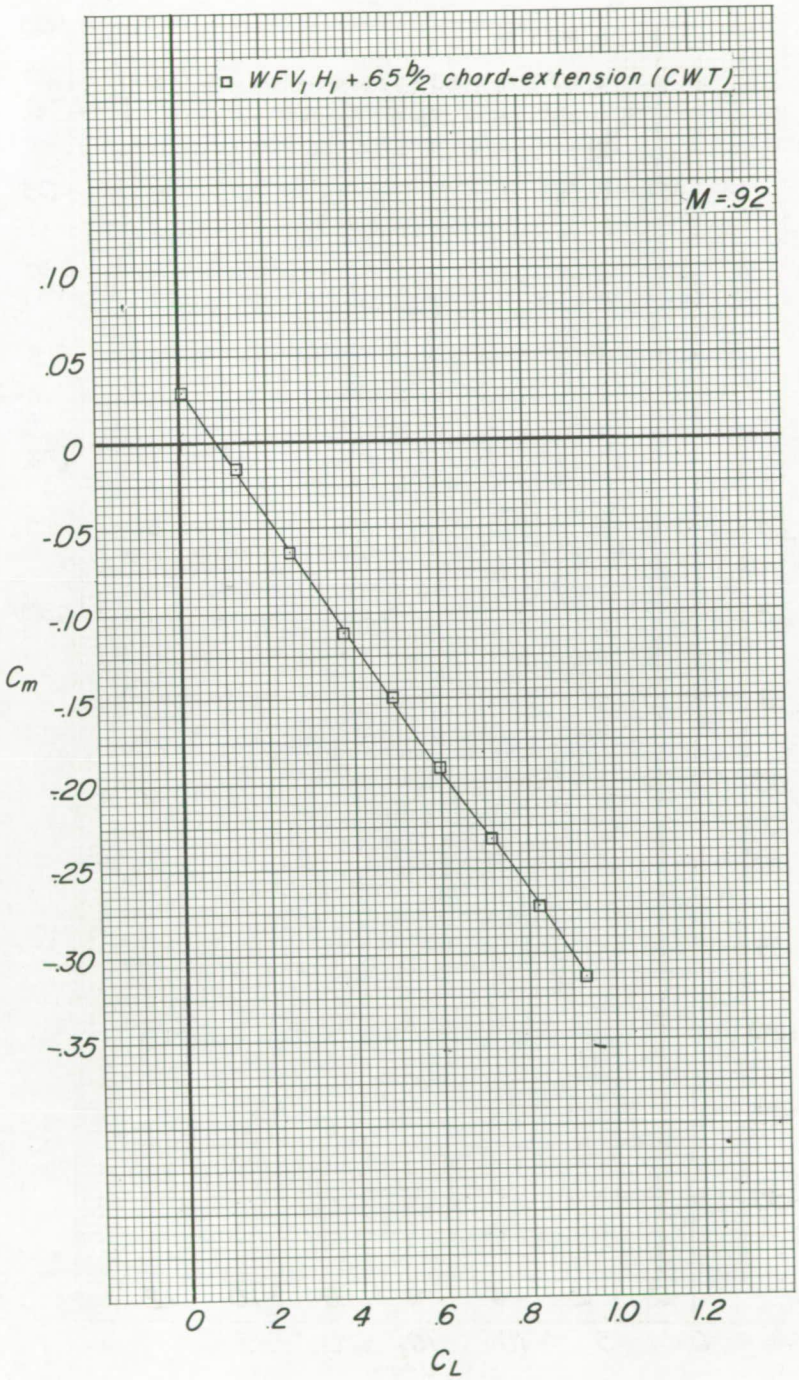

(b) Concluded.

Figure 15.- Continued.

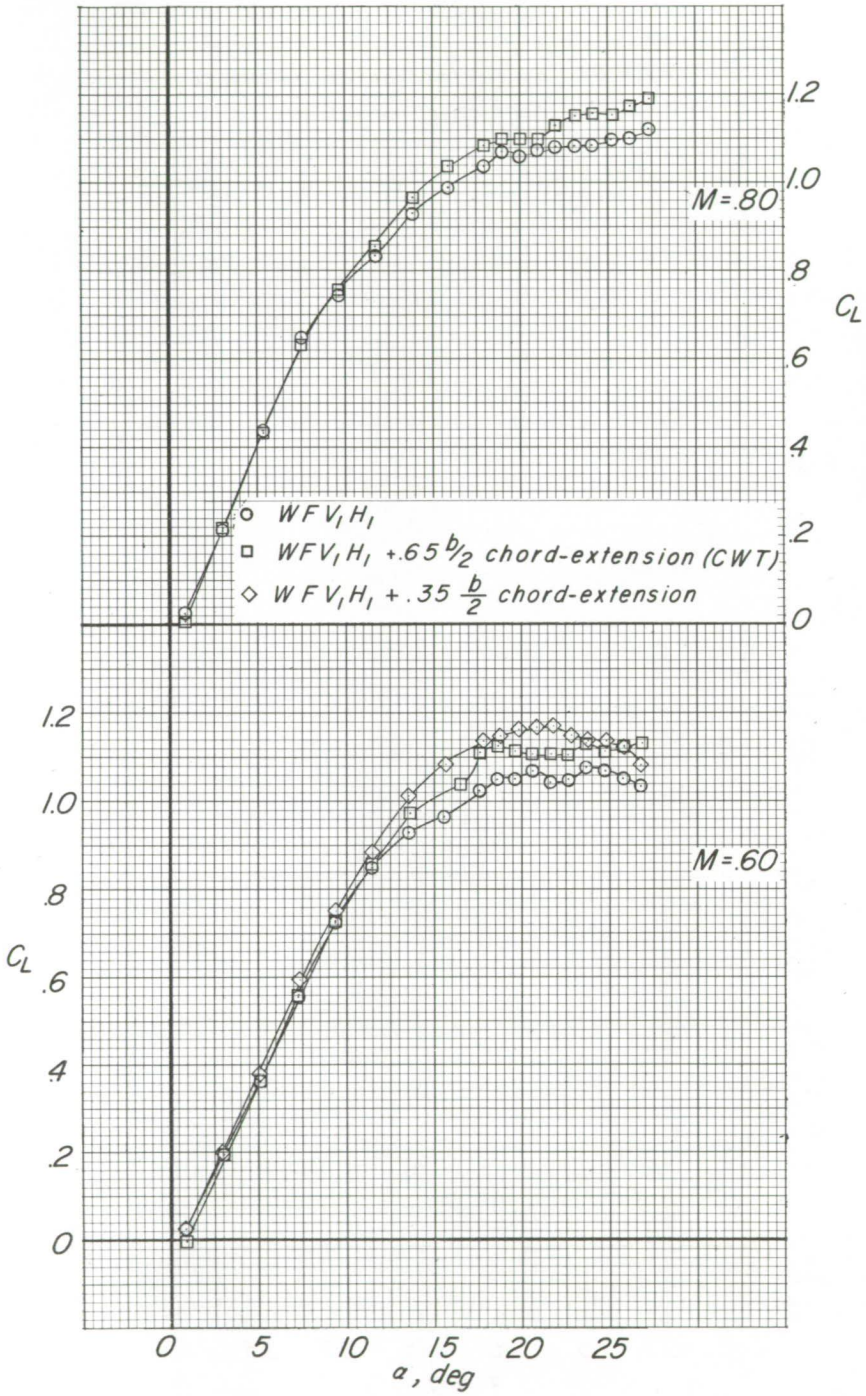

(c) C_L against α.

Figure 15.- Continued.

DECLASSIFIED

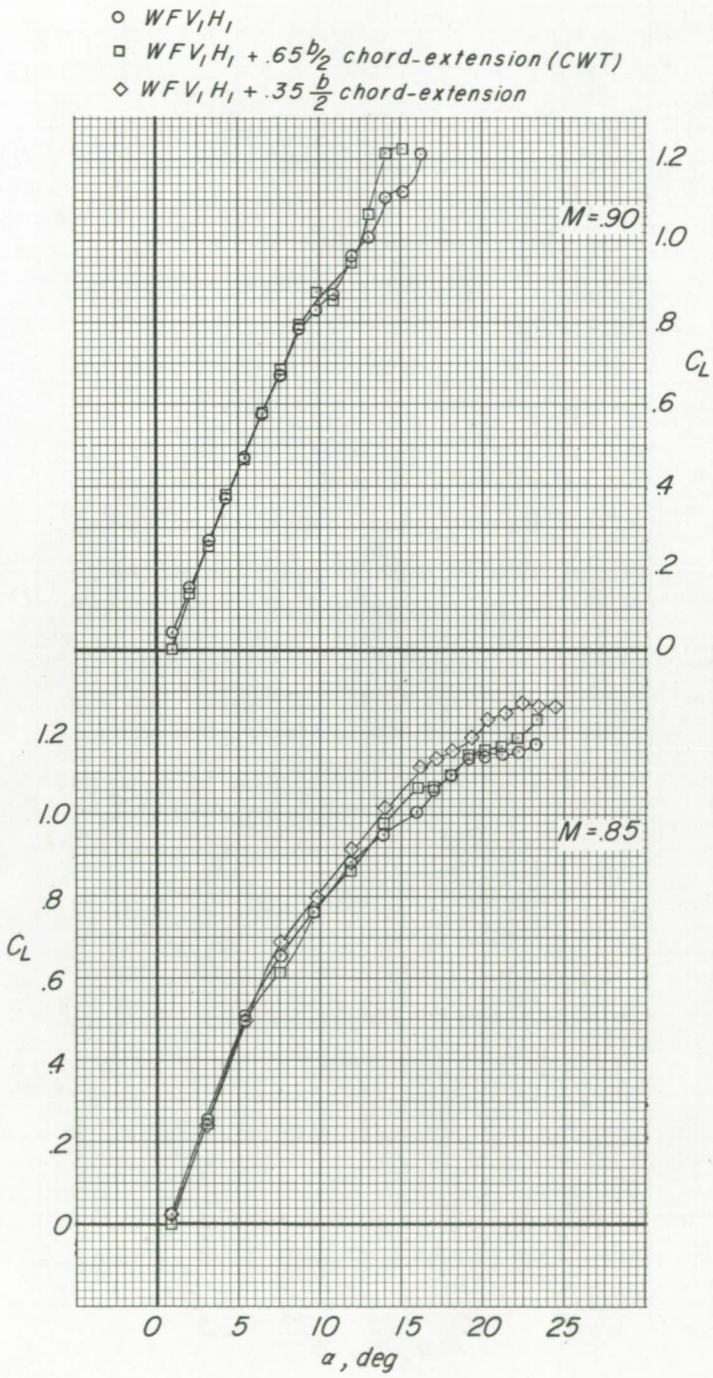

(c) Continued.

Figure 15.- Continued.

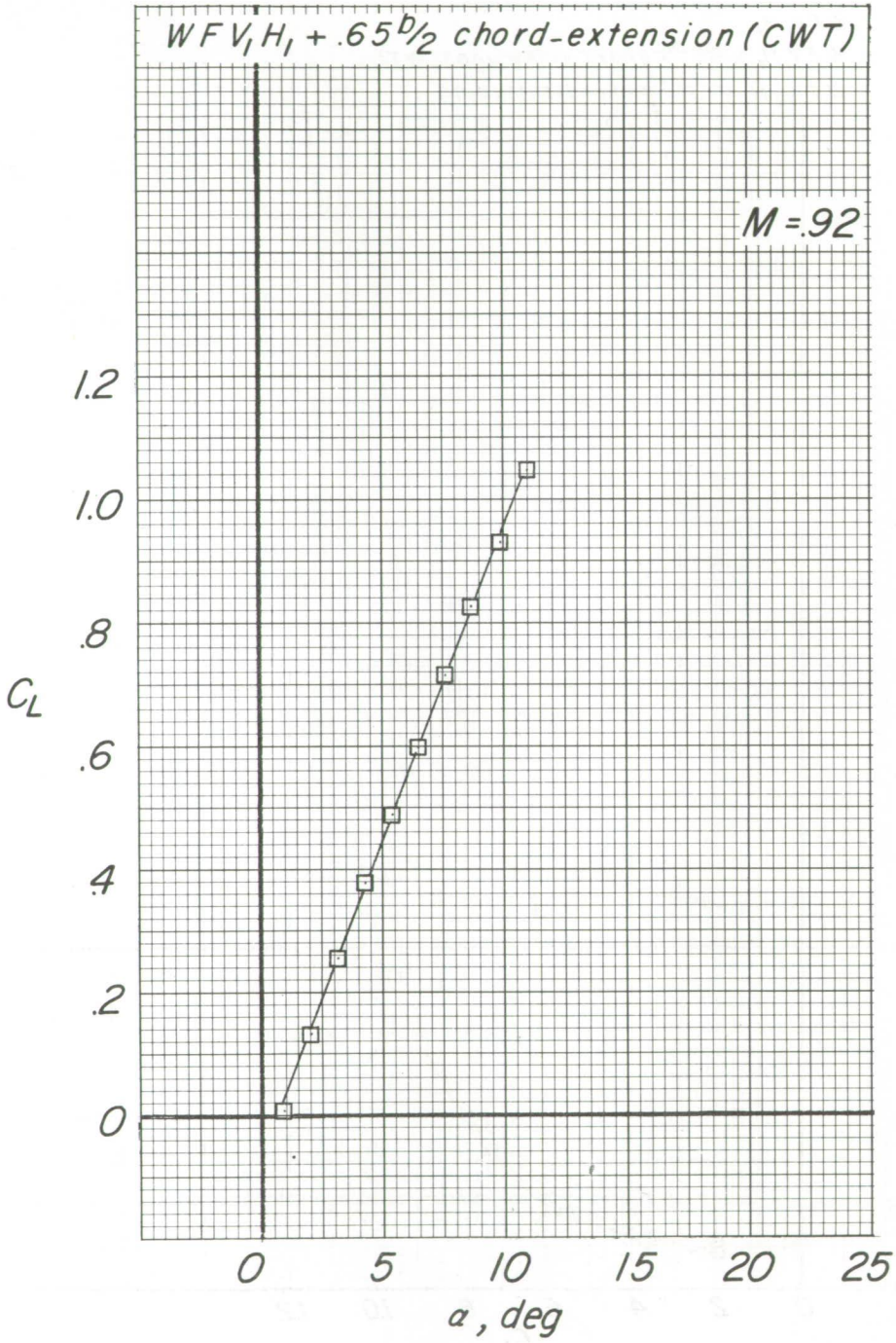

(c) Concluded.

Figure 15.- Continued.

DECLASSIFIED

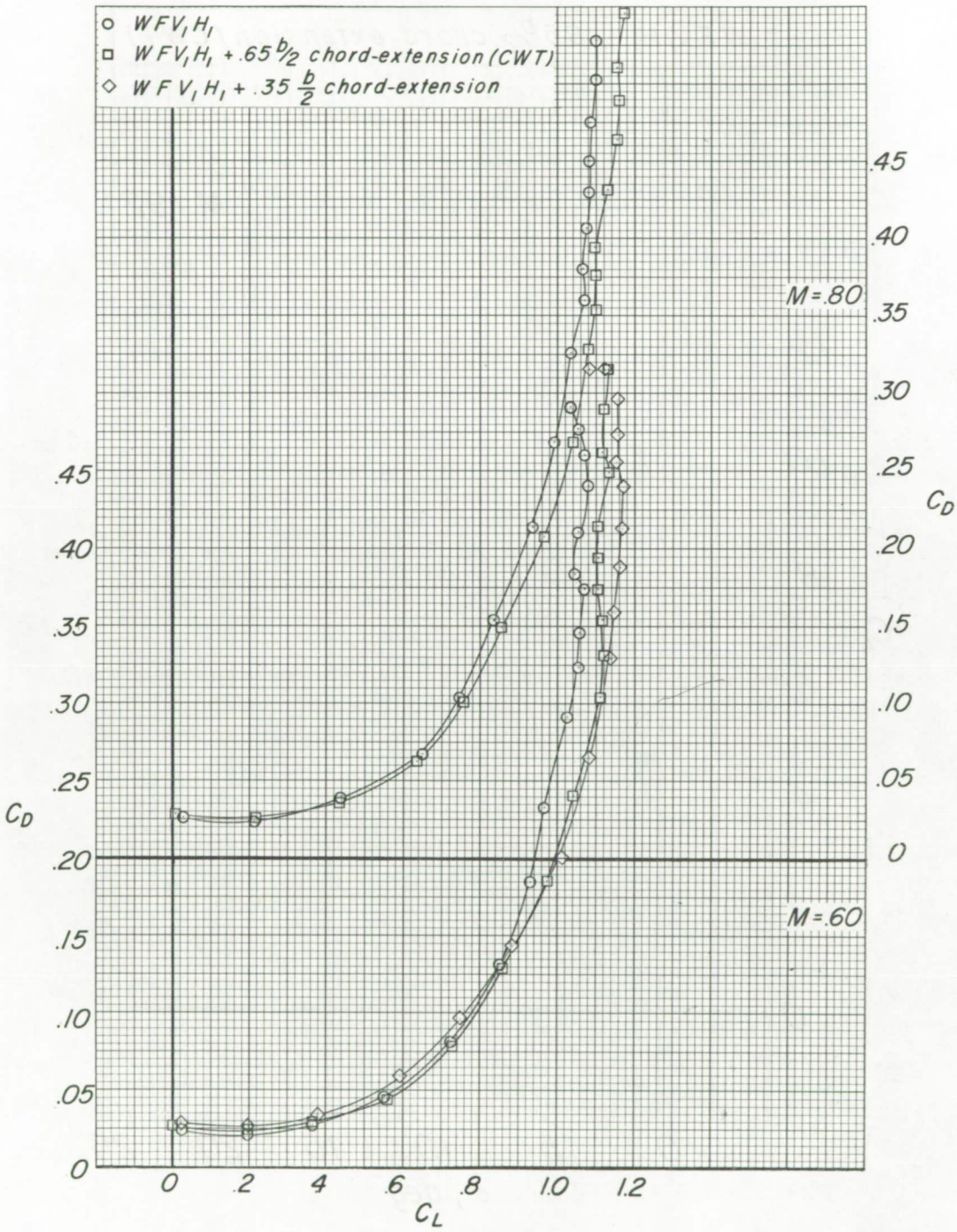

(d) C_D against C_L.

Figure 15.- Continued.

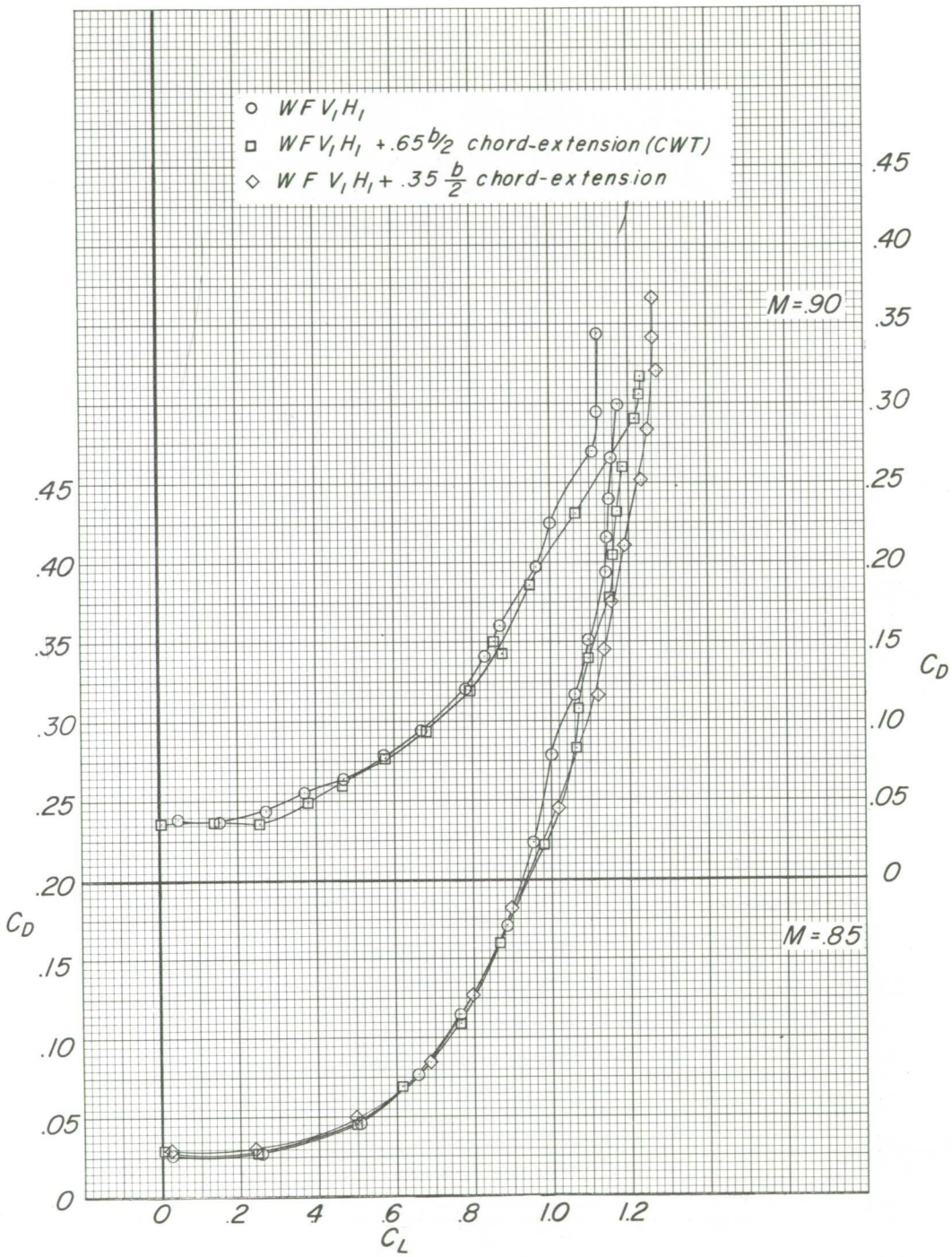

(d) Continued.

Figure 15.- Continued.

DECLASSIFIED

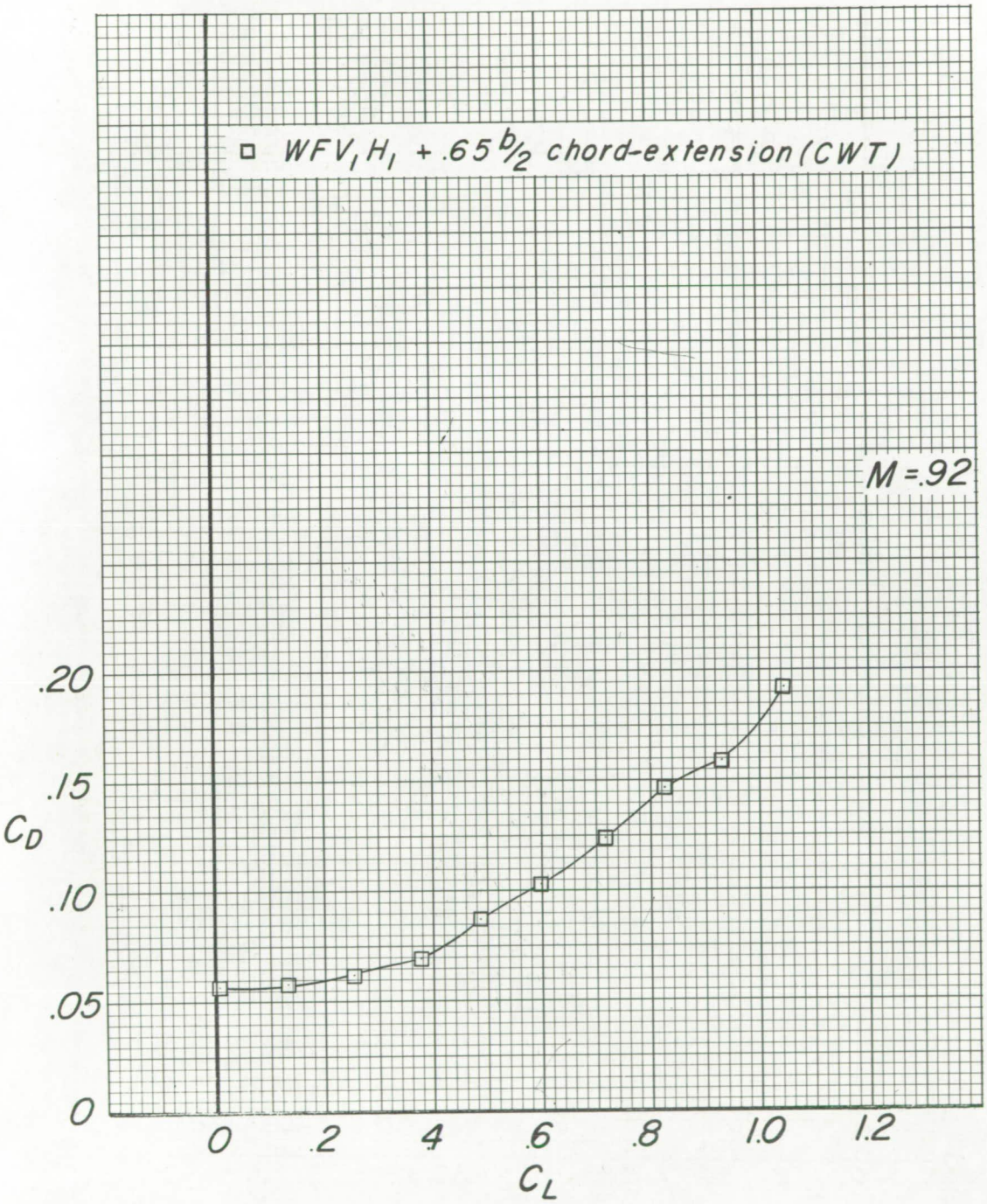

(d) Concluded.

Figure 15.- Concluded.

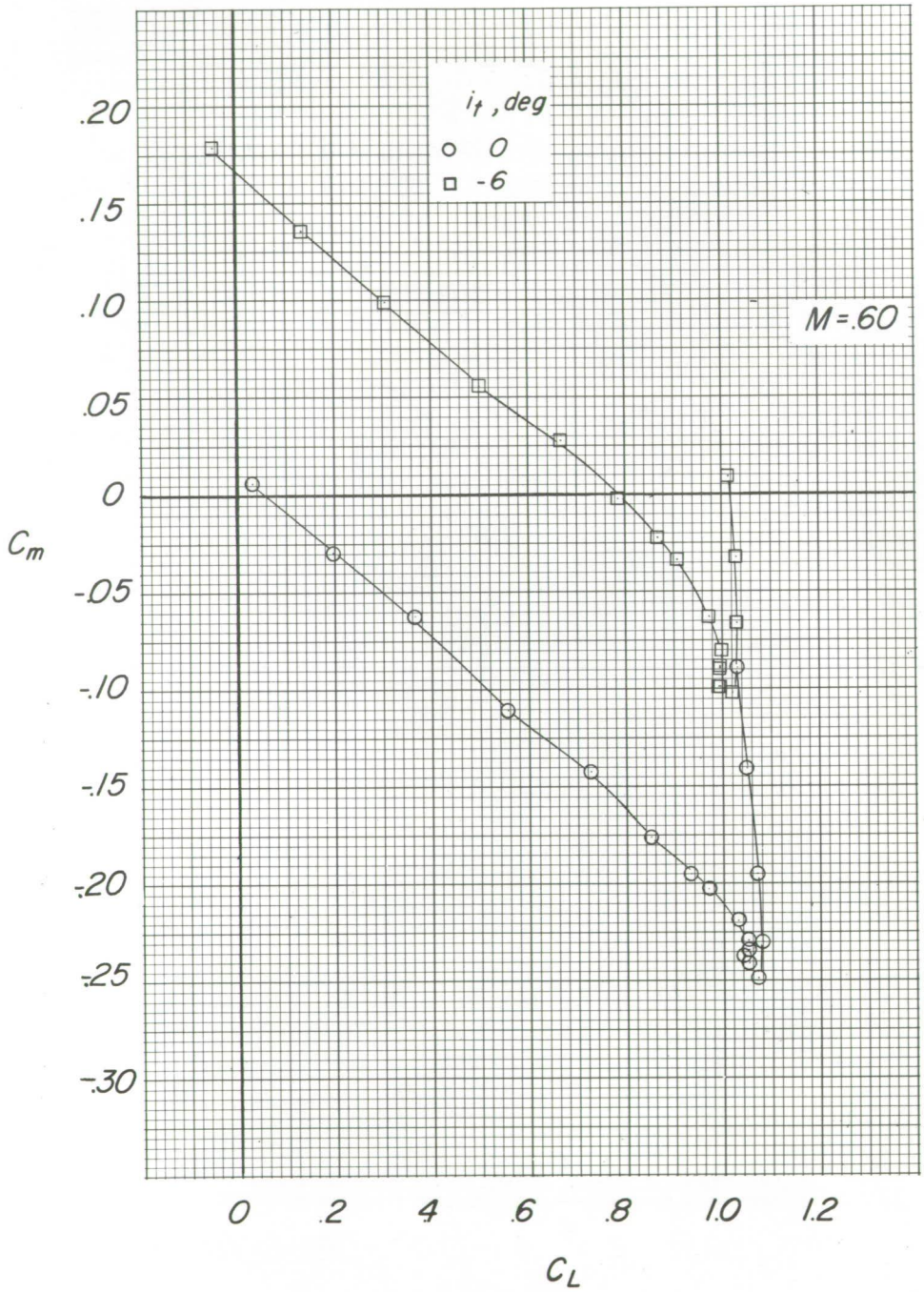

(a) C_m against C_L.

Figure 16.- Effect of stabilizer deflection on the longitudinal aerodynamic characteristics of the model with the new vertical and horizontal tail. WFV_1H_1.

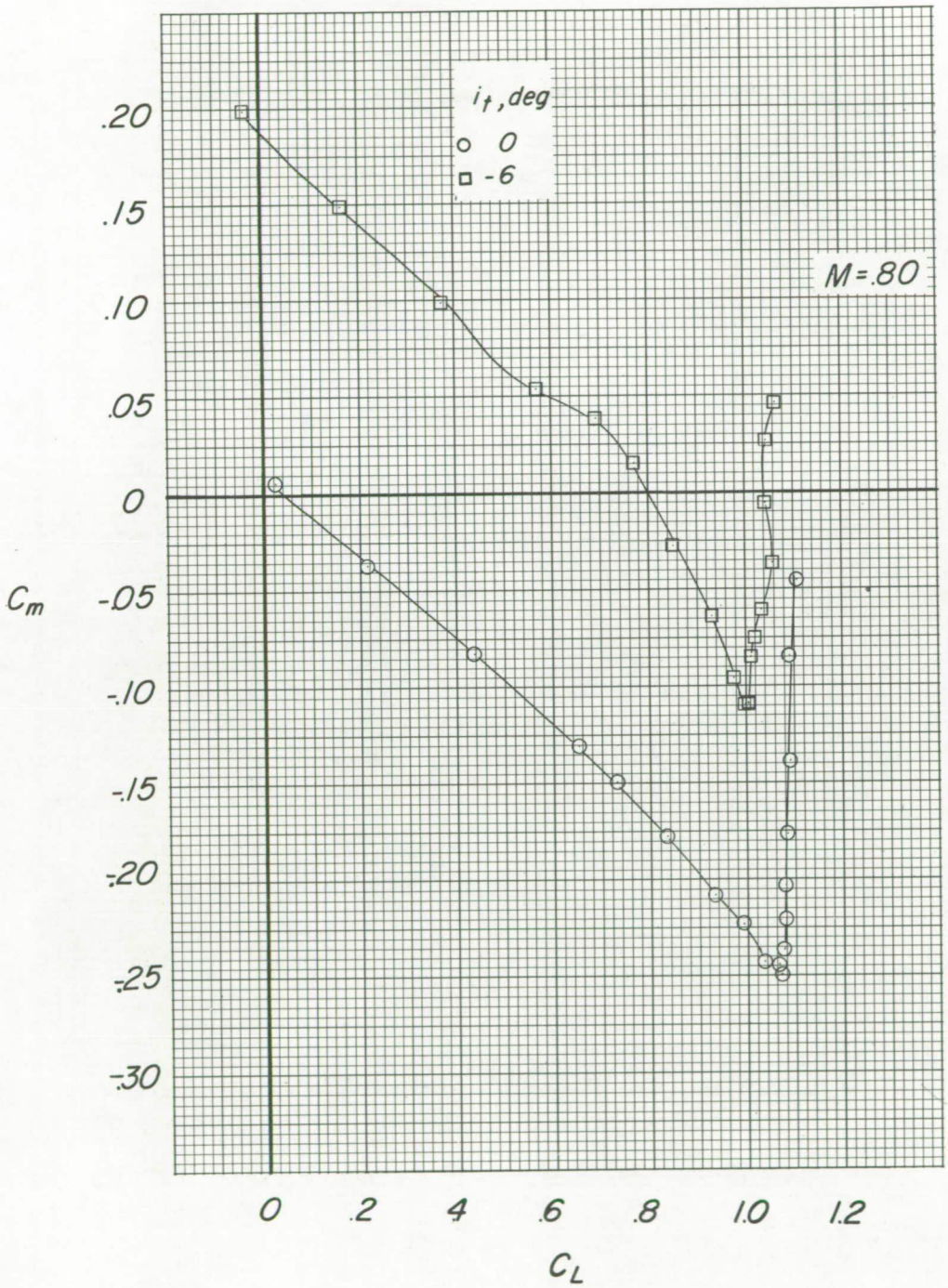

(a) Continued.

Figure 16.- Continued.

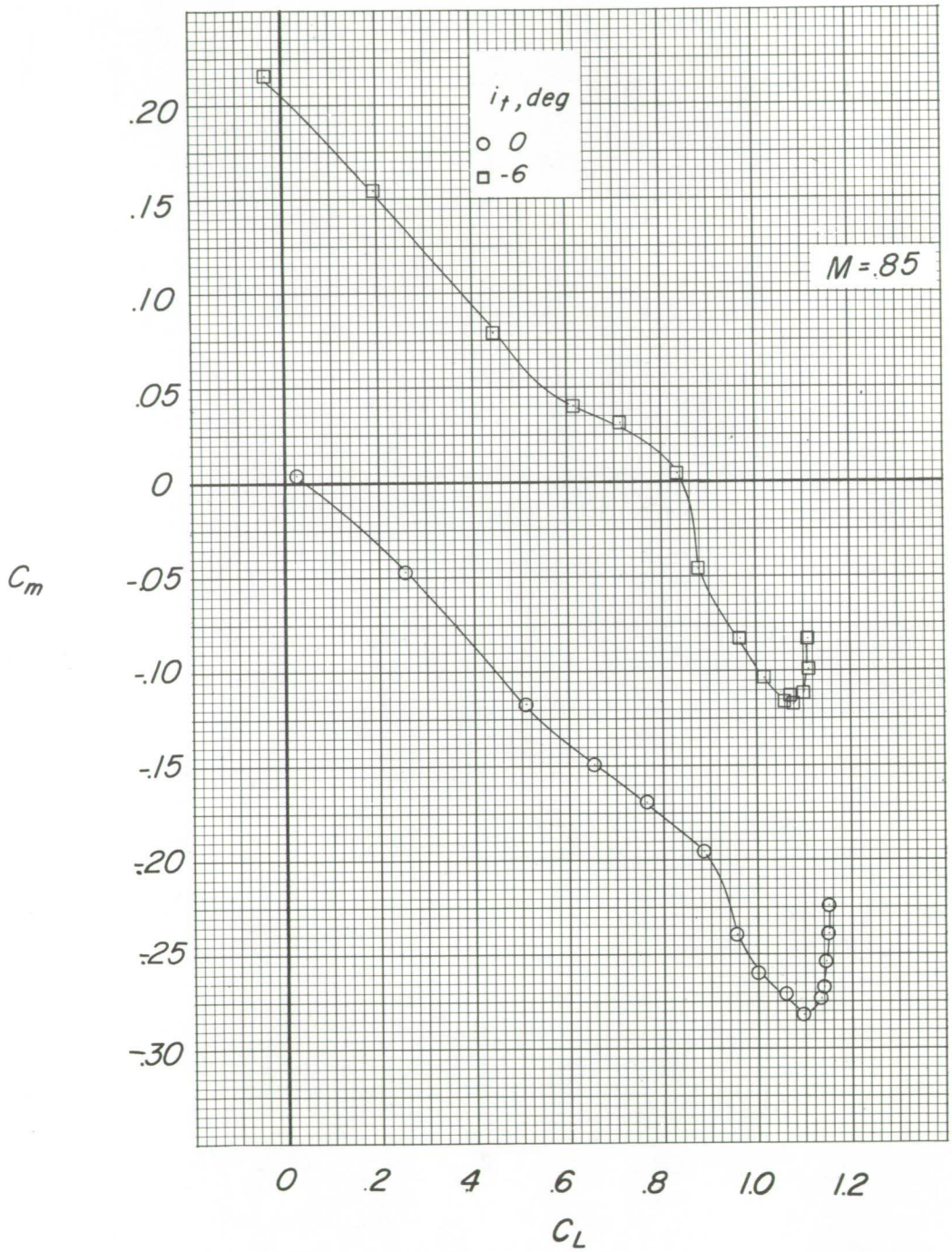

(a) Continued.

Figure 16.- Continued.

DECLASSIFIED

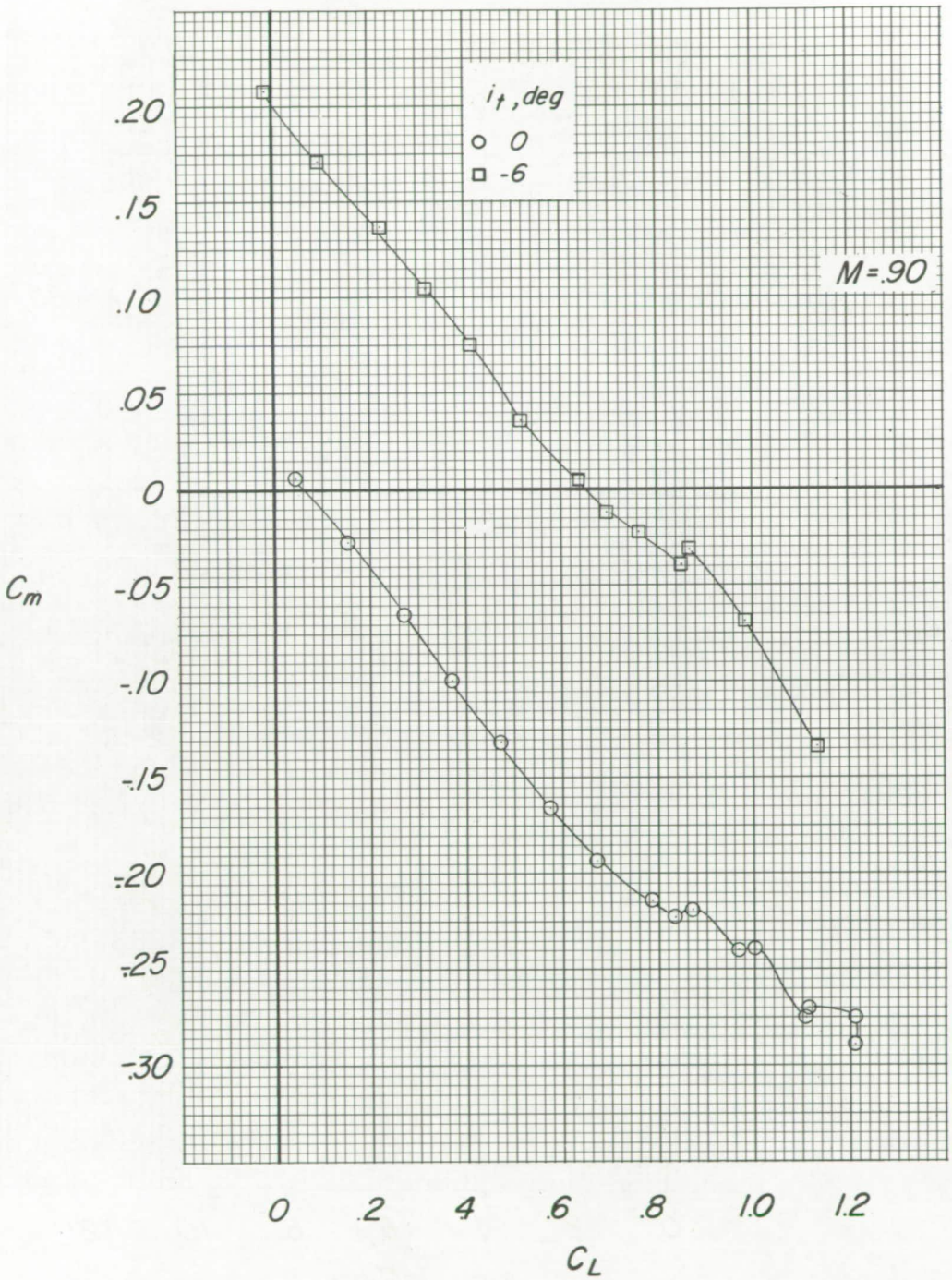

(a) Continued.

Figure 16.- Continued.

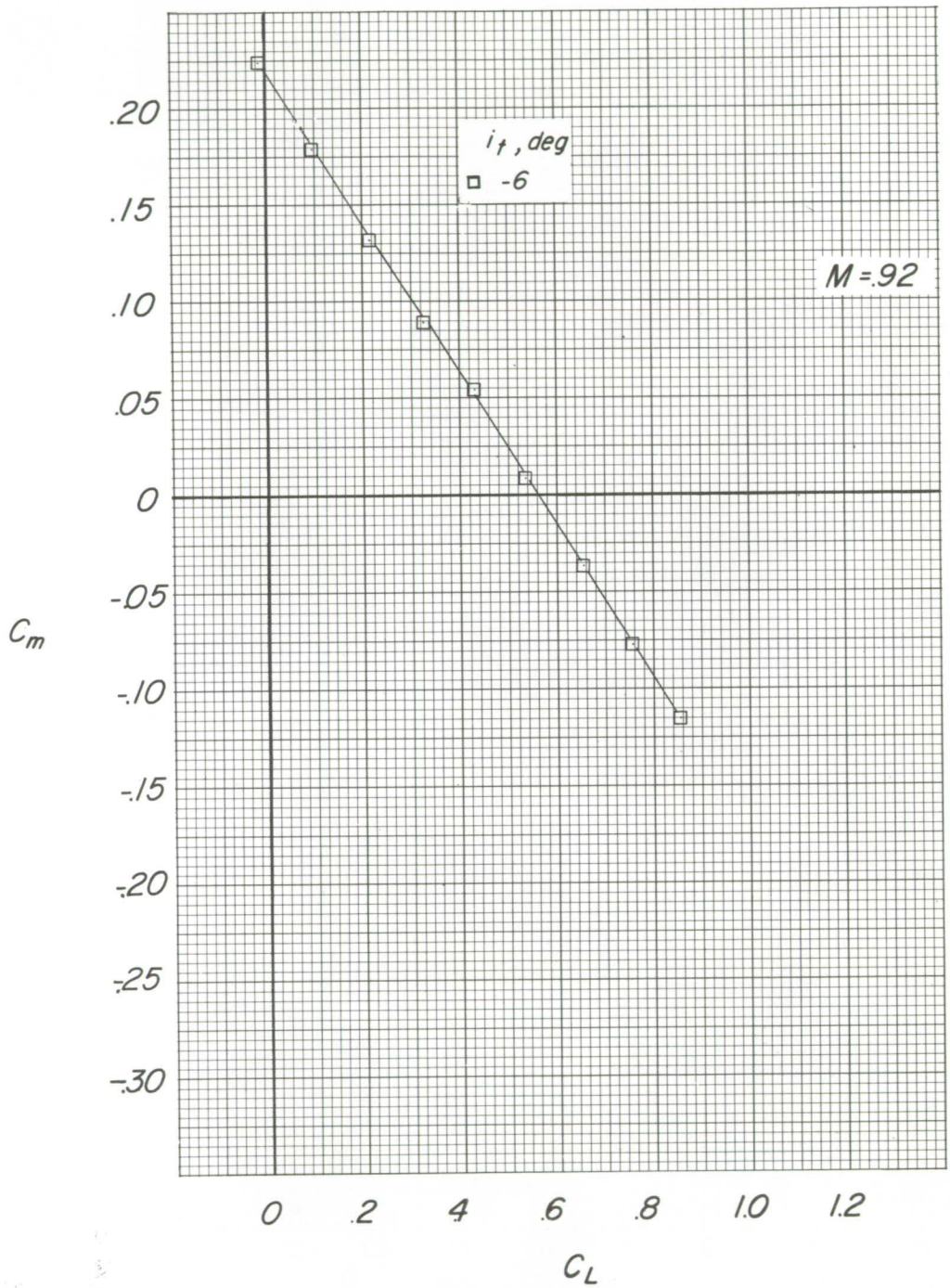

(a) Concluded.

Figure 16.- Continued.

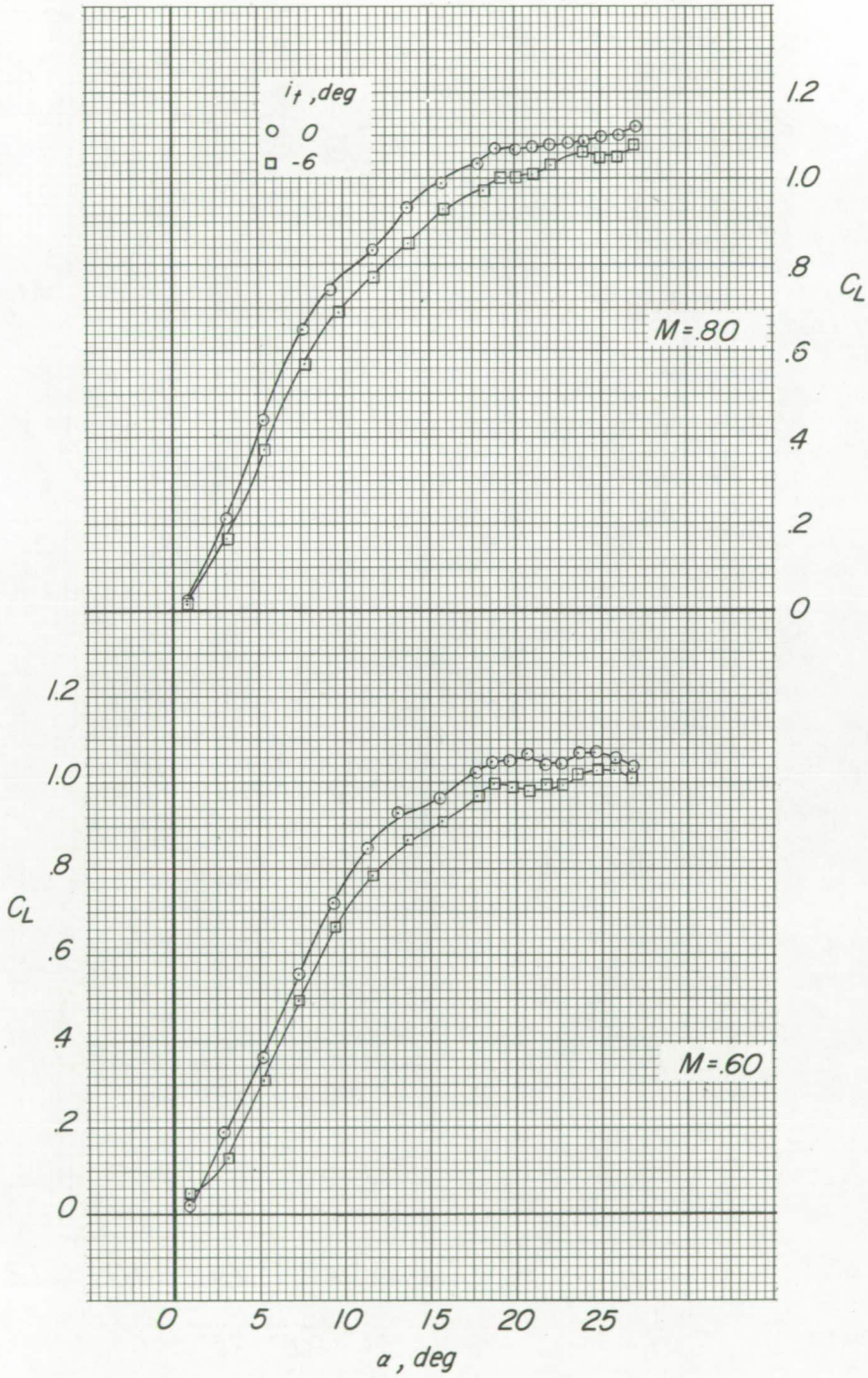

(b) C_L against α.

Figure 16.- Continued.

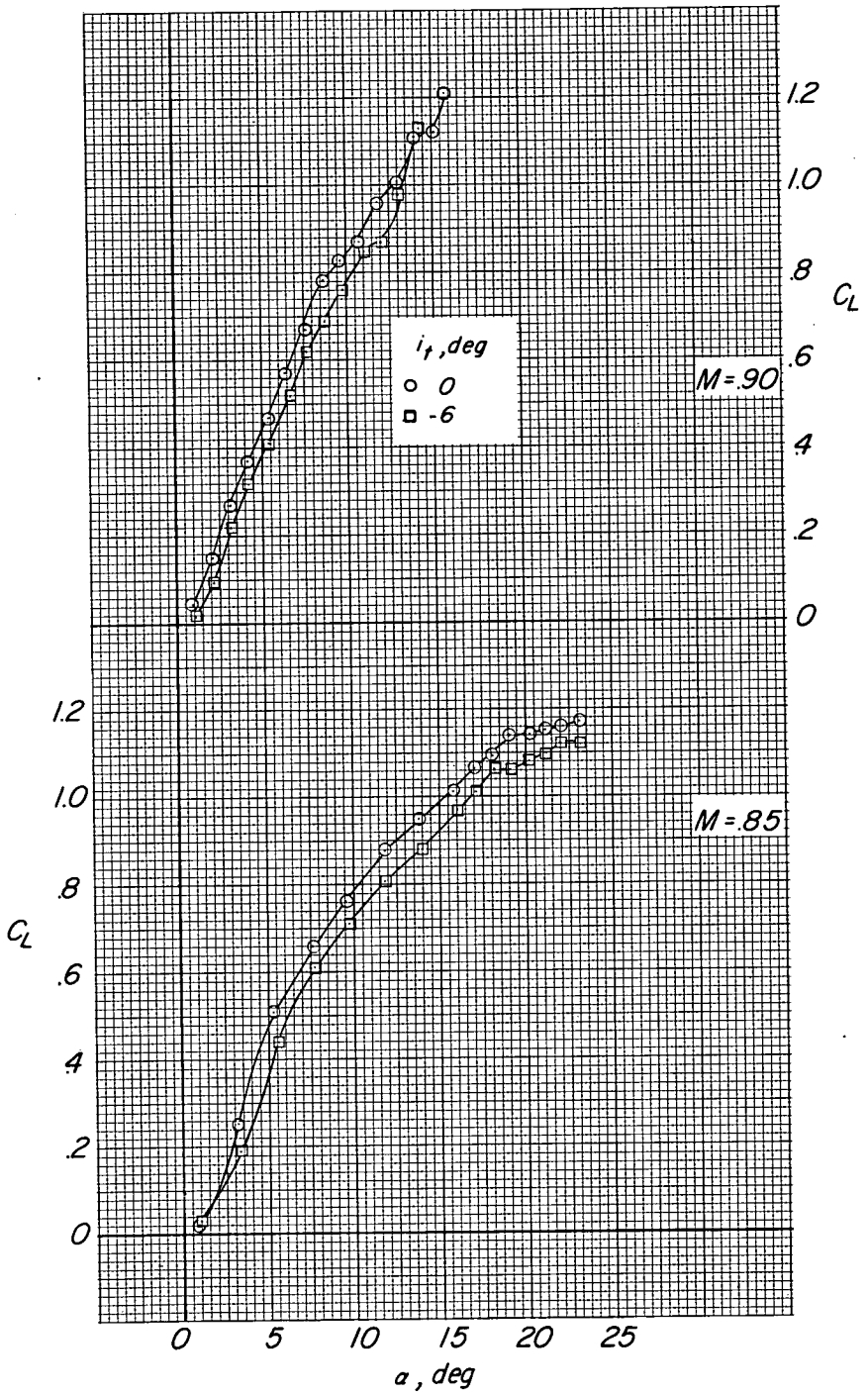

(b) Continued.

Figure 16.- Continued.

[redacted]

DECLASSIFIED

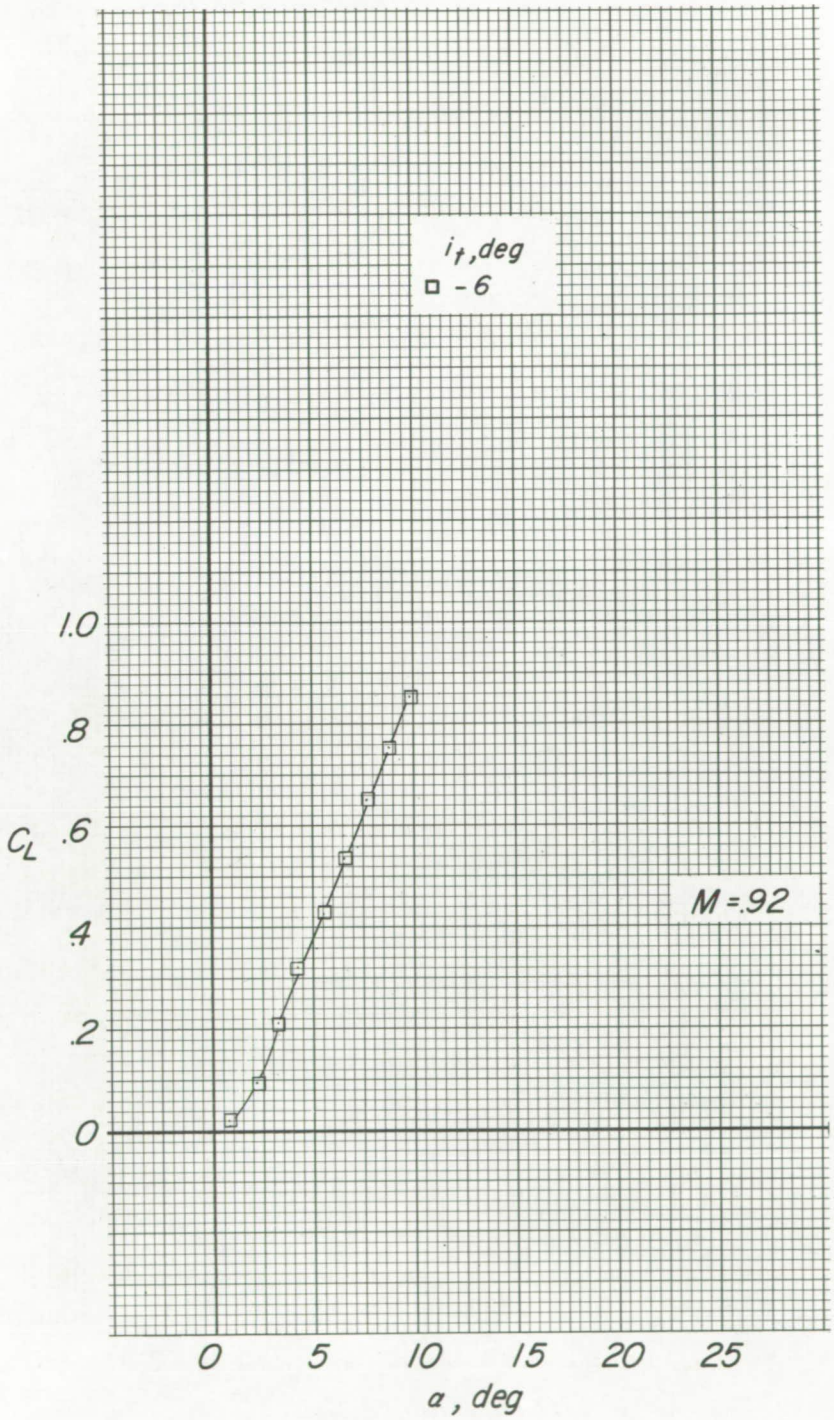

(b) Concluded.

Figure 16.- Continued.

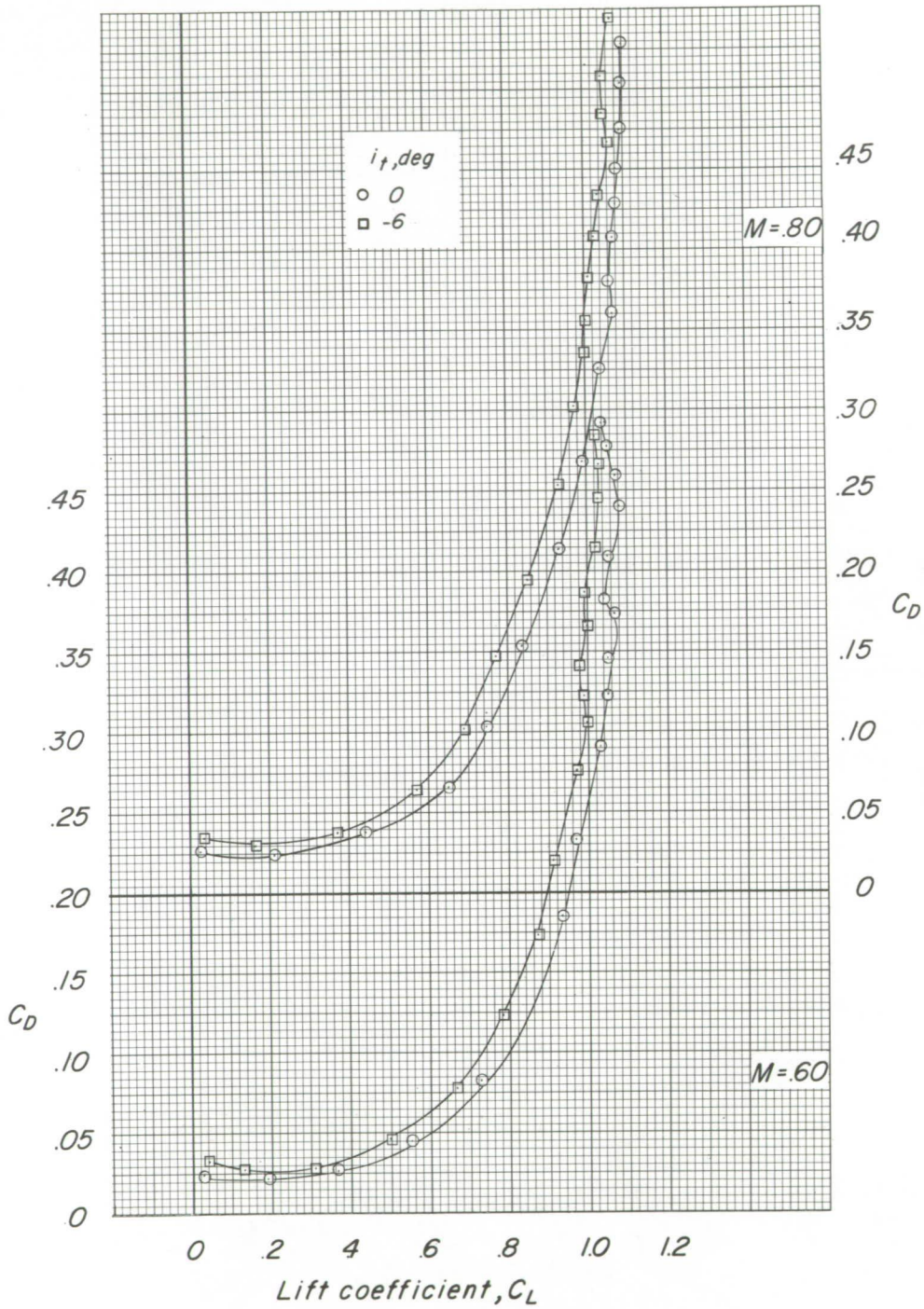

(c) C_D against C_L.

Figure 16.- Continued.

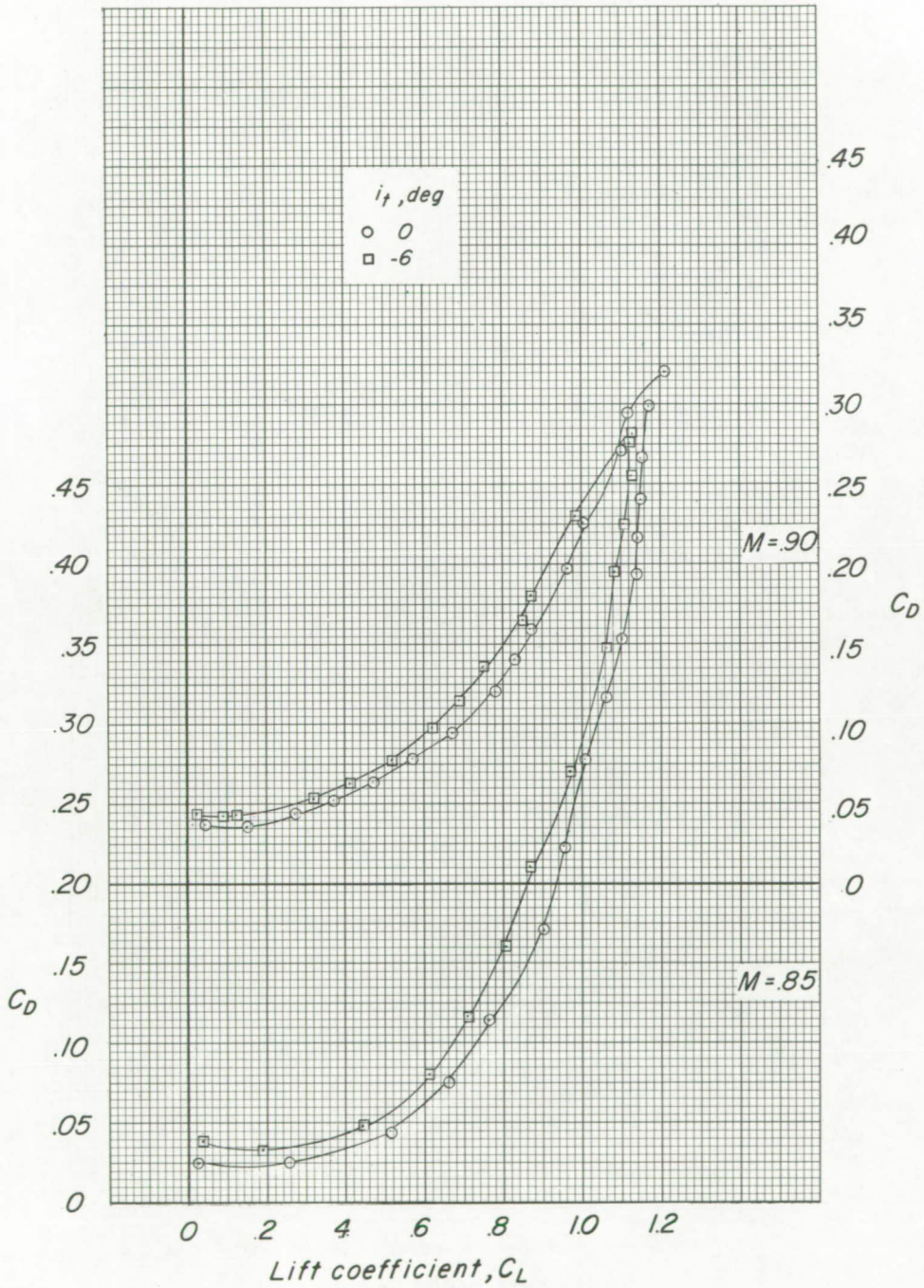

(c) Continued.

Figure 16.- Continued.

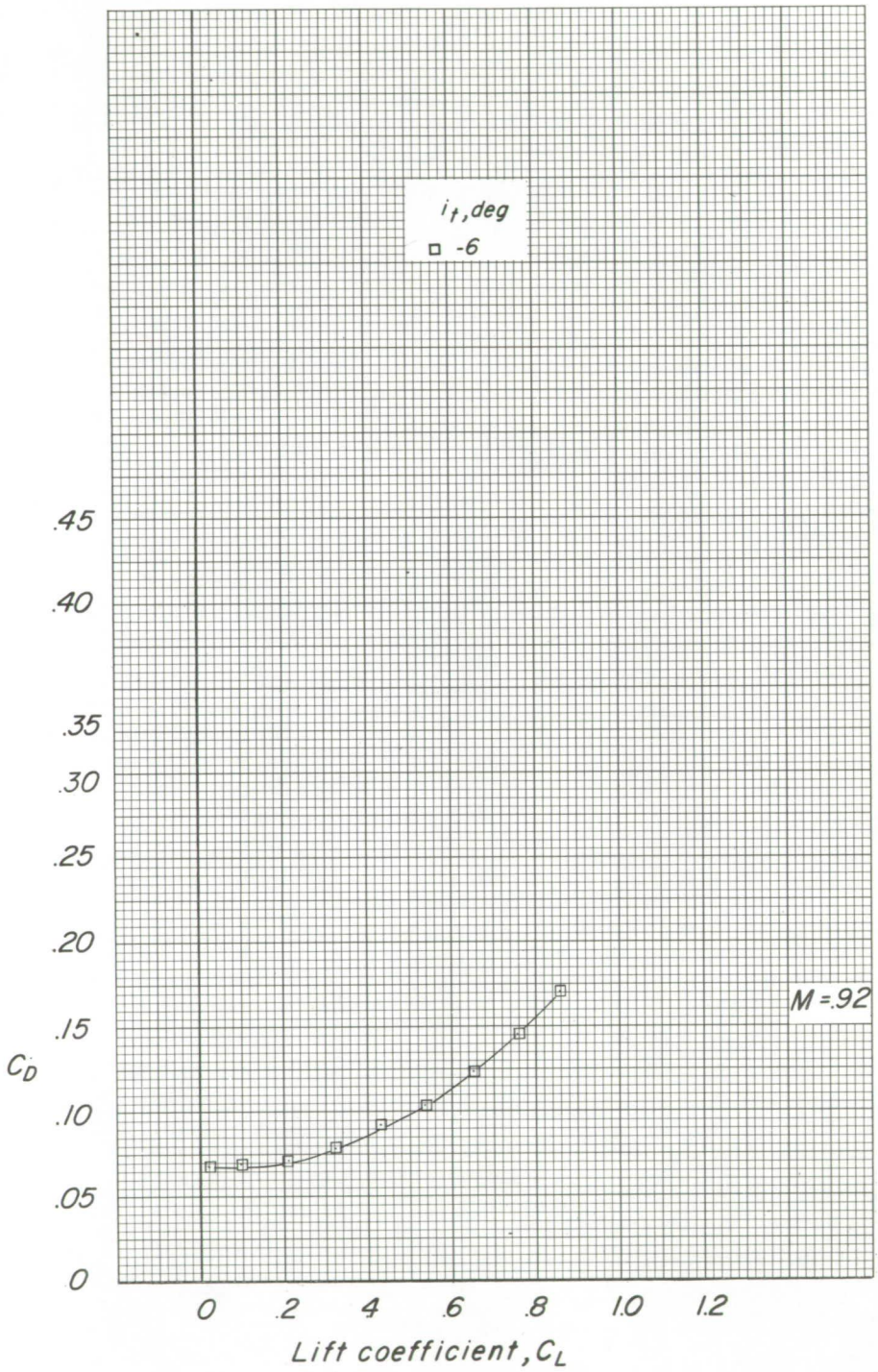

(c) Concluded.

Figure 16.- Concluded.

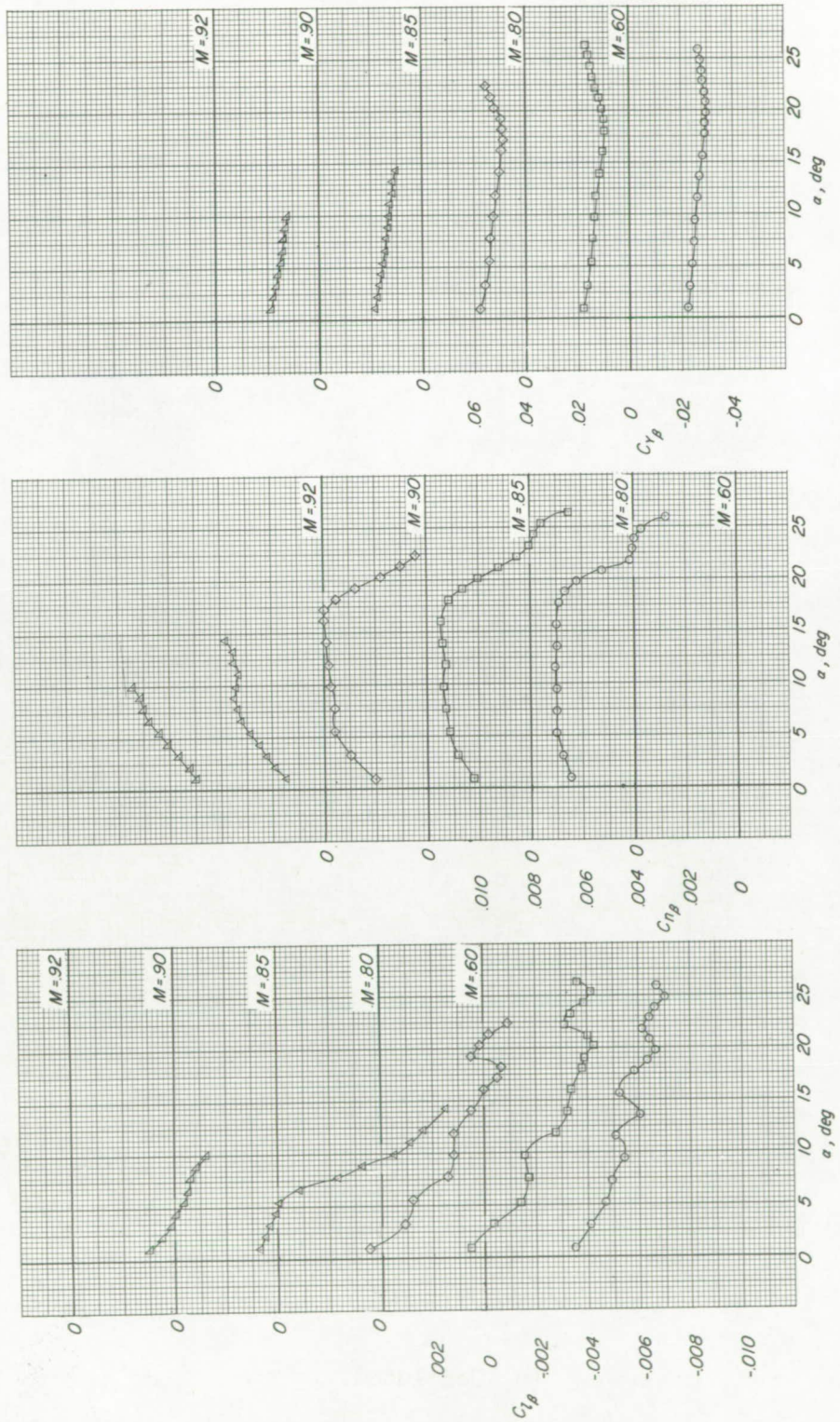

Figure 17.- Lateral stability derivatives of the model with the new vertical and horizontal tail. WFV_1H_1. $i_t = -6^\circ$.

[redacted]

[redacted]